THE MEASUREMENT OF TURBULENCE WITH THE BURST-TYPE LASER DOPPLER ANEMOMETER - ERRORS AND CORRECTION METHODS

by

Preben Buchhave

A dissertation submitted to the Faculty
of the Graduate School of State University
of New York at Buffalo in partial fulfillment
of the requirements for the degree of
Doctor of Philosophy

September 1979

Acknowledgements

The main body of this work was carried out during a one year leave of absence from DISA Elektronik A/S, Skovlunde, Denmark. The author wishes to express his appreciation to individuals and institutions, which made this arrangement possible, in particular to Dr. W. K. George, who issued the initial invitation and who has functioned as an inspiring advisor and co-worker. He also wishes to thank the staff and students of the Department of Mechanical Engineering, State University of New York at Buffalo and my colleagues at DISA Elektronik A/S for helpful discussions and excellent support in the development of both hardware and software.

He would like to issue a special thank you to Mr. R. L. Humphrey of DISA Electronics, New Jersey for his unfailing, round the clock support and to the secretaries, Ms. Birte Svenson and Mrs. Eileen Graber at DISA and SUNYAB respectively, for expert typing and secretarial help.

The research was supported by the Danish Science Research Council, the Danish Council for Scientific and Industrial Research, the U. S. National Science Foundation, Meteorology Program under Grant No. ATM-76-02157 and Fluid Mechanics Program under Grant No. ENG-76-17466 and the U. S. Air Force Office of Scientific Research, Aerospace Sciences Division under Contract No. F49620-78-C-0047.

Table of Contents

List of Figures

Figure No.	Figure Title
7.1	Oscilloscope traces showing (from bottom): The Doppler signal, the tracker VCO signal and the tracker output with drop-out protection (the threshold set to eliminate the large phase fluctuations).
7.2a	Tracker output in time domain. (Range 1.5 MHz, Bandwidth 4%).
7.2b	Tracker output in frequency domain.
7.3	Hot-wire spectrum corresponding to the tracker spectrum of Fig. 7.2b.
7.4a	Tracker output in the time domain. Drop-out pct 0 (Range 1.5 MHz, B.W. 4%, f_D-.2 MHz, f_s-.3 MHz)
7.4b	Spectrum corresponding to Fig. 7.4a.
7.5a	Tracker output in time domain. Drop-out pct. 10. (Parameters as in Fig. 7.4a)
7.5 b	Spectrum corresponding to Fig. 7.5a.
7.6a	Tracker output in time domain. Drop-out pct. 50. (Parameters as in Fig. 7.4a).
7.6b	Spectrum corresponding to Fig. 7.6a.
7.7	Spectrum of tracker output at drop-out pct. 80. (Parameters as in Fig. 7.4a).
7.8	Spectrum of LDA-counter analog out at a high data rate (d.r. 20 kHz).
7.9a	Analog out of counter in time domain. D.r. 6kHz. (high pass 16 kHz, low pass 4 MHz, f_D.2 MHz, f_s=.3 MHz)
7.9b	Spectrum corresponding to Fig. 7.9a.
7.10a	Counter analog out in time domain. D.r. 1.8 kHz. (Parameters as in Fig. 7.9a).
7.10b	Spectrum corresponding to Fig. 7.10a.
7.11	Spectrum of counter analog output at a data rate of 100 Hz. (Parameters as in Fig. 7.9a).
A1	The measuring volume projected onto the three coordinate planes θ = 20°.

ABSTRACT

The laser Doppler anemometer (LDA) is rapidly evolving as a major tool for fluid mechanics research. A relatively recent innovation in the development of this instrument is the "so-called" burst-processor or individual realization mode of operation. In this mode the instrument measures the velocity of individual particles as they arrive at the measuring volume. It is well-known that there are problems in interpreting the signals from these randomly arriving particles since the statistics of the particle arrival are correlated with the velocity.

In this work the functioning of the laser anemometer in the burst mode is investigated, and sources of errors in the velocity determination are analyzed and measured. The residence-time analysis of burst-type LDA signals is developed to encompass spectral measurements as well as moments of the velocity distribution. It is shown both analytically and experimentally that the complete time statistics of the velocity field can be recovered from the random burst-signal if the particle residence time is measured along with its velocity. Formulas for mean and mean square velocity, autocorrelation function and spectra are derived, and the differences in the results obtained by various data processing methods predicted from the theory are substantiated by measurements.

The experimental system is based on an LDA-counter processor coupled to a mini-computer through a special parallel interface with a buffer memory to absorb data arriving at random times. Results of the LDA data processing are compared to simultaneous measurements with conventional techniques.

1. Introduction

Although laser Doppler methods for fluid flow measurements have now been in existence for more than 15 years, new methods and results are continually being published and both optical and signal processing methods can be expected to continue to develop further in the coming years. In recent years the so-called burst-type or individual realization LDA (laser Doppler anemometer) has received the most attention. The properties of continuous Doppler signals are by now fairly well understood and signal processing methods like spectral analysis and frequency tracking are well established (although there is also here still room for improvements of both a practical and theoretical nature.) On the contrary burst-type signal processing has been the subject of some controversy regarding the correct methods of signal processing and data processing and concerning the so-called bias effect on the computed statistical flow parameters.

This report describes burst-type LDA measurements in turbulent flows and presents a rigorous derivation of the correct, bias-free method of processing randomly arriving, burst-type LDA signals in measurements in incompressible flow. Algorithms for the computation of moments of the velocity distribution, correlation functions and spectra are derived.

The theoretical results are substantiated by measurements of the properties of a free jet in air with the burst-type LDA and by comparisons to simultaneous measurements with a hot-wire anemometer and in some cases to a continuous LDA using a frequency tracker. The burst-type LDA data are likewise compared to existing theoretical and experimental information on the properties of the free jet in air. The free jet was

chosen because it represents a stable, reproducible, self-similar flow phenomenon, and because the rather high turbulence intensity present in the fully developed jet is needed in some cases to distinguish the results of the various experimental methods.

The complete optical and electronic LDA system for burst-type LDA measurements is described. The optical system is designed for optimum performance in single particle measurements. The signal processing system is based on the counter processor and includes optical and electronic frequency shift. The data processing is performed on a dedicated DP-11 minicomputer. The minicomputer is coupled to the LDA system via a special interface which allows both data collection and processing as well as output for control of experimental conditions, traversing of the measuring point, etc.

The software (in particular the higher level language FORTRAN programs) used for the evaluation of moments, autocorrelation function and spectrum--both by a method analogous to the Blackman-Tukey estimator for equidistantly sampled data and by a direct transform-- is described in the text.

The structure of the contents of the report is the following: In section 2 the optical system and transducer characteristics of an LDA-system optimized for burst processing are described. Then follows in section 3 a description of the electronic system including counter signal processor, frequency shift and computer system. In section 4 the correct, bias-free procedure for burst-type LDA data processing using the so-called residence time weighting is derived. Section 5 provides the experimental evidence for the correctness of the residence time weighting and also results of the so-called 1-dimensional weighting

as well as LDA-tracker and hot-wire measurements. Chapter 6 presents results of burst-type LDA measurements of autocorrelation functions and spectra computed from the autocorrelation function by the Blackman-Tukey method. Also presented are results of spectral measurements by a direct Fourier transform of the randomly sampled LDA data. Spectra from hot-wire and tracker measurements are presented for comparison. Finally in Chapter 7 the influence of drop-out in tracker data and the effect of the staircase-type signal from counter analog outputs on the measured spectrum is evaluated theoretically and substantiated by direct measurements of the spectrum of the frequency tracker and counter analog output in measurements in the free jet.

The burst-type or individual realization LDA mode is a particular mode of operation of the LDA as opposed to continuous operation or photon counting methods. The burst-type operation is particularly useful in situations, where the seeding particle concentration is relatively low, such as in many measurements in gases or where reference beam or other coherent detection schemes are not practical. Also the burst-type LDA has some particular advantages compared to the continuous type LDA. These advantages will be described several places in the following, but the main points may be summarized here: 1) The single particle LDA does not suffer from the so-called ambiguity noise present in continuous signal LDA signal processing. 2) The randomly arriving data from burst-type LDA's allow the formation of alias-free spectra and the elimination in the computed spectrum of some types of noise associated with Doppler signals. 3) In incompressible flows with statistically uniform seeding,

complete elimination of the so-called velocity bias is possible. In other types of flows with non-uniform seeding as, e.g. an unseeded jet issuing into seeded air or vice-versa or in combustion measurements, the burst-type LDA may perform a conditional sampling of flow data, which would be difficult to obtain by other means. Many of these possibilities remain to be explored and present a promising field for future research.

2. Optical System and Probe Characteristics of Burst-Type LDA

The burst-type LDA is a particular mode of operation of the LDA optimized for the detection of the velocity of single particles. To fully utilize the advantages of this system the various optical and electronic subsystems must be capable of adjustment for optimum operation in the burst-mode in the given flow situation and with the chosen or naturally occurring seeding particles. Many of the features of the burst-mode or single particle detection are well known and documented, but we shall take this opportunity to summarize the essential features of the burst-type LDA and describe the optical system used in the present measurements. As a general introduction to LDA methods two recent monographs may be recommended: Durst, Melling and Whitelaw (1976) and Durrani and Greated (1977). A recent review of the state of the art of turbulence measurements with the LDA is given in Buchhave, George and Lumley (1979).

2.1 Fringe-mode Optical System

The LDA-mode used in burst-type or single particle measurements is the so-called dual-beam mode (also called the differential- or fringe-mode). This mode of operation was investigated in the early seventies, see e.g. Rudd (1969), Drain (1972), Lading (1973) and Hanson (1974). The essential element of this system, which is shown in Figure 2.1, is the probe volume formed by the intersection of two equally intense laser beams by focusing two parallel beams into a common focal volume with a single lens (optics). In the intersection region a system of interference fringe planes is formed.

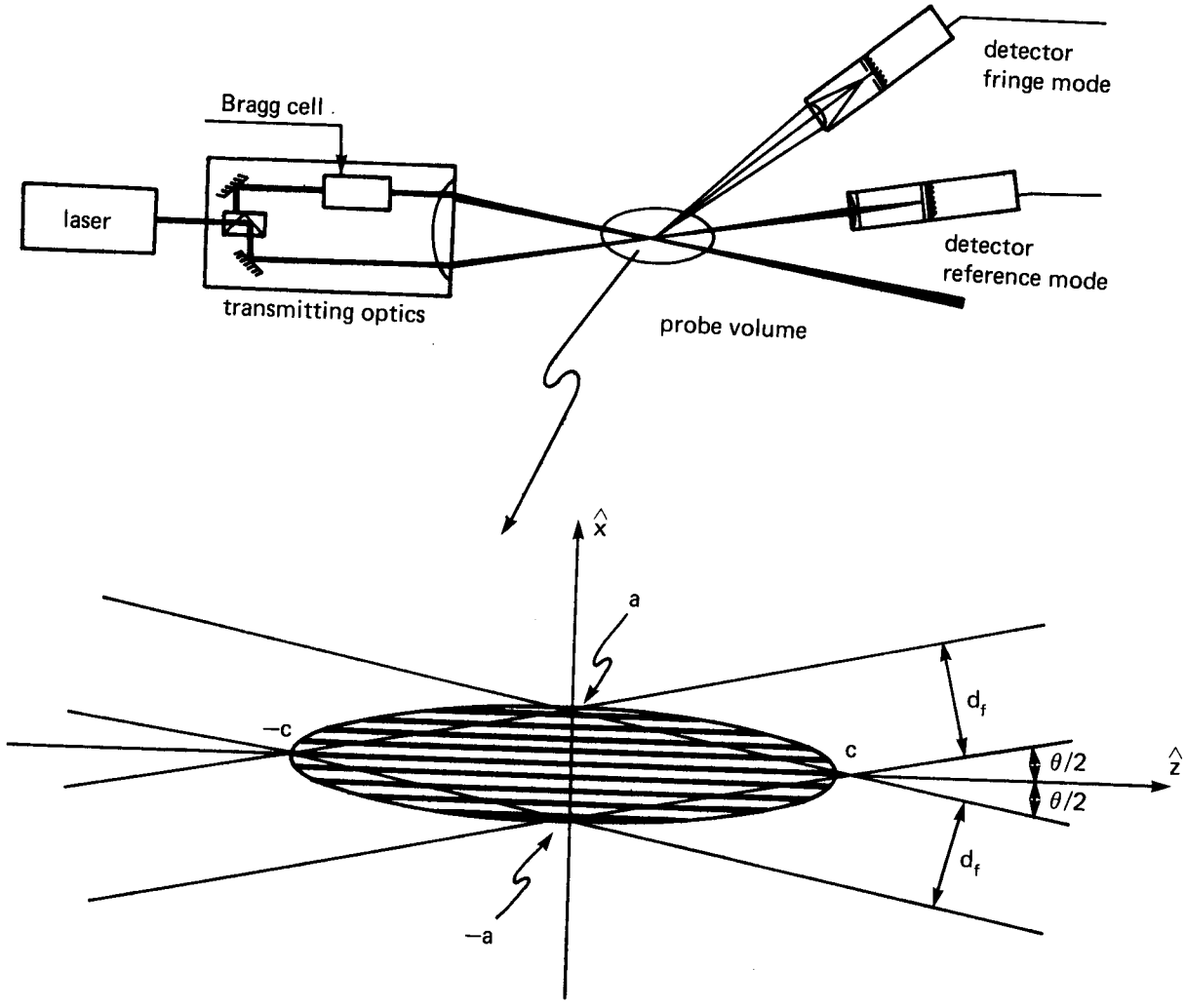

Fig. 2.1. Optical configuration of fringe mode LDA.

Three main principles or physical effects are utilized in the LDA:

- The Doppler shift of light scattered from particles moving through the focused laser beams.
- The optical heterodyning of the two scattered beams on a square-law photodetector.
- Frequency demodulation of the detector current to derive the velocity, which is proportional to the detected frequency.

2.2 Detection and Doppler Signal

The Doppler shift of light scattered from a single (point) particle at the time dependent position $\underline{x}(t)$ moving with velocity $\underline{u}(t) = (u(t), v(t), w(t))$ through the light field $\underline{E}(\underline{x},t)$ represented by the scalar, plane wave components $E(\underline{x},t)\, e^{i(\underline{k}\cdot\underline{x} - \omega_1 t + \phi)}$, where $\underline{k}$ is the wave vector, $\underline{x}$ and t position and time, ω_1 the light frequency and ϕ a phase term depending on the initial position of the particle, is given for steady velocities by

$$\omega_D = \underline{u}\cdot(\underline{k}_s - \underline{k}_i) \qquad (2.2.1)$$

where $\underline{k}_i$ and $\underline{k}_s$ are the wave vectors of the incident and scattered light respectively.

The Doppler shift can be measured by heterodyne detection of the light scattered from two different incident light beams represented by wave vectors $\underline{k}_{i,1}$ and $\underline{k}_{i,2}$ into a common scattered beam represented by the wave vector $\underline{k}_s$ directed towards the detector element dA at $\underline{x}_d$. The resulting photocurrent is then found by integration over the whole detector surface of the square of the total light field at each point of the detector surface:

$$i(t) \propto \int_A \left| E_{s,1}(\underline{x}_d,t) e^{i(\underline{k}_s \cdot \underline{x}_d - (\omega_1 + \omega_{D,1})t + \phi_1)} \right.$$

$$\left. + E_{s,2}(\underline{x}_d,t) e^{i(\underline{k}_s \cdot \underline{x}_d - (\omega_1 + \omega_{D,2})t + \phi_2)} \right|^2 dA \qquad (2.2.2)$$

It is the square-law characteristic of the photodetector which allows the detection of the difference in the two light frequencies.

Evaluation of the integral gives:

$$i(t) = i_1(t) + i_2(t) + 2\varepsilon\sqrt{i_1(t) i_2(t)} \qquad (2.2.3)$$

$$\cdot \cos\left(\underline{u} \cdot (\underline{k}_{i,2} - \underline{k}_{i,1})t + (\phi_2 - \phi_1)\right)$$

where $i_1(t)$ and $i_2(t)$ are the currents, which would flow in the detector with only one or the other beam present:

$$i_1(t) \propto \int_A |E_{s,1}(\underline{x}_d,t)|^2 \, dA \qquad (2.2.4)$$

$$i_2(t) \propto \int_A |E_{s,2}(\underline{x}_d,t)|^2 \, dA \qquad (2.2.5)$$

ε is the so-called heterodyning factor or visibility factor, which in the general theory accounts for misalignment of the two wave fronts on the photodetector surface or phase differences between the two scattered fields across the detector surface. When light is scattered from a single particle of dimensions of the order of the light wave length the coalignment criterion or antenna condition is automatically fulfilled and the heterodyning factor is unity even for large detector apertures. For larger particles this is not necessarily true and a better signal-to-noise ratio may be obtained when the detector aperture is reduced (Adrian and Orloff (1977). Generally speaking, though, much larger apertures can be utilized in single particle detection in the dual-beam mode than in many particle detection with the reference beam mode.

In the single particle, dual-beam system the wave vector of the scattered light drops out in the expression for the modulation frequency. The detected frequency is independent of the detector position and only the angle between the incident beams enters the expression for the relation between Doppler frequency and velocity.

In the coordinate system defined in Figure 2.1 the relation is:

$$f_D = \frac{2u}{\lambda} \sin(\theta/2). \tag{2.2.6}$$

However, the direction to the detector still enters through the strength of the optical field in the direction towards the detector. For optimum signal-to-noise ratio of the detector signal the two scattered beams should have equal intensity (Lading 1973). Thus for equal intensity incident beams the detector should be placed in the symmetry plane between the two incident beams (the y-z plane in Figure 2.1).

If a TEM_{00} mode laser of power P is used the intensity distribution in the intersection region is given by the following expression:

$$I(x,y,z) = \frac{1}{4\pi} \frac{P}{\sigma_f^2} e^{-\frac{1}{2\sigma_f^2}\left[(x\cos\frac{\theta}{2})^2 + y^2 + (z\sin\frac{\theta}{2})^2\right]}$$

$$\cdot\{\cosh\left(\frac{x\,z\sin\theta}{2\sigma_f^2}\right) + \cos(2k\,x\sin\frac{\theta}{2})\} \tag{2.2.7}$$

where σ_f is the standard deviation of the Gaussian intensity distribution in the focal plane of each beam. Equation (2.2.3) expressed in the coordinate system of Figure 2.1 becomes:

$$i(t) = i_1(t) + i_2(t) + 2\sqrt{i_1(t)i_2(t)}\cos(2\pi f_D t + \phi_p) \tag{2.2.8}$$

with

$$i_1(t) = i_{0,1} e^{-\frac{1}{2\sigma_f^2}\left|(x \cos\frac{\theta}{2} - z \sin\frac{\theta}{2})^2 + y^2\right|} \qquad (2.2.9)$$

and

$$i_2(t) = i_{0,2} e^{-\frac{1}{2\sigma_f^2}\left|(x \cos\frac{\theta}{2} + z \sin\frac{\theta}{2})^2 + y^2\right|} \qquad (2.2.10)$$

$i_{0,1}$ and $i_{0,2}$ are the detector currents resulting from a particle placed in the focal point of beam 1 and 2 respectively, ϕ_p is a phase term depending on the initial position of the particle, $\underline{x}(0)$, and $\underline{x}(t)$ is given by:

$$\underline{x}(t) = \int_0^t \underline{u}(t)\, dt + \underline{x}(0) \qquad (2.2.11)$$

where $\underline{u}(t)$ is the (Langrangian) particle velocity.

2.3 Probe Volume and Measuring Volume

The optical probe volume is often defined by the $1/e^2$ contour of the fringe modulation region. This is an ellipsoid with half axes a, b and c along the coordinate axes of Figure 2.1.

$$2a = 4\sigma_x = \frac{d_f}{\cos(\theta/2)}$$

$$2b = 4\sigma_y = d_f \qquad (2.3.1)$$

$$2c = 4\sigma_z = \frac{d_f}{\sin(\theta/2)}$$

where d_f is the $1/e^2$-diameter of the focused laser beam:

$$d_f = 4\sigma_f = \frac{4}{\pi}\frac{\lambda_f}{d_e} \qquad (2.3.2)$$

and d_e is the beam waist diameter of the laser beams before the focusing lens.

The interference fringes are parallel planes normal to the vector

$\underline{k}_{i,2}-\underline{k}_{i,1}$ (the x-axis in figure 2.1) with a constant mutual distance δ_f given by:

$$\delta_f = \lambda/(2 \sin(\theta/2)) \tag{2.3.3}$$

The number of fringes within the probe volume, N_f, is given by:

$$N_f = \frac{8}{\pi}\frac{f}{d_e}\tan(\theta/2) = \frac{4}{\pi}\frac{D_e}{d_e} \tag{2.3.4}$$

where D_e is the separation of the two parallel beams as they leave the focusing optics and f is the focal length.

Before we leave the subject of the burst-mode LDA probe volume the following comments should be made:

- The Doppler frequency can be explained as a modulation of the intensity of light scattered from a particle moving through the interference fringe pattern in the probe volume (the so-called fringe-model). This model is correct as long as the detection is non-coherent but fails in the case of coherent detection. Hanson (1974).

- The above description is based on the use of Gaussian laser beams. If the laser operates in a higher order mode or if the beams are distorted or vignetted along their way, the probe volume characteristics change.

- In the description of the focusing and interference of the laser beams some assumptions and approximations have been made. Specifically: Gaussian laser beams are used and it is assumed that the beam waist of the laser beam was placed at the focal distance f behind the front lens so that the fringe planes will be parallel (see e.g. Hanson 1973). It is also assumed that the scaler field approximation is valid, i.e. that a scaler field instead of the full E-M vector field is adequate for the description of the field distribution in the focal region. This approximation fails at low f-numbers (see e.g. Born and Wolf 1959) but is valid with sufficient accuracy for all f-numbers of importance in LDA work except possibly for the LDA microscope. If these conditions were not fulfilled the interference

fringes in the probe volume would not be equidistant and the zero crossings of the high-pass filtered Doppler burst would not be equidistant in time. Thus an important advantage of the burst LDA over the continuous LDA would be lacking.

The probe volume is not necessarily equal to the measuring control volume. Let us define the measuring volume as the region in space from which Doppler signals are detected. The size of this volume is determined by a number of factors including velocity direction, particle size and shape, detector optics, amount of frequency shift, laser power and overall gain of the system.

Most straightforward to assess is the influence of the detector optics. Figures 2.2a and 2.2b show two cases: In Figure 2.2a the field of view of the detector is limited by the pinhole in the focal plane of the detector lens. This reduces the measuring volume to at most the region of overlap of the fringe system probe volume and the cylinder in the focal plane of the detector optics defined by the pinhole. More subtle is the influence of the detector optics in the backscatter arrangement shown in Figure 2.2b. The focal region of the receiver lens may now reduce the measuring volume, since the pinhole is chosen to match the field of view to the probe volume diameter. The length of the focal region for the imaging of a pinhole attached to a probe volume by a diffraction limited receiver lens is approximately given by:

$$\ell_f \tilde{=} d_f \, D/f \qquad (2.3.5)$$

This is usually somewhat shorter than the length of the probe volume.

Particle size, laser power and system gain determine the measuring volume size by their influence on the amplitude of the signal relative to the trigger level in the signal processing electronics. Increasing

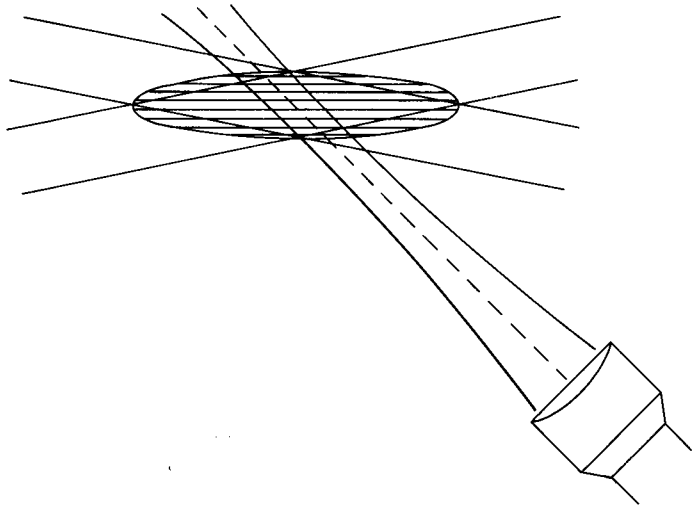

Fig. 2.2a Measuring volume, forward scatter.

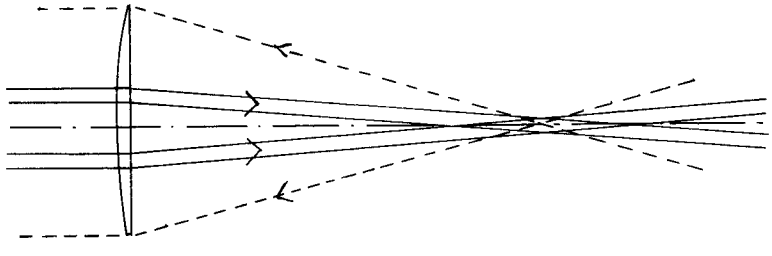

Fig. 2.2b Measuring volume, backscatter.

fringes in the probe volume would not be equidistant and the zero crossings of the high-pass filtered Doppler burst would not be equidistant in time. Thus an important advantage of the burst LDA over the continuous LDA would be lacking.

The probe volume is not necessarily equal to the measuring control volume. Let us define the measuring volume as the region in space from which Doppler signals are detected. The size of this volume is determined by a number of factors including velocity direction, particle size and shape, detector optics, amount of frequency shift, laser power and overall gain of the system.

Most straightforward to assess is the influence of the detector optics. Figures 2.2a and 2.2b show two cases: In Figure 2.2a the field of view of the detector is limited by the pinhole in the focal plane of the detector lens. This reduces the measuring volume to at most the region of overlap of the fringe system probe volume and the cylinder in the focal plane of the detector optics defined by the pinhole. More subtle is the influence of the detector optics in the backscatter arrangement shown in Figure 2.2b. The focal region of the receiver lens may now reduce the measuring volume, since the pinhole is chosen to match the field of view to the probe volume diameter. The length of the focal region for the imaging of a point by a diffraction limited receiver lens is approximately given by:

$$\ell_f \cong 8\, d\, \lambda^2\, f^2 \qquad (2.3.5)$$

This is usually much shorter than the length of the probe volume.

Particle size, laser power and system gain determine the measuring volume size by their influence on the amplitude of the signal relative to the trigger level in the signal processing electronics. Increasing

signal amplitude allows particles farther away from the probe volume center where the illumination is less intense to be detected, thereby increasing the effective measuring volume.

In many cases in turbulence measurements, e.g. in measurements of small scale turbulence or in strong shear layers, it is important to know approximately the size of the measuring volume. In such cases it may be necessary to determine the size of the measuring volume experimentally. Since control of the position of micron-size particles is difficult, one is often forced to estimate the measuring volume size from the signals from fine wires (e.g. hot-wire probes) which are moved about in the probe volume.

2.4 Angular Characteristics and Measuring Volume Cross Section.

The angular characteristics of the LDA measuring volume are determined not only by the optical configuration, but also by the method of signal processing employed. The main distinction is between continuous and burst-type processing. We shall consider the tracker and the counter as representative of these two methods.

Angular Characteristics, Tracker Processing

The tracker measures a Doppler frequency proportional to the component of velocity along the direction of measurement (the x-axis of Figure 2.1). If the frequency decreases below the range of the tracker, the instrument drops out and the measurement is interrupted. This leads to a particular "dead zone" depending on the velocity magnitude $|\underline{u}|$ as shown in Figure 2.3a. The graph shows a polar diagram of allowed angles ϕ between the measuring direction $\hat{x}$ and velocity vectors of magnitude u_m, 0.5 u_m and 0.1 u_m in the x-y-plane, where u_m is the maximum velocity

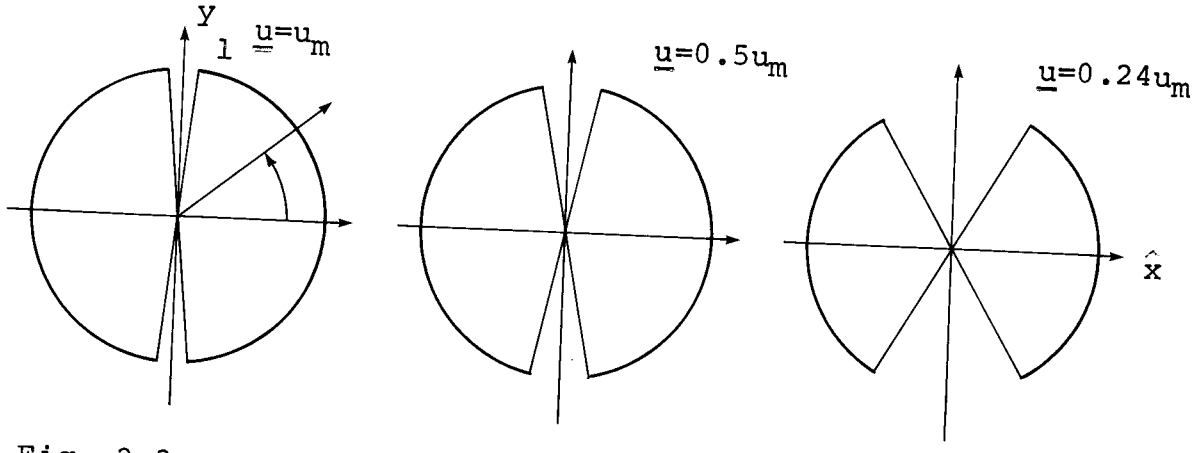

Fig. 2.3 a $u_s=0$

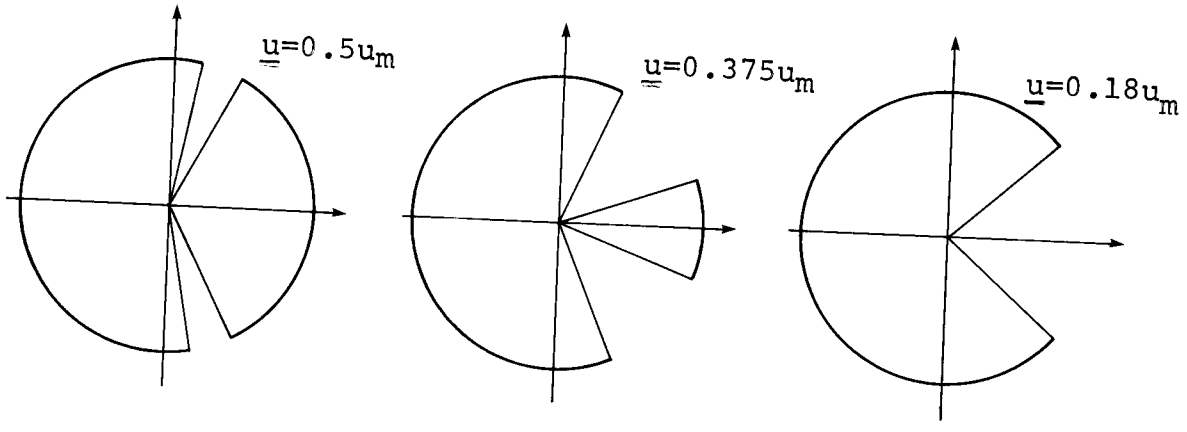

Fig. 2.3 b $u_s=0.5u_m$

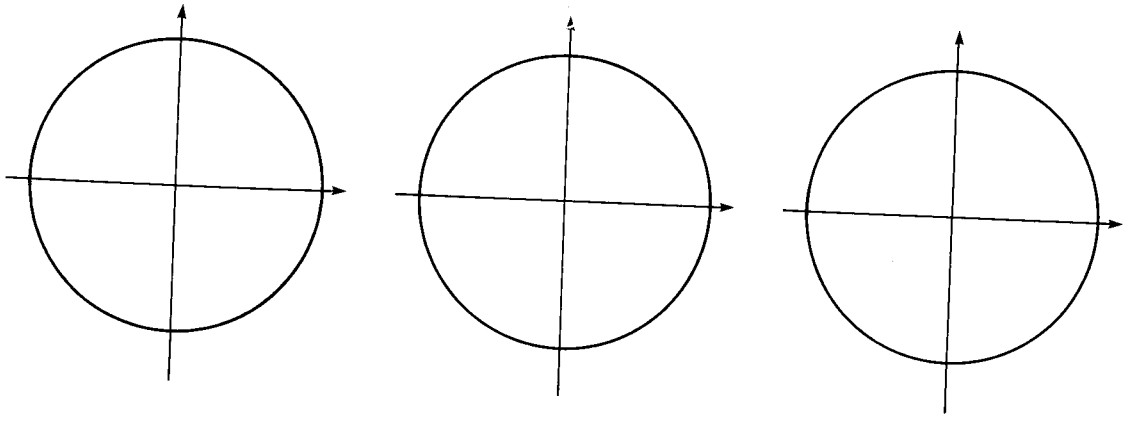

Fig. 2.3 c $u_s=2u_m$

Fig. 2.3 Polar diagram of measuring volume cross section and dead zones for LDA tracker signal processing.

within a given tracker range. The dead zone extends to velocities with non-zero z-components as well. The characteristics of Figure 2.3a are rotationally symmetric about the $\hat{x}$-axis. The dead zones are modified or completely removed by the addition of frequency shift. A frequency shift f_s corresponding to a motion of the interference fringes with velocity $u_s = \delta_f \cdot f_s$ results in the modified angular characteristics of Figure 2.3b. Finally, a shift greater than $f_s = u_m/\delta_f$ leads to the complete removal of dead zones, Figure 2.3c.

Angular Characteristics, Counter Processing

The angular characteristics of a burst counter LDA system are similar but more complicated. The complications arise because most counters require a certain minimum number of zero-crossings of the part of the burst whose amplitude is above the trigger level before a measurement can be completed.

For a given intensity of the scattered light, total system gain, trigger level and measuring volume the angular characteristics can be calculated or measured. In the following some examples of angular characteristics of a counter LDA with an ellipsoidal measuring volume of half axes a, b and c are computed and presented in the form of polar plots of the measuring volume cross section. The computed values are compared to measurements with the LDA in the backscatter mode.

Assuming that N_e zero-crossings are needed for a measurement and that the maximum number of fringes within the measuring volume (without frequency shift) along the x-axis is N_f, we present the data in terms of the parameter $Q = N_e/N_f$. The amount of frequency shift f_s is also an important parameter. Data is presented for various values of the equivalent fringe velocity $u_s = \delta_f/f_s$ relative to the magnitude of the

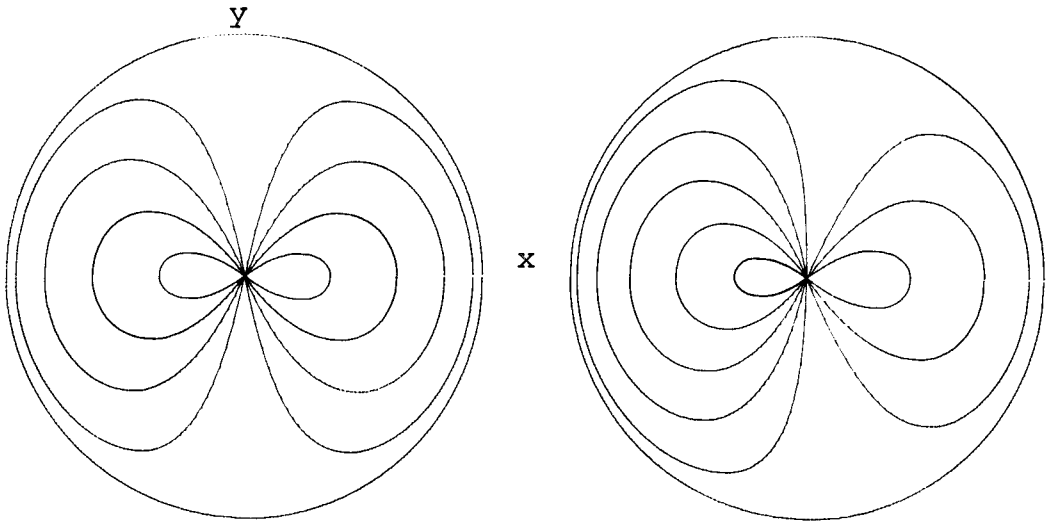

Fig. 2.4 a $u_s=0$

Fig. 2.4 b $u_s=0.2u_m$

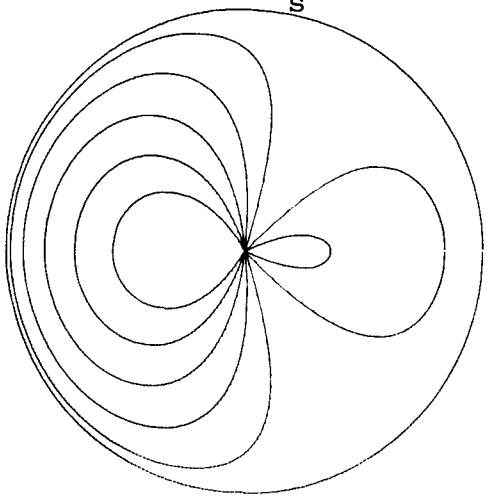

Fig. 2.4 c $u_s=0.5u_m$

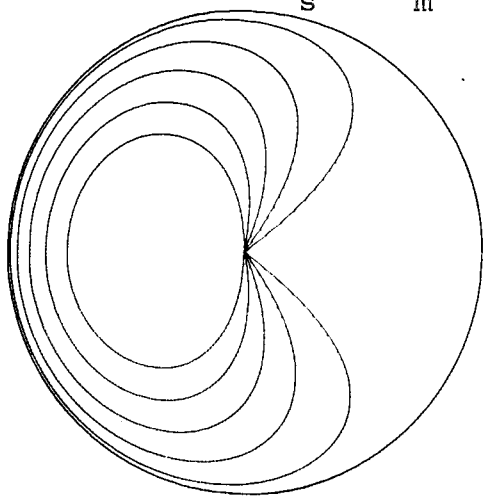

Fig. 2.4 d $u_s=u_m$

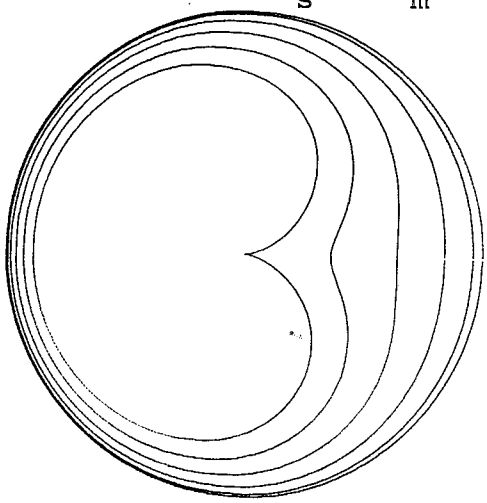

Fig. 2.4 e $u_s=2u_m$

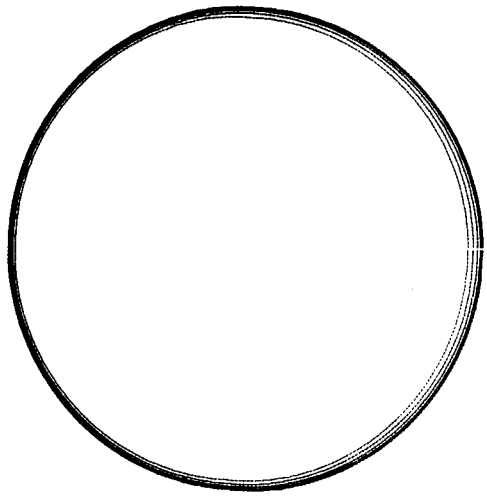

Fig. 2.4 f $u_s=5u_m$

velocity vector $|\underline{u}|$. The measuring volume cross section is defined as the area S normal to the instantaneous velocity within which a particle trajectory will lead to at least one measurement (Buchhave (1976)). The relative cross section σ is the ratio of S to the geometrical cross section of the measuring volume in the y-z-plane, πbc; that is, $\sigma = S/\pi bc$. The concept of a cross section requires that the flow velocity can be assumed constant across the measuring volume. Under this condition the following expression can be derived for the cross section including the effect of frequency shift (see Appendix I):

$$S = \pi abc\ R\ \{1 - a^2Q^2R^2\frac{|\underline{u}|^2}{(u - u_s)^2}\} \tag{2.4.1}$$

$$\sigma = a\ R\ \{1 - a^2Q^2R^2\frac{|\underline{u}|^2}{(u - u_s)^2}\} \tag{2.4.2}$$

with

$$R = \frac{1}{|\underline{u}|}\sqrt{\frac{u^2}{a^2} + \frac{v^2}{b^2} + \frac{w^2}{c^2}} \tag{2.4.3}$$

Figure 2.4 shows a polar diagram of the relative cross section for a particular optical configuration (f = 300 mm, λ = 0.633 nm, θ = 15°) for zero frequency shift. For $Q \to 0$, i.e. when the measurement is based on only a few of the available zero-crossings of a burst, the cross section tends towards the geometrical cross section of the measuring volume as seen from the flow direction. For finite values of Q (e.g. Q = 0.2 corresponding to 8 periods out of a maximum available of 40) a dead zone occurs as in the tracker case. However, in the counter case the cross section decreases gradually with increasing angle between the x-axis and the flow direction. With the addition of frequency shift the dead zone is moved forward and for a certain amount of shift ($u_s \leq u(1 - Q)$)

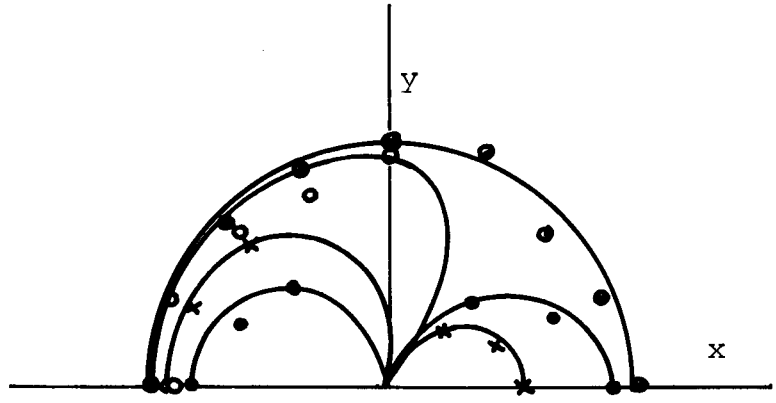

f_s= 10kHz, 100kHz, 1 MHz, 2 MHz

f_D= 1 MHz

Fig. 2.5 Polar diagram of measured data rate as a function of angle between x-axis and $\underline{u}$
Backscatter, = 15°, f = 310 mm.

the dead zone disappears. However, the shift must be appreciably greater than the maximum Doppler frequency before the cross section may be assumed to be equal to the geometrical cross section. Figure 2.4b, c and d show polar diagrams of the cross section with increasing amounts of frequency shift added. Figure 2.5 shows measured values of data rate for the same optical configuration. However the particle distribution for the measured values is not monodisperse, resulting in less pronounced dead angle effects for the measured data.

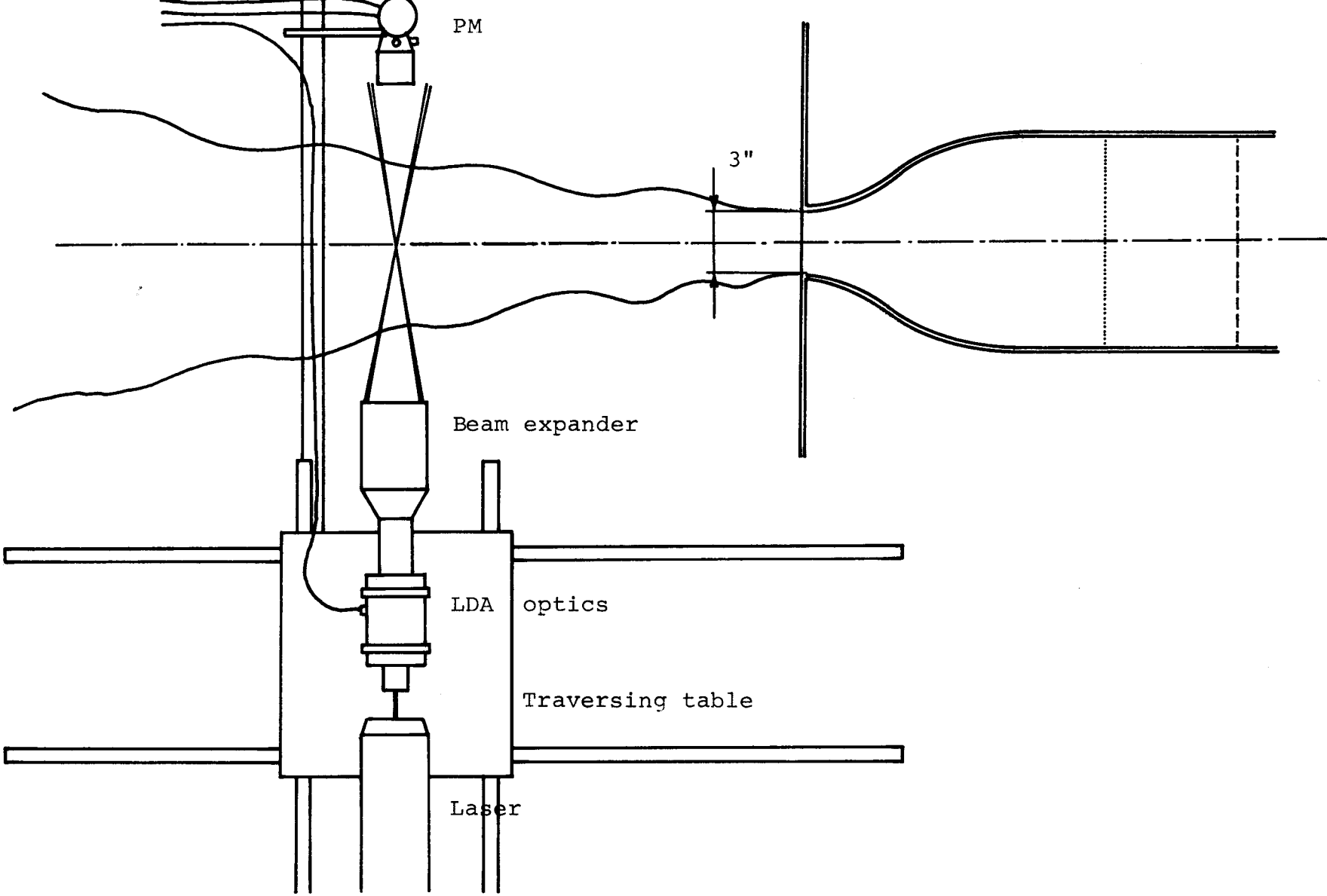

Fig. 3.1 Experimental arrangement.

3. Experiment and Apparatus

3.1 Experimental Set-up

The experimental arrangement with which most of the following measurements were performed is shown in Figure 3.1. The flow is a free jet in air issuing from a 3" diameter nozzle. The air flow is conditioned by passage through a 12" diameter plenum chamber. Swirl is removed by a honeycomb plate and turbulence is reduced by passage through a number of metal screens. The flow is finally accelerated through a 16:1 contraction having an axial profile of matched cubics designed for minimum pressure gradient in order to prevent separation (Morel (1975)).

The LDA optics is a DISA 55X modular optical system with Bragg cell frequency shift capable of operation in both forward and backscatter mode. The optical system is shown in Figure 3.2. In this figure is shown the position of the laser (Spectra-Physics model 124 15 mW He-Ne Laser or in some of the measurements Spectra-Physics model 165 0-5 W Ar-ion Laser). Also shown are the beam splitter modules, the Bragg cell, the backscatter module, the photodetector and the focusing optics. The transmitter optics includes a dual quarter-wave plate, one mounted on the laser and the other on the optical system, which allows rotation of the unit without changing the direction of polarization within the optical unit. The unit also contains the beam waist displacer, which allows the position of the laser beam waist to be adjusted to be coincident with the intersection point, the beam translator, which allows parallel displacement of the outgoing beams and the beam expander, which expands the aperture of the optical system by a factor 1.9. The focusing lens used in most measurements was a 300 mm focal length achromat of 95 mm diameter.

In the forward scatter mode this optical configuration with the

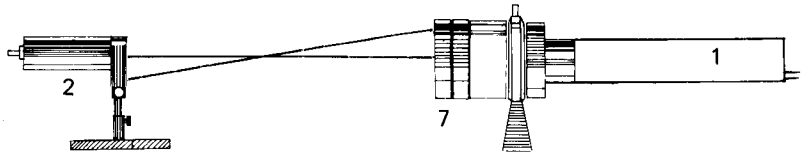

Minimum system

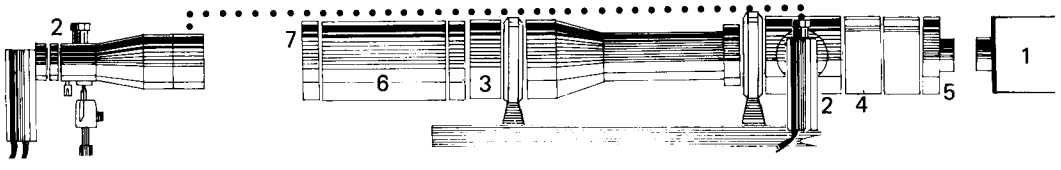

Full configuration

1. Laser
2. Detector (PM)
3. Beam translator
4. Bragg cell
5. Beam waist displacer
6. Beam expander
7. Front lens

Fig. 3.2 Modular LDA optical transducer (DISA 55X-system).

photodetector optics placed at a 30° angle to the optical axis results in a measuring volume approximately 0.1 mm in diameter and 0.3 mm in length located approximately 300 mm from the optical components.

In the backscatter mode the measuring volume is approximately 0.1 mm in diameter and 0.9 mm in length for an intersection angle of 15°.

The entire optical system can be traversed in two directions in the horizontal plane. The environment around the jet and the optical system can be sealed off to allow uniform seeding of the flow field. Droplets of a 50:50 pct. mixture of glycerin and water were used as seeding particles. The seeding generator was a DISA type 55 L 17 aerosol generator with cyclone separator. According to the specifications the particles generated have a size range from 0.5 μ to 5 μ with a peak at 2 μ.

The signal processing equipment is composed of standard DISA LDA components and is shown in Figure 3.3. The rack contains from the top two 55 L 90a counters, a 55 N 10 Frequency Shifter, a 57 G 20 Interface and Buffer, a DEC LSI-11 mini-computer and a DEC DX-11 Dual Floppy Disk System. A block diagram is shown in Figure 3.4. The digital output from the counter is transferred to the Interface and Buffer which handles up to eight parallel 12-bit input words and eight parallel 12-bit output words. Two of the interface output lines are used to communicate with the LSI-11 mini-computer. The computer is controlled through a Beehive B-100 terminal and storage is provided by the DEC DX-11 Dual Floppy Disk System.

The DISA 55 N 10 Dual Channel Frequency Shifter includes a Bragg cell driver operating at 40 MHz and two mixers with variable local oscillators phase locked to the Bragg cell. The resulting frequency shift can be selected individually for each channel from 10 kHz to 10 MHz with

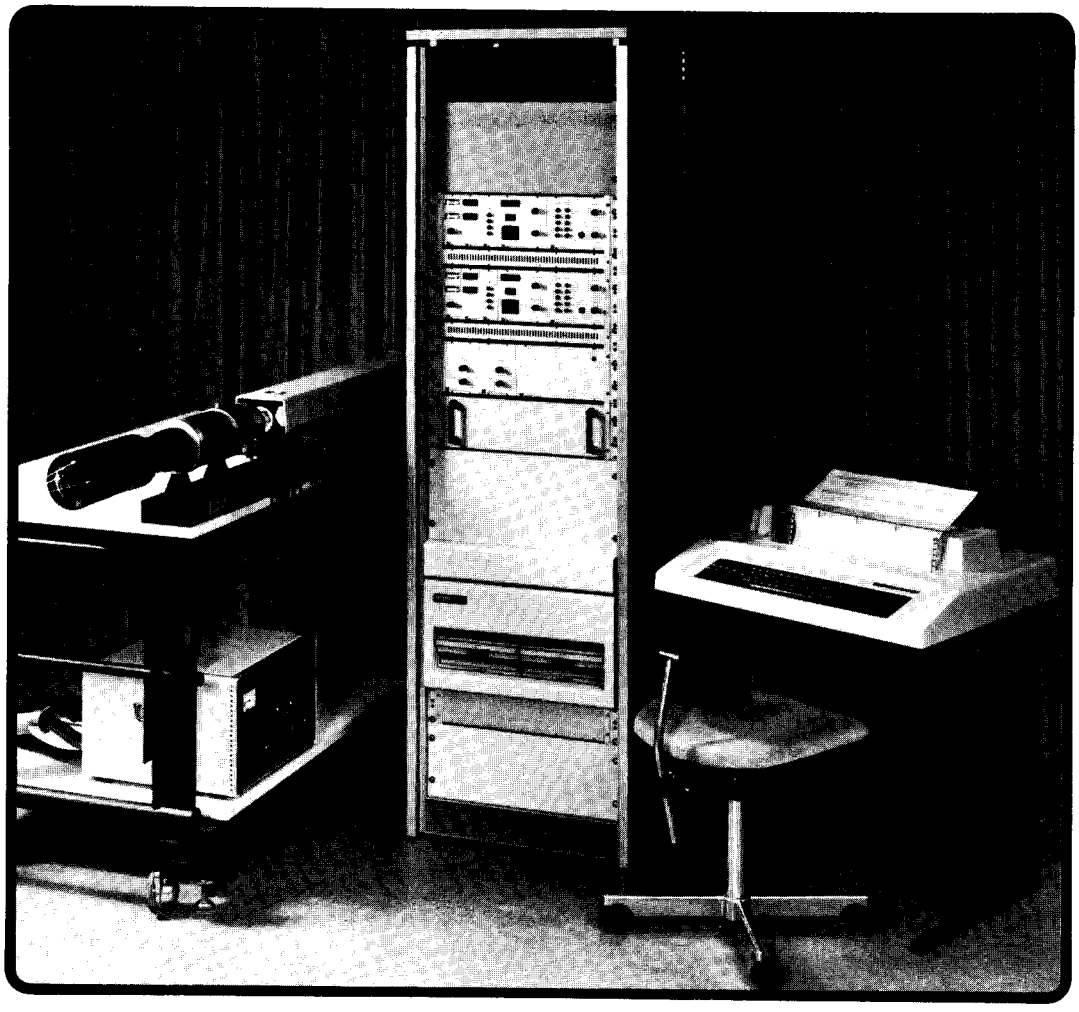

Fig. 3.3 Electronic instrumentation.

Fig. 5. Complete LDA Instrumentation comprising Two-Color Argon-Ion Laser, 55X Two-Color LDA Optics, 55N10 Frequency Shifter, two 55L90a LDA Counters, 57G20 Buffer Interface and Computer with key board terminal.

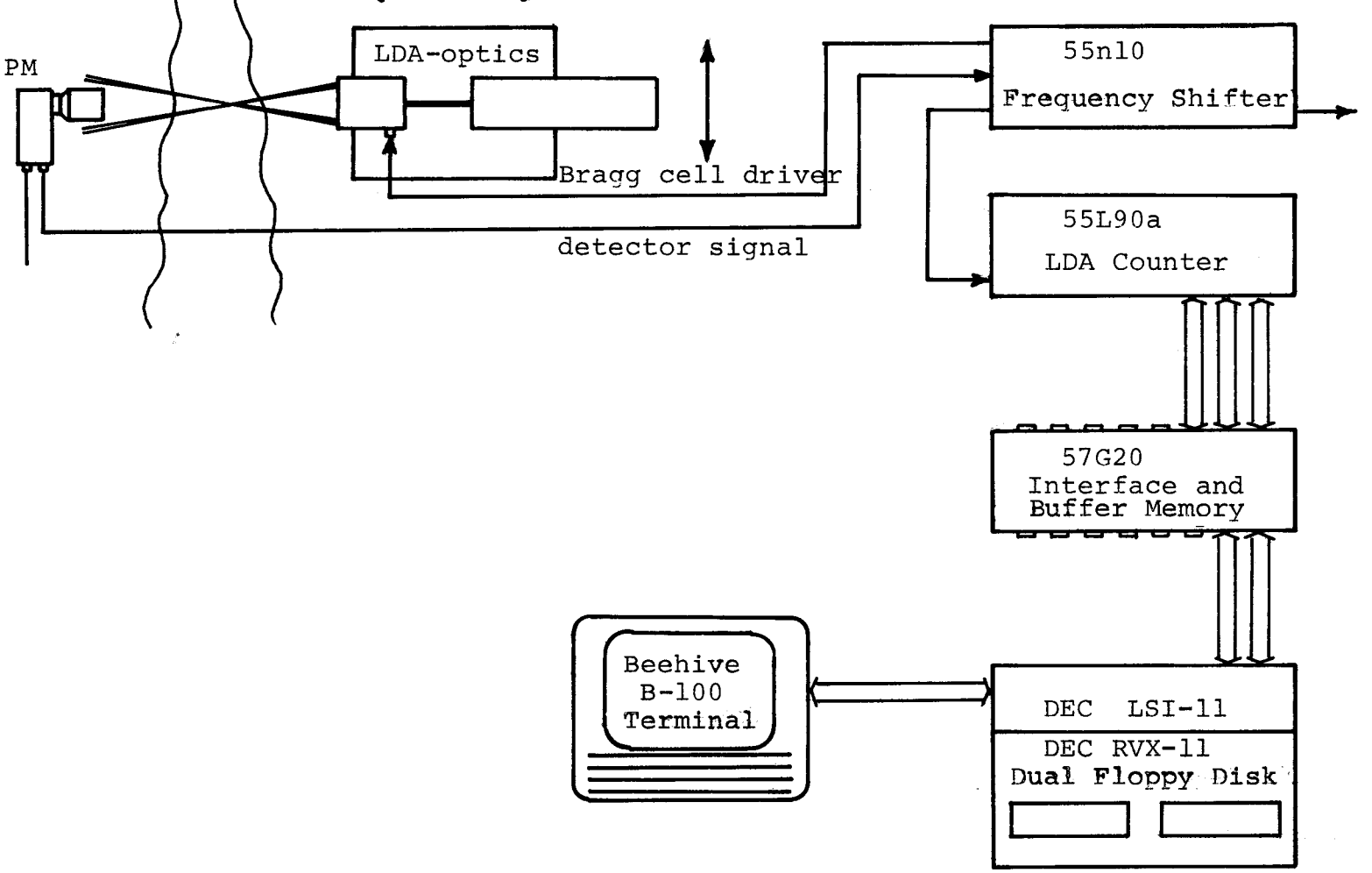

Fig. 3.4 Block diagram of signal processing equipment.

Mode	Name	Number of measurements	Validation	Output
1	Fixed N	Continuous	5:8 + 3	V , T
2	Combined	One per burst	5:8 + 3	V , T , N
3	Varible N	One per burst	3	V , T,, N
4	Time-of-flight	One per pulse pair	2	T

Fig. 3.5 Counter modes.

electronic selection of the sign of the apparent fringe velocity.

The Interface and Buffer contain a backplane with a number of print sockets and can be built up to the required complexity by inserting optional prints. The main ingredient is an input logic and buffer card, which handles incoming data, marks the data words so the source can later be identified, and stores the data in the 512 word SILO-type memory. The buffer can accept asynchronous data with a time spacing of only 1 μs (or by replacement of memory elements with somewhat more expensive, but pin-for-pin compatible chips, a spacing of only 70 ns). A high data reception rate is required by the interface to take advantage of the short time lags inherent in the random sampling of the LDA, especially if more channels are used. The function of the buffer is primarily to allow reception of asynchronous data and subsequent transmission to the computer. The buffer can be expanded if needed by insertion of additional memory cards with no change in logic circuitry. The function of the interface is controlled by the control logic card, and the output demultiplexer card allows communication through the remaining six 12-bit channels (in addition to the two occupied by the computer) for controlling external devices (flow parameters, traversing mechanisms or other).

The LDA-counter mode of operation is an important factor in the data processing and is explained with reference to Figure 3.5. The DISA 55 L 90a counter can operate in four modes of which one (the fourth) is primarily of interest in time-of-flight measurements.

Mode-1 is the most common mode of operation of conventional LDA counters. A measurement is initiated when the signal exceeds the fringe counter Schmidt trigger level. The first zero-crossing enables the counter, and counting of clock oscillator pulses is initiated at the second zero-

crossing if the counter is not reset by an error condition detected by the validation circuits (in which case the counter is immediately reset). The immediate reset allows the highest possible data rate and ensures that a burst is measured even if a fault should occur in the initial phase of the burst.

In mode-1 new measurements continue based on eight zero-crossings throughout the burst as long as Doppler periods exceeding the Schmidt trigger level are available. The measurement is checked by a 5:8 comparator circuit and three other validation schemes (burst amplitude exceeding preset level, measured velocity below preset range minimum and burst envelope dip detected by two-level sequency detector).

Mode-3 bases the measurement on the total number of periods in the burst (from 2 to 256), but outputs only one measurement per burst, and in addition to the velocity output makes available the number of zero-crossings measured per burst, N_z, in binary form at the output. However, in this mode the 5:8 comparison is not active and the counter is thus somewhat more sensitive to noise. The "velocity" output is based on a variable number of zero-crossings and must therefore be "normalized" relative to N_z.

Mode-2 combines the positive features of mode-1 and mode-3. The measurement is still based on eight zero-crossings, the 5:8 comparison is active, but only one measurement is made per burst and the total number of zero-crossings is available at the output. Unless the S/N is high, mode-2 works better than mode-3 which can give many data points based on only 2,3 or a low number of zero-crossings. Mode-3 may be somewhat less sensitive to the angular dependence described earlier in measurements where frequency shift is not used.

In the measurements describer here only mode-2 was employed and variable

frequency shift was always available.

In addition to the burst-type LDA equipment the following instruments were used at one time or another during the measurements: a DISA 55 L 22 Doppler Signal Processor (frequency tracker) with a 55 L 30 Frequency Translation Control Unit, two DISA type 55 M 01 CTA systems with standard 55 L 11 Bridge and a 55 K 10 Linearizers, a TSI type 1076 mean and RMS voltmeter and pressure taps for monitoring of plenum pressure and for use with a pitot tube.

The pressure drop and the measured mean velocity at the jet exit (with LDA methods) was stable within 1% during a full day's measurements. The turbulence level at the jet exit was not particularly low (of the order of 1% RMS), but this was not considered important in view of the purpose of the measurement, which was to study the data processing of LDA counter data in the high intensity turbulence of the fully developed jet.

4. Data Processing of Burst-type LDA Data

4.1 Particle Arrival Distribution and the Concept of Bias

Burst type LDA data are characterized by their random sampling-times. Data is only collected during a particle traversal of the measuring volume. In burst processing it is usually assumed that the seeding particle concentration is so low that the probability of two or more particles in the measuring volume at any one time is negligible. Thus the measured function is a highly intermittent series of data points, most often a direct digital output, and no real time signal is available.

As we shall see, however, even for average sampling rates far below the Nyquist rate it is possible to reconstruct all the basic statistical parameters of the flow such as moments, autocorrelation function and spectrum. The sampling method inherent in the burst-type LDA is in some ways advantageous: spectral aliasing is removed, some noise sources can be eliminated, relatively modest amounts of data points are used, and unique possibilities exist for conditional sampling.

With statistically uniform particle distribution in space and for constant flow velocity the distribution of particle arrival times is Poisson (equivalent to a shot noise process). However, fluctuations in particle velocity and direction of motion modify this basic distribution and the resulting distribution is <u>not</u> Poisson, but a weighted integral (the Mandel distribution):

$$P_M(n,T) = \int \frac{u^n}{n!} e^{-u} P(u)du \qquad (4.1.1)$$

where $P_M(n,T)$ is the probability of arrival of n particles in time T, $P(n,T) = (u^n/n!)e^{-u}$ is the regular Poisson distribution, and P(u) is the probability distribution for the process modulating the particle arrival rate. The Mandel distribution is known from photon counting spectroscopy

(see e.g. Mehta (1970)),but no generally applicable method exists for finding $P(u)$ from $P_M(n,T)$.

The variations in particle arrival rate result in errors if direct arithmetic averaging is applied to the sampled data. This in turn has led to the concept of biasing as a measure of the error in the computed statistical parameters. Various sources of bias exist. The correlation between flow velocity and sampling rate leads to the so-called velocity bias. Correlations between sampling rate and direction of flow may be termed directional bias. Bias may also result from density fluctuations, variations in particle concentration because of non-uniform seeding, mixing processes, combustion, etc. Bias may also be introduced due to electronic imperfections such as non-uniform filter characteristics, poor signal-to-noise ratio, etc. However, it must be emphasized that bias is not an inherent property of burst-type LDA's, but only a result of improper data processing. As we shall see, bias free processing of burst-type LDA data from uniformly seeded, incompressible flow is straightforward when directional bias is removed and when the so-called residence time --the time spent in the volume-- is measured and used as a weighting function.

4.2 Representation of the Burst-Type Signal

The representation of the signal and the following derivation is similar to the one used by George (1976) for LDA signals with the exception of the representation of the measuring volume and the form of the function g, which represents the statistics of the particle distribution.

The measured velocity $u_0(t)$ is written:

$$u_0(t) = \int u(\underline{a},t)\, W(\underline{x}(\underline{a},t))g(\underline{a})d^3\underline{a} \qquad (4.2.1)$$

$W(\underline{x})$ is a weighting function, which in essence defines the measuring volume, $u(\underline{a},t)$ is the (Lagrangian) velocity of the particle with initial position $\underline{a}$, $g(\underline{a})$ is a function describing the initial distribution of particles (e.g. a distribution of Dirac functions).

A measurement with the burst processor is initiated when the signal exceeds the trigger level (i.e. when the particle enters the measuring volume as defined above) and the measurement is concluded when the signal again drops below the level. Thus a reasonable form of W is

$$W(\underline{x}) = \begin{cases} 1 \text{ when the particle is in the volume} \\ 0 \text{ when the particle is outside} \end{cases} \qquad (4.2.2)$$

$u_0(t)$ then reproduces the velocity of individual particles, but only when they are in the volume. A typical $u_0(t)$ is shown in figure 4.1. The dotted line represents the velocity at the center of the volume.

Mapping from the Lagrangian to the Eulerian frame we can write:

$$u_0(t) = \int u(\underline{x},t)\ W(\underline{x})\ \ g_1(\underline{x},t)d^3\underline{x} \qquad (4.2.3)$$

where

$$\underline{x} = \underline{a} + \int_0^t \underline{u}(\underline{a},t)dt \qquad (4.2.4)$$

and

$$g(\underline{a}) \rightarrow g_1(\underline{x},t) \qquad (4.2.5)$$

The statistics of $g_1(\underline{x},t)$ are important for the properties of u_0. If we assume incompressibility and that the particles completely follow the flow (i.e. do not agglomorate, migrate sideways in gradients etc.) we may assume that the statistics of g_1 are the same as that of g, i.e. that the particle distribution does not change with time.

In Appendix II the first and second moments of g_1 are shown to be given by:

$$\overline{g_1(\underline{x},t)} = \mu \qquad (4.2.6)$$

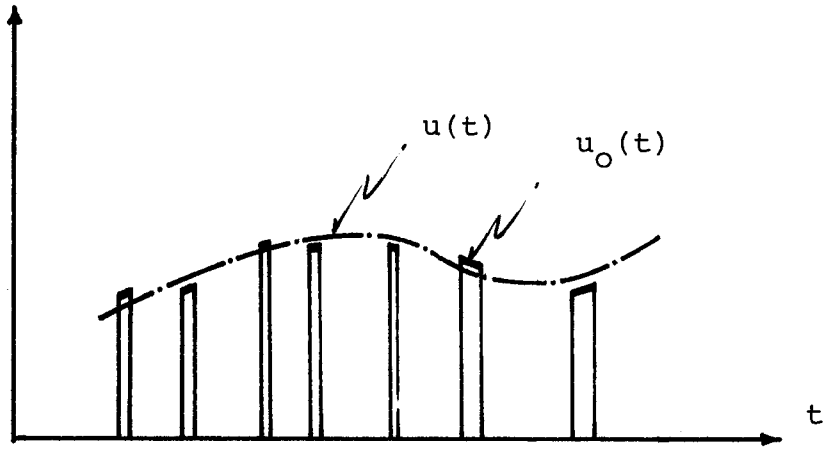

Fig. 4.1 The signal $u_o(t)$ measured by a burst-type LDA.

$$\overline{g_1(\underline{x},t)g_1(\underline{x}',t')} = \mu P(\underline{x},t|\underline{x}',t') + \mu^2 \qquad (4.2.7)$$

where $P(\underline{x},t|\underline{x}',t')$ is the probability that the particle at $\underline{x}$ at time t has moved to $\underline{x}'$ at time t', and μ is the expected number of particles per unit volume. For small times, a good approximation to $P(\underline{x},t\,|\underline{x}',t')$ is:

$$P(\underline{x},t|\underline{x}',t') \simeq \delta(\underline{x}'-\underline{x} - \overline{\underline{u}}\tau) \qquad (4.2.8)$$

where

$$\tau \equiv t'-t.$$

4.3 Mean Values

The average of $u_0(t)$ is given by:

$$\overline{u_0(t)} = \int \overline{u(\underline{x},t)}\, W(\underline{x})\, \overline{g_1(\underline{x},t)}\, d^3\underline{x} \qquad (4.3.1)$$

$$= \mu \int \overline{u(\underline{x},t)}\, W(\underline{x})\, d^3\underline{x} \qquad (4.3.2)$$

The measured velocity is thus a weighted average of the mean velocity within the measuring volume.

If we separate the velocity into mean and fluctuating parts and furthermore decompose the mean value into the value at $\underline{x}_0$, the center of the measuring volume, and a deviation from that value, Δu, we may write:

$$u(\underline{x},t) = \overline{u(\underline{x},t)} + u'(\underline{x},t)$$

$$= \overline{u}(\underline{x}_0) + \Delta\overline{u}(\underline{x}) + u'(\underline{x},t) \qquad (4.3.3)$$

Thus

$$\overline{u_0(t)} = \mu\overline{u}(\underline{x}_0) \int W(\underline{x})d^3\underline{x} + \mu \int \Delta u(\underline{x})\, W(\underline{x})d^3\underline{x} \qquad (4.3.4)$$

If furthermore we assume a weighting function of the form eq. (4.2.2) we get:

$$\overline{u_0(t)} = \mu V\, \overline{u}(\underline{x}_0) + \mu \int_{M.V.} \Delta u(\underline{x})d^3\underline{x} \qquad (4.3.5)$$

where the integral is over the measuring volume. Only if the $\Delta\overline{u}(\underline{x})$ is symmetric is the measured velocity equal to the velocity at the center of the measuring volume. In the simple case where we may assume uniform velocity within the measuring volume we find:

$$\overline{u_0(t)} = \mu V \, \overline{u(\underline{x}_0,t)} \tag{4.3.6}$$

We may also define the point of measurement $\underline{x}_0$ from the condition $\int_{M.V.} \Delta\overline{u}(\underline{x})d^3\underline{x} = 0$. The measuring point is then no longer at the center of the volume, but (4.3.6) holds exactly and the expresion for the extra mean square value due to mean gradients within the measuring volume (eq. 4.4.5) is simplified.

Thus the measured mean value is directly proportional to the desired Eulerian mean. However it must be emphasized that $\overline{u_0(t)}$ is arrived at by measuring $u_0(t)$ during all the time a particle is in the measuring volume. This is not the same as a simple average of all realizations.

To see this let us assume we form the averages by integration over a time T. There is then a simple relationship between the time average of $u_0(t)$ and that of $u(\underline{x}_0,t)$. Using eq. (4.3.6) we find:

$$\overline{u_0(t)} \simeq \frac{1}{T}\int_0^T u_0(t)dt = \mu V \, \overline{u(\underline{x}_0,t)}$$

or

$$\overline{u(\underline{x}_0,t)} \simeq \frac{1}{\mu VT}\int_0^T u_0(t)dt \tag{4.3.7}$$

But μVT is (with the previous assumptions on particle density) exactly the fraction of time a particle is in the volume, and in which $u_0(t)$ is non-zero. Thus the correct mean is given by averaging only during those periods where there is a signal.

Most burst-processors measure the average velocity during a particle

traversal. This implies that the velocity must be approximately constant during a burst. If there is only a single output during each burst, the time integral (4.3.6) can be approximated by:

$$\overline{u(\underline{x}_o,t)} \simeq \frac{1}{\mu VT}\int_0^T u_o(t)dt \simeq \frac{\sum_i u_o(t_i)\Delta t_i}{\sum_i \Delta t_i} \qquad (4.3.8)$$

where $u_o(t_i)$ is the i_{th} realization of the velocity (at time t_i) and Δt_i is the time the i^{th} particle spends in the volume, the residence time. Thus the correct time average can be formed by measuring both the velocity and the residence time and forming the weighted sum (eq. 4.3.8) - the so-called residence time weighting.

4.4 Mean Square Value

Squaring and averaging the expression for the measured velocity (eq. 4.2.3) we obtain:

$$\overline{u_o(t)\,u_o(t')} = \iint \overline{u(\underline{x},t)u(\underline{x}',t')\,W(\underline{x})\,W(\underline{x}')} \cdot \overline{g_1(\underline{x},t)\,g_1(\underline{x}',t')}\,d^3\underline{x}\,d^3\underline{x}' \qquad (4.4.1)$$

We first consider the case $t = t'$ for which $P(\underline{x},t|\underline{x}',t') = \delta(\underline{x} - \underline{x}')$ (eq. 4.2.8). This corresponds to the measured mean square velocity. Inserting we find:

$$\overline{[u_o(t)]^2} = \mu \int \overline{[u(\underline{x},t)]^2}\,W^2(\underline{x})d^3\underline{x} + (\text{terms of order } (\mu V)^2) \qquad (4.4.2)$$

Due to our assumptions on low particle concentration the second term is negligible compared to the first. (Note that the reverse was true for the continuous LDA, where the first term was negligible compared to the second, cf. George and Lumley, 1973.)

Separating again into mean and fluctuating components, and considering again the mean velocity as composed of the mean velocity at the center $\bar{u}(\underline{x}_0)$ and a deviation away from the center $\Delta\bar{u}(\underline{x})$ we find:

$$\overline{[u_0(t)]^2} = \mu \int \overline{[u'(\underline{x},t)]^2}\, W^2(\underline{x})d^3\underline{x} + \mu \int [\Delta\bar{u}(\underline{x})]^2 W^2(\underline{x})d^3\underline{x}$$

$$+ 2\mu\, \bar{u}(\underline{x}_0) \int \Delta\bar{u}(\underline{x})W^2(\underline{x})d^3\underline{x} + [\bar{u}(\underline{x}_0)]^2 \int W^2(\underline{x})d^3\underline{x} \qquad (4.4.3)$$

Assuming again $W(\underline{x})$ to be given by eq. (4.2.2) we find:

$$\overline{[u_0(t)]^2} = \mu \int_{M.V.} \overline{[u'(\underline{x},t)]^2 d^3\underline{x}} + \mu \int_{M.V.} [\Delta\bar{u}(\underline{x})]^2 d^3\underline{x}$$

$$+ 2\mu\, \bar{u}(\underline{x}_0) \int_{M.V.} \Delta\bar{u}(\underline{x})d^3\underline{x} + \mu V[\bar{u}(\underline{x}_0]^2 \qquad (4.4.4)$$

The measured mean square is thus a spatial average over the measuring volume of the actual mean square plus two noise terms caused by gradients within the volume. The last term is due to the intermittent nature of the u_0 signal.

With the definition of the measuring point given in Section 4.3.6 the third term disappears and the fourth term is just the square of the mean measured when a particle is in the volume. Thus

$$\overline{u_0'^2} \equiv \overline{[u_0(t)]^2} - \mu V[\bar{u}(x_0)]^2$$

$$= \mu \int_{M.V.} \overline{[u'(\underline{x},t)]^2} d^3x + \mu \int_{M.V.} [\Delta\bar{u}(\underline{x})]^2 d^3\underline{x} \qquad (4.4.5)$$

We see that the measured mean square velocity is always increased when mean gradients of velocity are present within the measuring volume.

As in the case of mean values we can show the equivalence between the mean square time average and the residence time weighted mean square

when the velocity can be considered uniform across the measuring volume:

$$\overline{[u'(\underline{x}_o)]^2} \simeq \frac{1}{\mu VT}\int_0^T u_o'^2\, dt \simeq \frac{\sum_i [u_o(t_i) - \bar{u}\,]^2\, \Delta t_i}{\sum_i \Delta t_i} \qquad (4.4.6)$$

4.5 Correlation Function

We now investigate the covariance function eq. (4.4.1) for $t \neq t'$. Applying eqs. (4.2.6), (4.2.7) and (4.2.8) we find

$$\overline{u_o(t)u_o(t+\tau)} = \mu\iint \overline{u(\underline{x},t)u(\underline{x}',t')}\; W(\underline{x})W(\underline{x}') \cdot \delta(\underline{x}'-\underline{x}-\bar{\underline{u}}\tau)d^3\underline{x}d^3\underline{x}' \qquad [I(\tau)] \qquad (4.5.1)$$

$$+ \mu^2\iint \overline{u(\underline{x},t)u(\underline{x}',t')}\; W(\underline{x})W(\underline{x}')d^3\underline{x}d^3\underline{x}' \qquad [II(\tau)]$$

In the following, the first term is denoted $I(\tau)$ and the second $II(\tau)$. It will now be shown that the first term is a noise term generated by the intermittent nature of the signal $u_o(t)$, whereas the second term represents the desired information.

Consider the term $I(\tau)$. Integrating once we get:

$$I(\tau) = \mu\int \overline{u(\underline{x},t)u(\underline{x}+\bar{\underline{u}}\tau,t+\tau)}\; W(\underline{x})W(\underline{x}+\bar{\underline{u}}\tau)d^3\underline{x} \qquad (4.5.2)$$

We have a spatial average over the overlap of the measuring volume with itself at a (averaged) position time τ earlier.

If we can assume uniform velocity within the volume the expression simplifies to:

$$I(\tau) = \mu V\overline{[u(\underline{x}_o,t)]^2}\;\rho_1(\tau) \qquad (4.5.3)$$

where

$$V\rho_1(\tau) \equiv \int W(\underline{x})W(\underline{x}+\bar{\underline{u}}\cdot\tau)d^3\underline{x} \qquad (4.5.4)$$

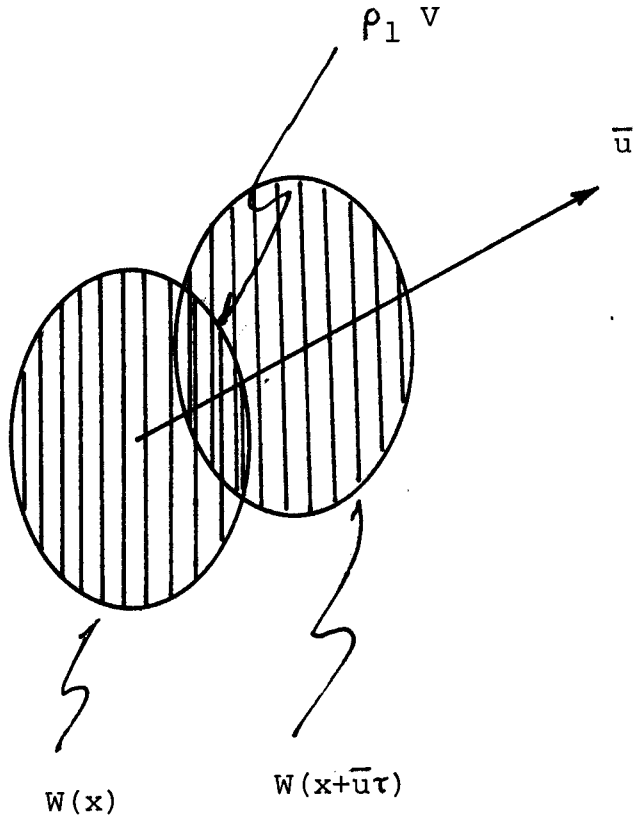

Fig. 4.2 Overlap volume equal to $V\rho_1$.

or using eq. (4.2.4) for $W(\underline{x})$:

$$V\rho_1(\tau) = \int_{\text{M.V. overlap}} d^3\underline{x} \tag{4.5.5}$$

which is just the overlap-volume between the measuring volume at times t and $t+\tau$. Thus the function $\rho_1(\tau)$ is a function of unity height at $\tau = 0$ which falls off to zero within a time corresponding to the mean transit time of a particle through the measuring volume. (Fig. 4.2)

Since LDA burst processors normally require a time of the order of a transit time to process the measured signal, it is normally assumed that the minimum scales of interest in a measurement are greater than the measuring volume dimensions and that no significant change occurs in the flow velocity within a time of the order of the transit time. Thus the first term in eq. (4.5.1) does not contain any information of interest, but only adds noise if kept in the correlation function. The effect on the corresponding spectrum would be the addition of a wide band, constant noise level of high intensity. Fortunately, as we shall see later it is simple to avoid this noise by not including self-product terms in the algorithms for correlation function and spectra.

We now consider the second term in eq. (4.5.1) Decomposing the velocity into mean and fluctuating parts yields:

$$\begin{aligned} II(\tau) = {} & \mu^2 \iint \overline{u}(\underline{x})\overline{u}(\underline{x}')\, W(\underline{x})W(\underline{x}')d^3\underline{x}d^3\underline{x}' \\ & + \mu^2 \iint \overline{u'(\underline{x},t)u'(\underline{x},t')}\, W(\underline{x})W(\underline{x}')d^3\underline{x}d^3\underline{x}' \end{aligned} \tag{4.5.6}$$

The first term is precisely the square of the volume-averaged mean velocity given in eq. (4.3.2) and the second represents the volume-averaged space-time correlation. If we assume uniform velocity within

the measuring volume we can write:

$$II(\tau) = \bar{u}_o^{\,2} + (\mu V)^2 B_v(\tau) \tag{4.5.7}$$

where

$$V^2 B_v(\tau) = \iint \overline{u'(\underline{x},t)u'(\underline{x},t')}\, W(\underline{x})W(\underline{x}')d^3\underline{x}d^3\underline{x} \tag{4.5.8}$$

is the volume-averaged correlation.

Assuming as before the form eq. (4.2.2) for $W(\underline{x})$ we find:

$$V^2 B_v(\tau) = \iint_{M.V.} \overline{u'(\underline{x},t)u'(\underline{x}',t')}d^3\underline{x}d^3\underline{x} \tag{4.5.9}$$

where the integrals are over the measuring volume.

In summary, $I(\tau)$ represents the autocovariance function for the signal while one particle traverses the measuring volume; $II(\tau)$ is the covariance between two different particles, not simultaneously present within the volume. In view of our usual presumption that $u(\underline{x},t)$ does not change appreciably within the transit time it is clear that $I(\tau)$ represents a noise term primarily caused by the intermittency of the $u_o(t)$ signal. This noise can be eliminated by considering only correlations between the signal from two different particles, i.e. the term $II(\tau)$.

Now let us consider the influence of velocity gradients within the measuring volume on the covariance $II(\tau)$.

Again we consider the mean velocity $\bar{u}(\underline{x}_o)$ at a fixed point $\underline{x}_o$ within the volume and the deviation of the mean velocity $\Delta\bar{u}(\underline{x})$. If we use the previous definition of the measuring point, we have the condition:

$$\int \Delta\bar{u}(\underline{x})\, W(\underline{x})d^3\underline{x} = 0 \tag{4.5.10}$$

The first term of II (τ) now becomes:

$$\mu^2 \iint \overline{u}\,(\underline{x})\overline{u}(\underline{x}')W(\underline{x})W(\underline{x}')d^3\underline{x}d^3\underline{x}'$$

$$= \mu^2 \iint [\overline{u}(\underline{x}_0)+\Delta\overline{u}(\underline{x})][\overline{u}(\underline{x}_0')+\Delta\overline{u}(\underline{x}')]W(\underline{x})W(\underline{x}')d^3\underline{x}d^3\underline{x}' \qquad (4.5.11)$$

But this is equal to:

$$= \mu^2 \int [\overline{u}(\underline{x}_0)+\Delta\overline{u}(\underline{x})]W(\underline{x})d^3\underline{x} \cdot \int [\overline{u}(\underline{x}_0')+\Delta\overline{u}(\underline{x}')]W(\underline{x}')d^3\underline{x}'$$

$$= \mu^2 V^2[\overline{u}(\underline{x}_0)]^2 \qquad (4.5.12)$$

Thus, if we define the measuring volume as done above, mean velocity gradients within the volume do not contribute any noise to the autocovariance function. We can subtract the square of the mean velocity at $\underline{x}_0$ from both sides of eq. (4.5.7) and obtain the (volume averaged) autocorrelation function of $u'(\underline{x},t)$ without gradient noise.

To find the autocovariance function expressed by the measured velocity samples $u(t_i)$ and residence times Δt_i we proceed as before. We replace the ensemble averages by time averages and obtain:

$$\overline{u'(\underline{x}_0,t)u'(\underline{x}_0,t')} = \frac{1}{(\mu V)^2}\overline{u_0'(t)u_0'(t')}$$

$$= \frac{1}{(\mu V)^2 T}\int_0^T u_0'(t)t_0'(t')dt \qquad (4.5.13)$$

or

$$\overline{u'(\underline{x}_0,t)u'(\underline{x}_0,t+\tau)} = \frac{1}{(\mu V)^2 T}\int_0^T u_0'(t)u_0'(t+\tau)dt \qquad (4.5.14)$$

From the intermittent nature of the signal $u_0(t)$ we know that $u_0(t)$ is only non-zero, when a particle is within the measuring volume as defined previously. Thus the integral eq. (4.5.14) is only non-zero when there is a particle in the volume at t and one at $t+\tau$. If we consider

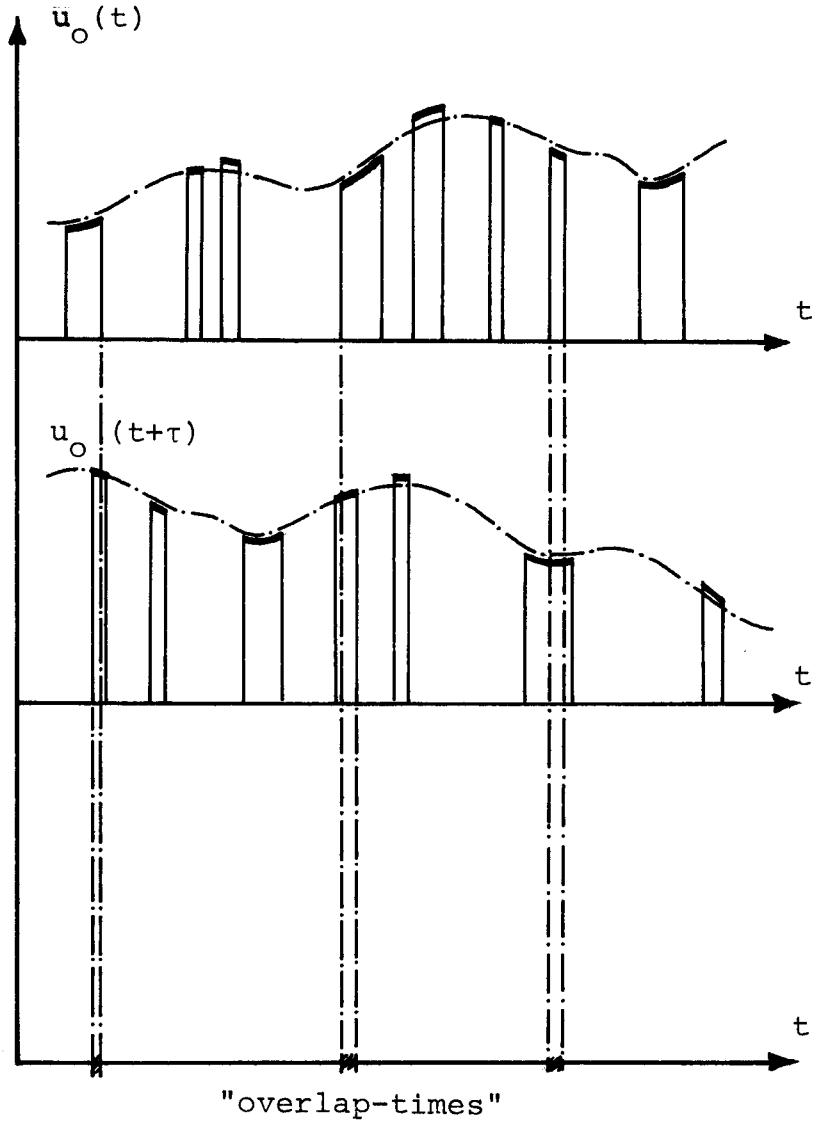

Fig. 4.3 "Overlap-times" for realizations of $u_o(t)$ and $u_o(t+\tau)$.

figure 4.3, which shows the signal $u_o(t)$ and a signal $u_o(t+\tau)$ displaced in time by the lag τ,we see that the integral should only be computed during the time of overlap of realizations of $u_o(t)$ and $u_o(t+\tau)$. Thus we may write:

$$C(\tau) \equiv \overline{u'(\underline{x}_o,t)u'(\underline{x}_o,t')} \simeq \frac{1}{(\mu V)^2 T} \sum_{i\neq j} u_o'(t_i)u_o'(t_j)\, \Delta t_{ij}(\tau) \tag{4.5.15}$$

where $\Delta t_{ij}(\tau)$ are the "overlap-times", i.e. the times where $u_o(t)$ and $u_o(t+\tau)$ are both non-zero, and $\tau = t_j - t_i$. The factor $(\mu V)^2 T$ is the total fraction of the time T one particle is in the measuring volume and another is in the volume at $t+\tau$:

$$(\mu V)^2 T = \left(\frac{\Sigma \Delta t_i}{T}\right)^2 \cdot T \tag{4.5.16}$$

However, since we have excluded the possibility of two particles in the measuring volume simultaneously, a more correct expression for the total overlap-time is:

$$\sum_{i\neq j} \Delta t_{ij}(\tau) = \left[\left(\frac{\Sigma \Delta t_i}{T}\right)^2 - \sum_i \left(\frac{\Delta t_i^2}{T}\right)\right] \cdot T = \frac{1}{T} \sum_{i\neq j} \Delta t_i \Delta t_j \tag{4.5.17}$$

The expression (4.5.15), which is still a function of τ albeit a discontinuous one, is impractical because its implementation would not only require storage of velocity, residence time and time of occurrence for each realization, but also computation of the overlap-time $\Delta t_{ij}(\tau)$ for each value of τ.

It is more practical to form discrete estimates of $C(\tau)$ corresponding to the actually occurring pairs of samples $u_i' \equiv u_o'(t_i)$ and $u_j' \equiv u_o'(t_j)$ and assign those to the lag value $\tau_{ij} = t_j - t_i$. Each sample must be assigned a weight factor according to its "integrated overlap-time" when used in

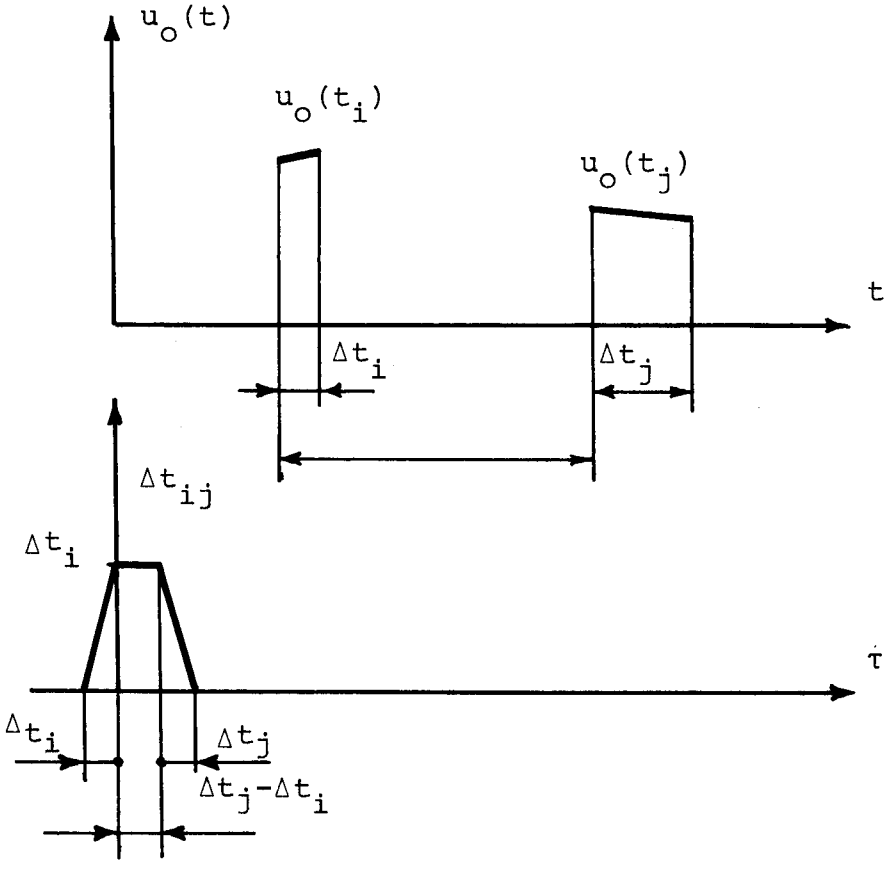

Fig. 4.4 "Overlap-time", Δt_{ij}, for realizations $u_o(t_i)$ and $u_o(t_j)$ as a function of τ.

ensemble averages.

For computational purposes it is practical to collect realizations of the autocovariance function with lags within a given time-slot:

$$C(n\Delta\tau) = \frac{1}{\Delta\tau} \int_{(n-1/2)\Delta\tau}^{(n+1/2)\Delta\tau} C(\tau)d\tau$$

$$= \frac{1}{\Delta\tau} \frac{T}{\sum_{i\neq j} \Delta t_i \Delta t_j} \int_{(n-1/2)\Delta\tau}^{(n+1/2)\Delta\tau} \sum_{i\neq j} u_i u_j \Delta t_{ij}(\tau)d\tau \qquad (4.5.18)$$

The overlap-time is a simple function of τ as shown in figure 4.4, and the integral is easily evaluated:

$$\int \Delta t_{ij}(\tau)d\tau = \Delta t_i \Delta t_j \qquad (4.5.19)$$

Thus

$$C(n\Delta\tau) = \frac{T}{\Delta\tau} \frac{\sum_{i\neq j} u_i u_j \Delta t_i \Delta t_j}{\sum_{i\neq j} \Delta t_i \Delta t_j} \qquad (4.5.20)$$

for

$$(n-\tfrac{1}{2})\Delta\tau < t_j - t_i \leq (n+\tfrac{1}{2})\Delta\tau$$

$\Delta t_i \Delta t_j$ can be considered weighting factors which must be assigned to the cross product $u_i u_j$ in the formation of the autocovariance estimate just as Δt_i can be considered a weighting factor in the formation of ensemble averages of functions of a single variable, i.e.:

$$\overline{f(u)} = \frac{\sum_i f(u_i)\Delta t_i}{\sum \Delta t_i} \qquad (4.5.21)$$

4.6 Spectral Estimators

The spectrum of the function $u_o(t)$ is defined by $S_{u_o}(\omega) = \overline{|\hat{u}_o(\omega)|^2}$ where $\hat{u}_o(\omega)$ is the Fourier transform of $u_o(t)$:

$$\hat{u}_o(\omega) = \frac{1}{2\pi}\int_{-\infty}^{\infty} u_o(t)e^{i\omega t}dt \tag{4.6.1}$$

Thus

$$S_{u_o}(\omega) = \frac{1}{(2\pi)^2}\iint_{-\infty}^{\infty} \overline{u_o(t)u_o(t')}e^{i\omega(t-t')}dt\,dt' \tag{4.6.2}$$

It is well known that by changing variables and carrying out partial integration this can be shown to be equivalent to the Fourier transform of the autocovariance function (the Wiener-Khinchine theorem):

$$S_{u_o}(\omega) = \frac{1}{(2\bar{u})^2}\int_{-\infty}^{\infty} C(\tau)\, e^{i\omega t}dt \tag{4.6.3}$$

As shown in the previous section, use of the representation (4.2.3) for the measured velocity leads to the expression $\mu^2V^2B_v(\tau)$ for the autocovariance function of the velocity (eg.(4.5.9)). Thus we can form a spectral estimator from the autocovariance samples (4.5.15) by inserting into eq. (4.6.3):

$$\hat{S}_1(\omega) = \frac{T}{2\pi\sum_{i\neq j}\Delta t_i\Delta t_j}\int_{-\infty}^{\infty} u_iu_j\Delta t_{ij}(\tau)\cos(\omega(t_j-t_i))d\tau \tag{4.6.4}$$

Integrating the overlap times as in (4.5.20) we get

$$\hat{S}_1(\omega) = \frac{T}{2\pi\sum_{i\neq j}\Delta t_i\Delta t_j}\sum_{i\neq j} u_i\Delta t_iu_j\Delta t_j\cos(\omega(t_j-t_i)) \tag{4.6.5}$$

This spectral estimator is analogous to the usual Blackman-Tukey estimator in usual equidistant sampling power spectrum computations. However, it is important to note that no self-products occur in eqs. (4.6.4) and (4.6.5)

By simply rewriting the exponential form of the cosine and rearranging terms this can be shown to be equivalent to an expression analogous to the classical periodogram minus the d.c. spike at the origin:

$$\hat{S}_2(\omega) = \frac{T}{2\pi[(\sum_i \Delta t_i)^2 - \sum_i (\Delta t_i)^2]}\left[\left|\sum_i u_i \Delta t_i e^{i\omega t_i}\right|^2 - \sum_i (u_i \Delta t_i)^2\right] \tag{4.6.6}$$

As suggested by George (1979), we see that we could have arrived at (4.6.5) by using a special form of the periodogram estimator:

$$\hat{S}_2(\omega) = \frac{\left|\hat{u}_{o_T}(\omega)\right|^2}{(\mu V)^2 T} \tag{4.6.7}$$

where $\hat{u}_{o_T}(\omega)$ is a finite time estimate of the direct Fourier transform of $u_o(t)$ given by

$$\hat{u}_{o_T}(\omega) = \frac{1}{2\pi}\int_0^T u_o(t)\, e^{i\omega t}\, dt \simeq \frac{1}{2\pi}\sum u_i \Delta t_i e^{i\omega t_i} \tag{4.6.8}$$

Substituting into eq. (4.6.7) and ignoring self-products for the same reason The direct estimate of the Fourier transform of the velocity can be of interest in its own right. Estimator (4.6.6) requires only a single summation compared to the double sum in (4.5.20) or (4.6.5), but requires evaluation of both sin- and cos-functions. Which method is best still needs to be evaluated.

The properties of purely Poisson sampled time series have been investigated by several authors (see e.g. Gaster and Roberts (1975) and (1977) and Masry and Lui (1976) and Masry (1978)). These investigations show that the estimators $\hat{S}_1(\omega)$ and $\hat{S}_2(\omega)$ are asymptotically unbiased and that the variance is given by:

$$\text{var}[\hat{S}(\omega)] = \left[S(\omega) + \frac{C(0)}{2\pi\nu}\right]^2 \tag{4.6.9}$$

where ν is the average data rate. From (4.6.5) we see that the average sample rate ν must of of the order of the Nyquist rate to avoid excessive increase of the variability of a spectral estimate. Since the residence time weighting reestablishes the properties of the purely Poisson sampled series, it can be expected that the residence time weighted estimators have properties closely related to them. This equivanence was proven by George (1979) who showed that for both residence time weighted autocorrelation and spectral estimators the variance is given exactly by (4.6.5) with ν replaced by the equivalent sampling rate of the burst LDA, which is easily shown to be related to the average residence time by

$$\nu = \frac{\mu V}{\Delta t} \tag{4.6.10}$$

However, the measured residence time is in itself a stochastic variable and it can be expected to add to the variability of the estimates. The influence of the stochastic nature of the measured residence time has not yet been investigated.

In the actual computation of spectra based on the estimators $\hat{S}_1(\omega)$ and $\hat{S}_2(\omega)$, suitable window functions must be introduced to smooth the spectrum thereby reducing the resolution. Block averaging of the spectra of short blocks of the record can be used for the same purpose. The reader is referred to standard texts on spectral estimation and to recent reviews on standard and randomly sampled signal processing by George (1979) and Mayo (1979). Specific examples will be discussed in Chapter 6.

4.7 Bias Correction

It is clear that the method of residence-time weighted data processing developed above provides the correct statistical results, since it was shown to be equivalent to conventional time averages. Thus the concept of bias does not enter at all. However, the method is only correct for uniformly seeded flows of constant, uniform density. It was also assumed that no other sources of bias existed, e.g. directional bias due to the finite fringe number effect or electronic biasing.

The concept of bias in burst-type LDA measurement and methods of bias correction were introduced in 1974, when it became clear that the results of direct arithmetic averaging contained errors, so-called bias errors, especially for measurements in high intensity turbulence. One of the first treatments on the problem was given by McLaughlin and Tiederman (1974), who defined the problem and proposed a method of correction based on the weighting of the measured data, $u_0(t_i)$, with the inverse of the numerical value of the measured velocity component, i.e. with the factors $u_0(t_i)^{-1}$. The algorithms for the computation of mean and mean-square values by this method, from here on termed the one-dimensional or 1-D correction, are:

$$\overline{u(\underline{x}_0)}_{1\text{-}D} = \frac{\sum_i u_0(t_i)|u_0(t_i)|^{-1}}{\sum|u_0(t_i)|^{-1}} \tag{4.7.1}$$

and

$$\overline{[u'(\underline{x}_0)]^2}_{1\text{-}D} = \frac{\sum_i \left[u_0(t_i)-\bar{u}(\underline{x}_0)\right]^2 |u_0(t_i)|^{-1}}{\sum_i |u_0(t_i)|^{-1}} \tag{4.7.2}$$

McLaughlin and Tiederman investigated the accuracy of the 1-D correction by numerical simulation of certain 2-dimensional flow cases.

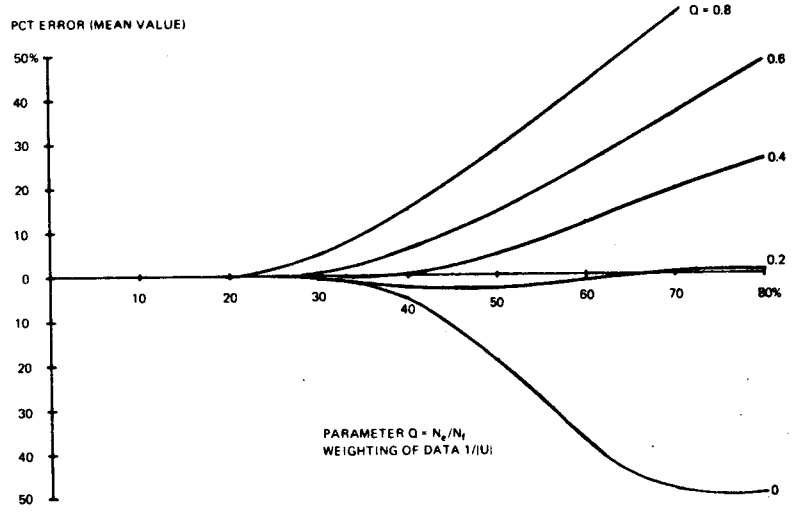

Bias error for 3-D Gaussian velocity distribution including effects of measuring volume cross-section.

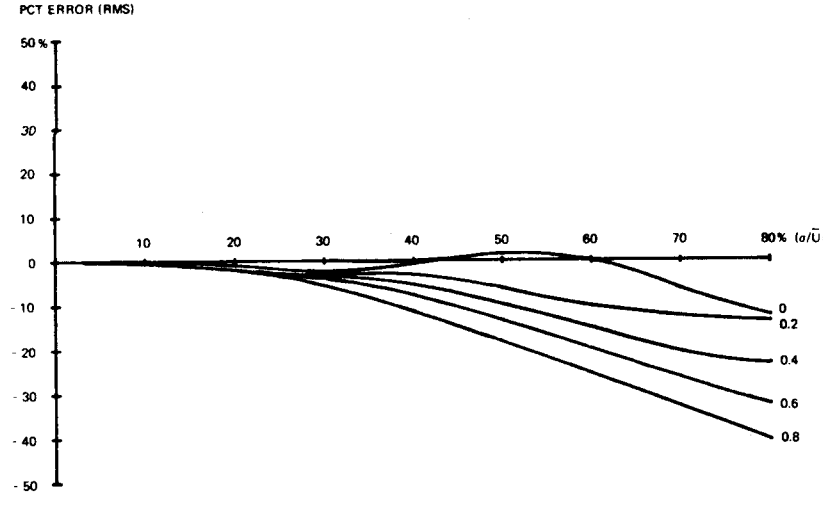

Bias error of r.m.s. velocity for a 3-D Gaussian velocity distribution including effects of measuring volume cross-section.

Figure 4.5 Errors in computed mean and mean-square velocity as a function of turbulence intensity.

However, they did not consider three dimensional cases and did not consider the directional bias due to the finite fringe number effect. Buchhave (1976) investigated the accuracy of 1-D correction data by simulating data from isotropic turbulence, and included the directional bias. It was shown that the 1-D correction over-compensates for the velocity bias and leads to large errors for turbulence intensities above 15-20%. However, the angular bias, which occurs for many types of LDA counters used up to this time, pulls in the other direction, and for some Q-values (c.f. eq. 2.4.2) quite good results may be obtained in certain situations even for turbulence intensities in the order of 50%. Figure 4.5 from Buchhave (1976) shows the errors in computed mean and mean-square values as a function turbulence intensity of an isotropic, Gaussian turbulence superimposed on a constant mean velocity.

The concept of residence-time weighting was discussed for the first time at the 1974 Purdue meeting (see e.g. Durst (1974)). The theory was further developed by George (1976) along the lines presented earlier in this chapter. Hösel and Rodi (1977) also developed the theory from considerations on the average data sampling rate for varying velocities and provided some experimental results to support the theory. Later Erdman and Gellert (1976) studied the correlation between velocity and particle arrival rate and showed results which substantiate the ideas about proportionality between data rate and velocity in one-dimensional flows.

Some investigators, however, report a weaker correlation between velocity and data-rate than expected from the preceeding theory (see e.g. Smith and Meadows (1974)). In these cases electronic noise may have caused secondary effects, since these measurements were made at rather high velocities.

More recent measurements by Karpuk and Tiederman (1976) and Quigley and Tiederman (1977) in the viscous sublayer in pipe flow show good agreement between mean and rms values computed by the 1-D correction method and hot-wire data. The measurements were made with an optical system especially designed to give a probe volume with small spatial dimensions in the direction of the mean velocity gradient. The authors note that the data rate did not seem to be correlated with direction, but unfortunately no details are given on the ratio of the number of fringes needed for operation of the signal processor to the total number available in a burst.

Finally, concerning velocity bias it may be mentioned (as already pointed out by McLaughlin and Tiederman) that in simultaneous measurement of all three velocity components (or in the case of two-dimensional measurements in flows in which the fluctuations in the third direction are negligible) it is of course possible to compute the magnitude of the velocity $\underline{u}_i$ and assign a weighting factor proportional to $|\underline{u}_i|^{-1}$ to each sample set (u_i,v_i,w_i), and even to correct for directional bias based on the knowledge of the direction of $\underline{u}$. Such corrections might be carried out on stored data-points after the measurement, but it appears that this method has not yet been tried in actual measurements.

The question of whether other factors influence the data-rate is still largely unresolved. Tiederman (1977) raised the question of whether differences in signal-to-noise ratio of fast and slow bursts might influence the data rate. Other physical effects that cause correlation between data rate and flow velocity include density variations caused by pressure or temperature fluctuations, mixing of fluids with different particle concentration, and chemical reactions. Asalor and Whitelaw (1976) derived

expressions for the correlation between combustion induced temperature, pressure and concentration fluctuations, and computed the data rate based on assumptions about the velocity-temperature and velocity-pressure correlations in a diffusion flame. From this analysis and subsequent measurements the authors concluded that in this particular flow the bias effects due to velocity fluctuations confirmed the velocity-data rate correlations expected from the residence time analysis and e.g. MacLaughlin and Tiederman's assumptions. Velocity-pressure and velocity-temperature correlation effects were found to be negligible.

George (1976) discusses briefly the extension of the arguments leading to the residence-time weighting to flows with density fluctuations. No previous attempts seem to have been made on weighting or bias-correction in LDA measurements of correlation functions or spectra.

The slotted-time-lag autocovariance method developed by Gaster and Roberts (1975) was simultaneously being developed by Mayo and others (see e.g. Mayo (1974), Smith and Meadows (1974), and Scott (1974). Measurements on the turbulence of a free jet were reported by Smith and Meadows. The basic feasibility of measurements of turbulence power spectra with burst-type LDAs was proven. Later also other measurements were reported (Mayo *et al (1974) and Bouis et al. (1977)). However none of these report any* attempt to consider weighting of the data along the lines discussed above or to correct for biasing. Wang (1976) and Asher, Scott and Wang (1974) discuss various sources of error and noise in LDA-counter measurements of power spectra and conclude that the quantizing of the output from the LDA-counter due to the finite resolution of the counter itself is the greatest source of error. However, these reports did not consider the "apparent turbulence" caused by the finite dimensions of the measuring volume in the

presence of gradients within the volume as described in Chapter 4.5, nor did it consider the biasing effects introduced by using uncorrected data. It should be apparent that bias effects will modify the computed spectra as well as mean and mean square values, and that bias correction methods should be applied to spectral measurements as well.

The theoretical considerations presented earlier indicate that the phenomenon of bias need not exist in the sense that it had been considered here and results only from incorrect signal processing. In the next two chapters we shall consider experimental evidence for the correctness of this theory from the measurements of mean and rms values in the free jet as well as from measurements of autocorrelation functions. We shall also consider those bias correction theories which have been developed for situations where the residence time information is not available.

5. Mean and RMS Velocity Measurements in a Free Jet with Burst-type LDA.

5.1 Purpose and Method

The purpose of this part of the investigation is to test the theory of residence-time weighted burst-type LDA data processing as outlined in the preceeding sections. A fully developed free jet in air was used as a test flow because it provides a stable, self-similar flow phenomenon with easy access for LDA measurements and with easily controlled seeding characteristics. The free jet also provides the high turbulence intensity needed to test the theory. The turbulence intensity relative to the local mean along the jet axis reaches approximately 23 pct. in the fully developed part of the jet beyond x/D = 20 and can exceed 100 pct. off axis. It is a problem with this experiment that no absolute reference for judging the accuracy of the various experimental methods is available. Both conventional experimental methods such as hot-wires or pitot tubes as well as available theoretical models can be expected to contain appreciable errors at the locations in the jet where the various LDA correction methods begin to display significant differences. Thus the results are displayed as comparisons between different experimental methods, and between the LDA data and previously established experimental and theoretical results.

5.2 LDA Measurements

The continuous LDA measurement with a frequency shifted Doppler signal appears to be the method most suited as an experimental standard of reference, at least for mean value measurements. With Doppler signals of good signal-to-noise ratio and low drop-out percentage, and in cases where no significant velocity gradient is present within the measuring volume, the

tracker based LDA should provide an unbiased measurement of the velocity component in the measuring direction of the LDA (see e.g. Edwards et al. (1971), George and Lumley (1973) and Lading and Edwards (1976)). However, because of the large fluctuations relative to the mean and because of the possibility of flow reversals it is necessary to add an amount of frequency shift to the Doppler frequency of about the same magnitude as the Doppler frequency corresponding to the mean velocity at the jet axis.

The LDA tracker is less suited for high frequency, small signal measurements because of the well known ambiguity noise problem (see e.g. George and Lumley (1973) and Berman and Dunning (1974)), and the measured rms and high frequency spectra must be expected to show too high values especially in parts of the flow where the turbulence intensity is relatively low.

It is difficult to provide enough seeding to obtain a sufficiently continuous signal of good signal-to-noise ratio in order to keep the tracker operating well with low drop-out percentage in the highly turbulent flow in the outer part of the jet. At the same time it is desirable to be able to make simultaneous burst-type measurements for comparison. However, it turned out to be possible to use a sufficiently dilute seeding of 2-5 μm size particles from the DISA 55 L 17 aerosol seeding generator to ensure proper burst-type operation and at the same time provide a quasi-continuous signal of sufficient signal-to-noise ratio for continuous tracker operation. This was made possible by the use of two sources of seeding particles: The seeding generator mentioned above to provide relatively large particles for the counter, and another generator which provided a denser smoke of much smaller particles of glycerin vapor from a smoke generator. The high concentration of very small particles allowed the detection of a low level,

continuous signal for the tracker. Only one photodetector was used and the same signal was divided between the two processors, but the tracker was operated with a relatively high gain, whereas the counter was operated with a relatively low gain to ensure that only the larger particles were able to exceed the trigger level of the counter.

The resulting tracker signal enabled the tracker to operate with a drop-out percentage of between 10 and 50 pct., while the counter operated with a data rate between 50 and 200 measurements per second.

The experimental set-up was described in Section 3. The following more specific parameters apply to the mean and rms measurements: The optical configuration was a dual-beam, off-axis forward scatter arrangement. The focusing optics consisted of a 300 mm focal length achromatic front lens preceeded by a 2:1 achromatic expander optics. The laser was a Spectra-Physics model 124 15 mW He-Ne laser. The resulting measuring volume was about 0.10 x 0.30 mm. The intersection angle used for most measurements was 15°. This gives a conversion factor of:

$$u/f_D = \left(\lambda/2 \sin \frac{\theta}{2}\right) = 2.42 \ (ms^{-1}/MHz) \qquad (5.2.1)$$

The signal from the photodetector was connected to the mixer input of the DISA 55 N 10 Frequency Shifter and from there passed to both the DISA 55 L 95 Counter and the DISA 55 L 22 Tracker. The tracker output voltage was measured with the TSI voltmeter, while the Counter digital output was connected to the DISA 57 G 20 Interface.

5.3 Hot-wire Measurements

Simultaneously with the LDA-measurements a DISA 55 M 01 CTA (Constant Temperature Anemometer) with a 55 M 10 Standard Bridge was used. Both a

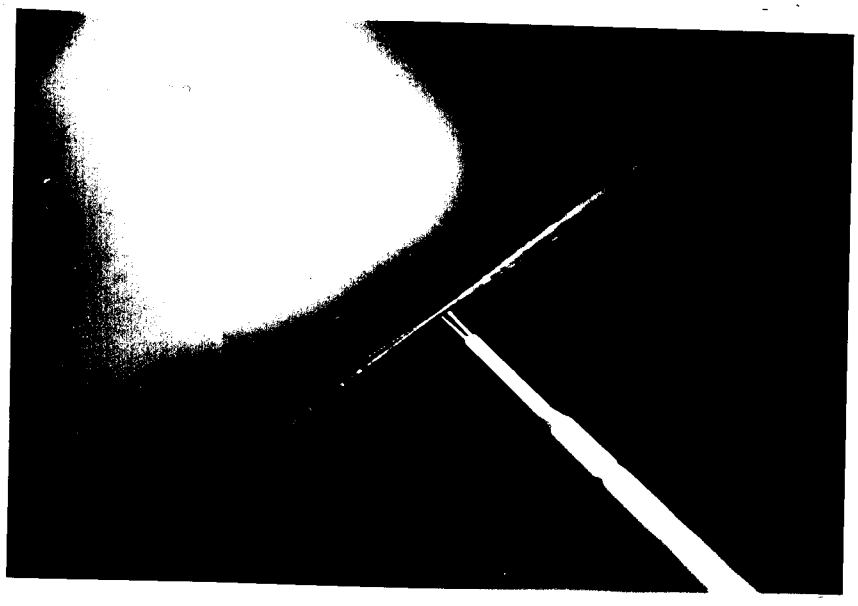

Fig. 5.1 Hot-wire probe and LDA probe volume.

DISA P-11 5μ x 1mm tungsten wire and a P-51 X-wire probe were used. The CTA output was measured with the TSI voltmeter. In some measurements the CTA output was linearized with a DISA 55 D 10 Linearizer. The wire was mounted parallel to the optical axis of the LDA about 1 mm downstream from the LDA measuring volume (see Figure 5.1).

The hot-wire calibration curve was measured before and after each experiment. The laser anemometer was used as a calibration standard close to the jet exit, where the flow was approximately laminar and bias negligible.

Of particular interest was the influence of glycerin seeding on the wire characteristics. The impact of individual seeding particles on the wire was clearly visible on a scope display of the CTA output as short spikes. However, no effect was measured on the calibration curve, neither at the moments following the initial start of the seeding generator nor from a full day's exposure to a seeded air flow.

For the non-linearized hot-wire measurements a calibration curve of the form:

$$E^2 = A + Bu^n \text{ or } u = \left(\frac{E^2 - A}{B}\right)^{\frac{1}{n}} \tag{5.3.1}$$

was assumed. Here E is the output from the CTA and A, B and n are constants. With n = 0.45 a good approximation to the calibration curve was obtained. In the rms measurement the sensitivity of the CTA at each value of u (or E) was computed from:

$$\frac{du}{dE} = \frac{2E}{nB}\left(\frac{E^2 - A}{B}\right)^{\frac{1}{n}-1} \tag{5.3.2}$$

and the rms velocity found from:

$$\sqrt{\overline{u'^2}} = \frac{du}{dE}\sqrt{\overline{e'^2}} \tag{5.3.3}$$

where e' is the fluctuating part of E.

Most of the hot-wire measurements were made with a single wire and the results are displayed without correction for cross flow sensitivity. The errors in hot-wire measurements of mean and rms velocity in turbulent flow are analyzed in e.g. Hinze (1974). These errors are complicated functions of the turbulent velocity field and no general correction procedure can be applied. For a perfectly linearized CTA the effective cooling velocity for small turbulence intensity can be approximated by:

$$u_{eff} = \sqrt{(\bar{u}+u')^2 + v'^2} \tag{5.3.4}$$

Expanding the square root and averaging results in:

$$\overline{u_{eff}} = \bar{u}\left(1+ \frac{\overline{v'^2}}{2\bar{u}^2} + o\left(\frac{u'}{\bar{u}}\right)^3\right) \tag{5.3.5}$$

A similar analysis for the non-linearized CTA assuming a static calibration law of the form (Generalized King's law):

$$E^2 = (A + Bu_{eff}^{\,n})\,(T_w - T_g) \tag{5.3.6}$$

where E is the output voltage, A, B and n are constants and T_w and T_g are the temperatures of the wire and the gas respectively, results in the following expression:

$$\overline{u_{eff}} = \bar{u}\left(1 + (n-1)\frac{\overline{u'^2}}{2\bar{u}^2} + \frac{\overline{v'^2}}{2\bar{u}^2} + o\left(\frac{u'}{\bar{u}}\right)^3\right) \tag{5.3.7}$$

However, for a finite length wire it is necessary to carry out a more refined analysis taking into account the temperature distribution along the wire. The resulting expression is very complicated (Hinze p.109). The correction terms may be substantially different from eqs. (5.3.5) or (5.3.7).

depending on the structure of the turbulence. In isotropic turbulence and a wire under normal operating conditions the correction terms for a linearized, a non-linearized and a non-linearized finite length wire are, respectively:

$$\overline{u_{eff}} \cong \bar{u}(1+ \frac{1}{2} \frac{\overline{u'^2}}{\bar{u}^2} + \sigma(\frac{u'}{\bar{u}})^3) \tag{5.3.8}$$

$$\overline{u_{eff}} \cong \bar{u}(1 + \frac{1}{4} \frac{\overline{u'^2}}{\bar{u}^2} + \sigma(\frac{u'}{\bar{u}})^3 \tag{5.3.9}$$

and

$$\overline{u_{eff}} \cong \bar{u}(1 + \frac{11}{16} \frac{\overline{u'^2}}{\bar{u}^2} + \sigma(\frac{u'}{\bar{u}})^3) \tag{5.3.10}$$

Because of the difficulties in estimating the error terms in non-isotropic turbulence, in particular in the outer region of the jet, the CTA data are displayed uncorrected.

5.4 LDA-Counter Data Processing

The data processing software is organized in data collection and transfer subprograms (COLLEC, TRANSFER and SORT) written in the RT-11 operative system assembly language (MACRO) for the PDP-11 computer family (Digital Electronics Corp.). This ensures maximum speed and efficiency in the data collection process. These programs are contained in the standard DISA LDA software package for operation through the 57 G 20 interface. The program COLLEC organizes the collection of a batch of NDATA data points and stores the data in memory. A total of NBATCH batches may be collected in the total measurement. The programs TRANSFER and SORT transfer data from a particular counter output to the user FORTRAN program. The data words transferred to the main program are organized as an

array D(I,J), where D(1,J), J = 1,2,···, NDATA are the measured velocities, derived from the measured frequencies:

$$D(1,J) = CALIB*(FMEAS(J)-FREQSH) \tag{5.4.1}$$

D(2,J), J = 1,2,···, NDATA are the measured time increments since the preceeding data ready pulse:

$$D(2,J) = t_j - t_{j-1} \tag{5.4.2}$$

and D(3,J), J = 1,2,···, NDATA are the measured number of zero-crossings in a burst:

$$D(3,J) = N_Z(J) \tag{5.4.3}$$

FMEAS is the measured frequency transferred directly from the counter:

$$FMEAS = 14.96 \cdot D \tag{5.4.4}$$

where D is the data word at the connector.

FREQSH is the chosen frequency shift (positive if the shift adds to the Doppler frequency of a particle moving in the X-direction).

CALIB is the calibration factor:

$$CALIB = WAVELE/(2*SIN(BEAMAN/2)) \tag{5.4.5}$$

(equivalent to eq. (5.2.1)) where WAVELE is the laser wavelength λ and BEAMAN the intersection angle between the laser beams θ.

As described in Section 2 the DISA 55 L 95 LDA-counter operates in four different modes of which three are of interest in LDA measurements. In mode 3, FMEAS is computed on the basis of a variable number of zero-crossings. The measured velocity in mode 3 must therefore be computed from the formula:

$$D(1,J)_{MODE\ 3} = CALIB*(FMEAS(J)*D(3,J)/8-FREQSH) \tag{5.4.6}$$

D(2,J) and D(3,J) in mode 3 are the same as in mode 1 and 2.

With the data array D(I,J), I = 1,2,3 and J = 1,2,···, NDATA corresponding to one batch from the counter, the quantities entering formulas (4.3.8),(4.4.6) and(4.5.20) in Chapter 4 are given by:

Velocity $u_o(t_j) \equiv u_j = D(1,J)$ (5.4.7)

Time increment: $t_j - t_{j-1} = D(2,J)$ (5.4.8)

Number of zero crossings: $N_{Z,j} = D(3,J)$ (5.4.9)

Further we have:

Residence time:

$$\Delta t_j = D(3,J)/[D(1,J)/CALIB + FREQSH] \quad (5.4.10)$$

Weighting factors:

Arithmetic averaging:

$$(W_j)_{AR} = 1 \quad (5.4.11)$$

1-D weighting:

$$(W_j)_{1-D} = 1/ABS(D(1,J)) \quad (5.4.12)$$

Residence time weighting:

$$(W_j)_{RT} = D(3,J)/[D(1,J)/CALIB + FREQUSH) \quad (5.4.13)$$

With these quantities we can immediately use the general formulas for mean and mean square velocity valid for all modes and for any correction method:

$$\bar{u} = \frac{\sum_{j=1}^{NDATA} u_j W_j}{\sum_{j=1}^{NDATA} W_j} \quad (5.4.14)$$

and

$$\overline{(u')^2} = \frac{\sum_{j=1}^{NDATA} (u_j - \bar{u})^2 W_j}{\sum_{j=1}^{NDATA} W_j} \qquad (5.4.15)$$

In the actual batch processing it may be more convenient to compute the quantity:

$$\overline{u^2} = \frac{\sum_{j=1}^{NDATA} u_j^2 W_j}{\sum_{j=1}^{NDATA} W_j} \qquad (5.4.16)$$

and find the mean square velocity from:

$$\overline{u'^2} = \overline{u^2} - \bar{u}^2 \qquad (5.4.17)$$

5.5 Batch Processing of Burst-type LDA Data

In the development of the theory of residence time weighting in Chapter 4 it was assumed that all the data measured were processed and that the record length was sufficiently long to give a good estimate of the time average, i.e. much longer than the integral scale of the flow (c.f. e.g. Tennekes and Lumley (1972)). The integral scale is defined as:

$$T_u = \int_0^\infty \rho_u(\tau) d\tau \qquad (5.5.1)$$

where $\rho_u(\omega)$ is the autocorrelation function. In a random process the integral scale is a measure of the large scale correlation or "memory" of the flow. The record length, TREC, should be at least two times the integral scale for two reasons. Firstly, it is a condition for the use of the residence time weighting that the data is sampled at the rate at which it occurs naturally from particles swept through the volume, i.e. that the data is not resampled by the computer at more or less equidistant intervals (see section 5.5). Secondly, with a batch length longer than

twice the integral scale we are sure that each batch can be considered an independent sample of the flow. From the theory of the measurement of random variables we know that the variance on a statistical estimate is related to the number of integral scales contained within a record (see e.g. Jenkins and Watts (1968) or Tennekes and Lumley (1972). In a recent survey by George (1979) the forms applicable to randomly sampled data were presented. The variance of the measured mean and mean-square are respectively:

variance of mean values:

$$\text{var}\,[\bar{u}_T] \cong \overline{u'^2}\left[\frac{2T_u}{T} + \frac{1}{\nu T}\right] \tag{5.5.2}$$

variance of mean square values:

$$\text{var}[\overline{u_T'^2}] \cong (\overline{u'^2})^2\left[\frac{2T_u}{T} + \frac{1}{\nu T}\right] \tag{5.5.3}$$

We see that the contribution to the variance from the first term reduces in proportion to the number of times we can have a record length of $2T_u$ within the total record length T, i.e. to the total number of independent samples of the flow, $T/2T_u$. The second term in the bracket shows that a certain average data rate is needed to prevent an unacceptable increase in variance due to the random sampling. From the form of eqs. (5.5.2) and (5.5.3) it is easy to see what happens in the limiting cases of very high and very low data rate. When the data rate is high the variance is essentially that of the continuous time function, i.e. dominated by the factor $2T_u/T$. In the limit of very low data rate all data points are independent and the variance is determined by $1/\nu T = 1/N$, the total number of data points measured.

In practice very long records would require a large buffer memory or other type of fast, digital mass storage device, or a fast real-time computer.

Often it is possible to use a much smaller buffer memory which contains a smaller amount of data--one batch of data. We do the required computations on one batch, then sample a new batch, and continually form an updated average of all batches.

This method was used in the processing of data in the present system. However, in the processing of randomly sampled LDA data precautions must be taken not to violate the basic assumptions behind the residence time weighting. The basic effect of the residence time weighting is to restore the ensemble averaging to a time integral. Thus one must be sure not to introduce another preferential sampling by the batch processing.

There are two basically different ways of handling batch processing: One can sample for a fixed sampling time at regular intervals, or one can sample a fixed number of data points again at regular intervals.

1. Batch length fixed.

This method is exactly the process described in Chapter 4. Within each batch, residence time weighting must be applied to restore the correct time integral over the batch sampling time. Each batch represents an independent realization of the flow process and thus batches must be averaged arithmetically. The interval between batches (which will often be the computing time) must be constant in order not to introduce a preferential sampling of the flow. If determined by computing time, the intervals are unlikely to be equal. Then the intervals must be at least two integral scales to prevent correlation between individual batches; such intervals also assure optimal convergence. Sampling in a fixed time is used in the direct spectral estimator described in section 4.6 and 6.4, where the window determines the batch record length.

2. Batch size fixed.

This method is most easily implemented, since no real-time clock is

needed. However, conceptually the method is more difficult to handle. Within each batch residence time weighting must be applied to prevent biasing. However, even if batches are spaced by equal size intervals or intervals greater than the integral scale, batch averaging can not just be performed by an arithmetic mean. Each batch must be longer than the integral scale to represent an independently unbiased realization of the flow. The batch may be composed of a small number of samples (NDATA small), but the sampling rate must be so low that more than an integral scale is covered by one batch length.

If records are very short compared to the integral scale and computing time long compared to the record length the situation is one approaching equidistant sampling and the theory of burst-type LDA data processing does not apply. These considerations are even more important in the formation of autocorrelation and spectrum (see sections 6.3 and 6.4).

The measurements described in this report were all performed with fixed batch sizes, but in the spectral measurements described in section 4.6 and 6.4, the window imposed on the record effectively converts the sampling method to the first case - fixed sampling time. Thus high frequency estimates can be made with short batches of high data rate.

5.6 Results and Conclusions

In general the experimental results confirm the theory given in the preceeding sections. The mean and rms data support the theory of residence-time weighted burst-type LDA measurements. Within experimental errors caused by the randomness of the flow variables measured, the residence-time weighted mean velocity and the mean values measured by the LDA tracker are identical. The mean values computed by arithmetic averaging and by the 1-D weighting deviate from the residence-time weighted mean value in the expected manner, i.e. the arithmetic averaging results in

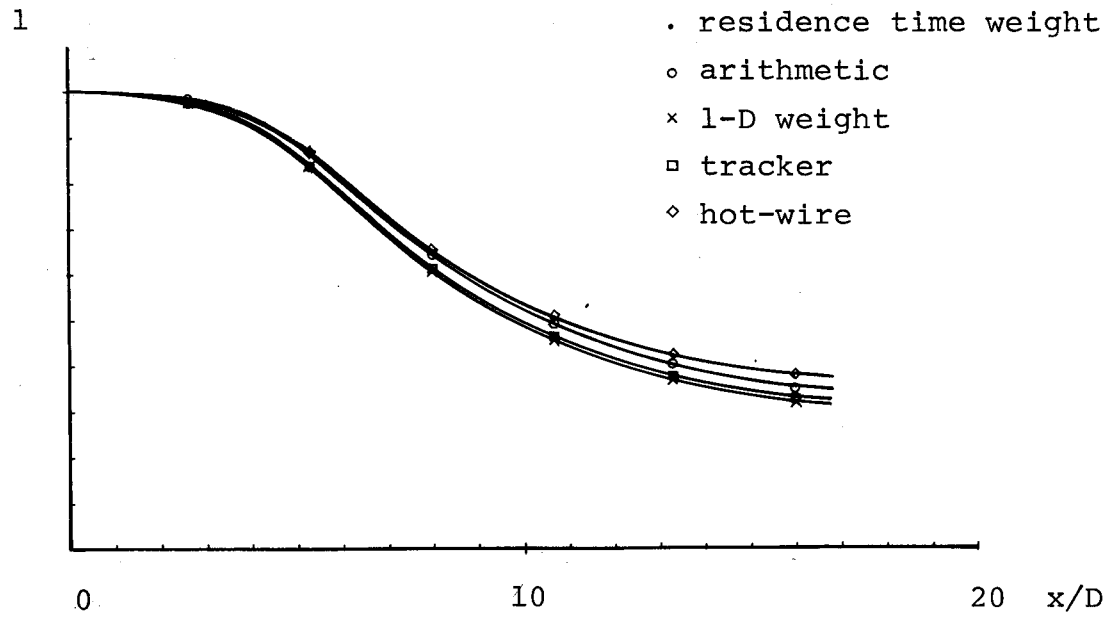

Fig. 5.2 Mean velocity along axis, Re=10000, f_s=.3 MHz.

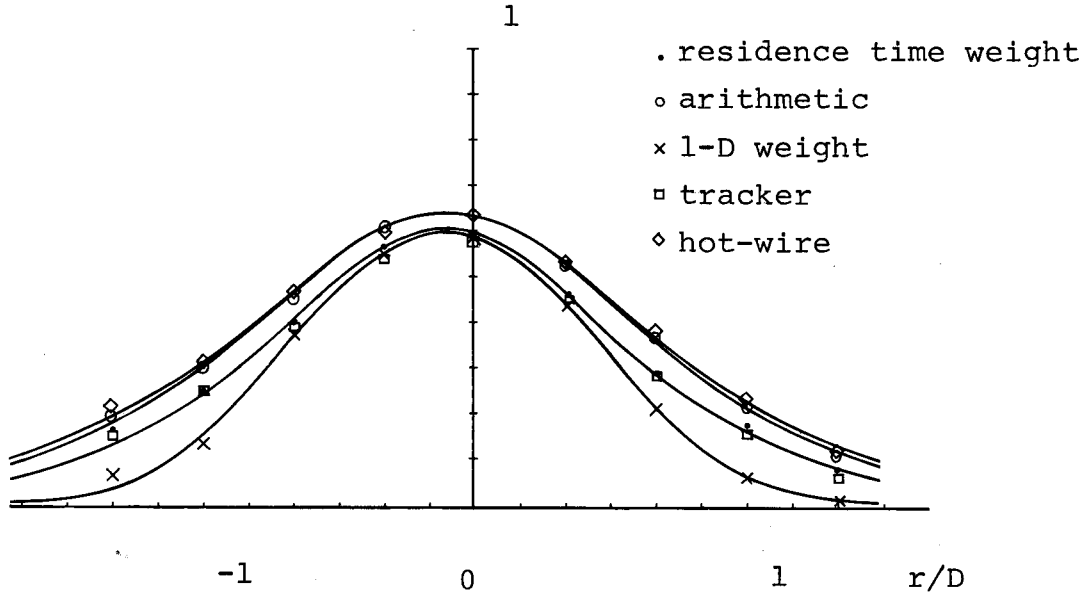

Fig. 5.3 Mean velocity, $\bar{u}$, transverse scan at x/D=10.6

mean values that are too high and the 1-D weighting results in mean values that are too low and become meaningless when measured data points close to $u \approx 0$ begin to occur. The mean values from hot-wire measurements are also too high as expected - about as much as the arithmetic averages. The X-wire data show the same trend in accordance with the fact that an X-wire only measures the correct u-component in a flow with 2-dimensional fluctuations in the plane of the two wires. In the 3-dimensional jet flow no particular advantage is gained by using an X-wire for u-measurements.

The rms results are surprisingly similar regardless of the type of instrument used. In fact, with the averaging times used in this experiment (100 sec. time averages) it was not possible to observe any differences in the rms values from counter, tracker or hot-wire measurements, except quite close to the jet exit. At the jet exit the LDA instruments, in particular the tracker, measured a higher rms value than the hot-wire, as would be expected.

The effect of different amounts of frequency shift relative to the measured Doppler frequency is also apparent in the data. It can be seen that the 1-D correction is best when the frequency shift is not too high, i.e. when the over-compensation introduced by the 1-D correction in a 3-dimensional flow measurement is counter-balanced by some directional bias.

Of course these effects are difficult to estimate in an arbitrary flow situation, but the data shows that the 1-D correction may work quite well up to turbulence intensities of 10-20 pct. At higher turbulence intensities as are encountered in swirling flows or flows behind steps, expansions etc., or in the free jet, residence-time weighting or tracker measurements would be the only reliable LDA data processing methods.

Figures 5.2 and 5.3 show measured mean values along the jet axis and at a transverse scan through the jet at $x/D = 11$. Figures 5.4 and 5.7

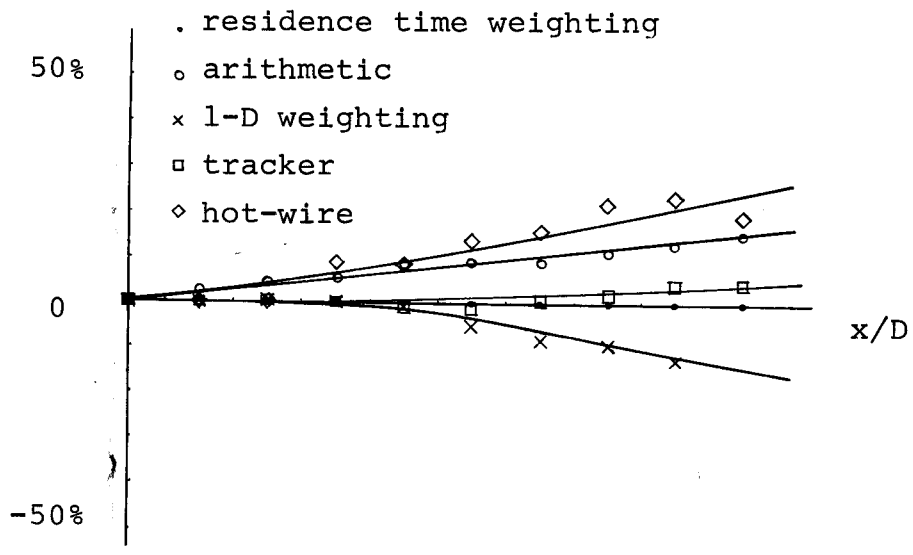

Fig. 5.4 Relative error in mean value, axial scan. Re=10000, f_s=.3 MHz.

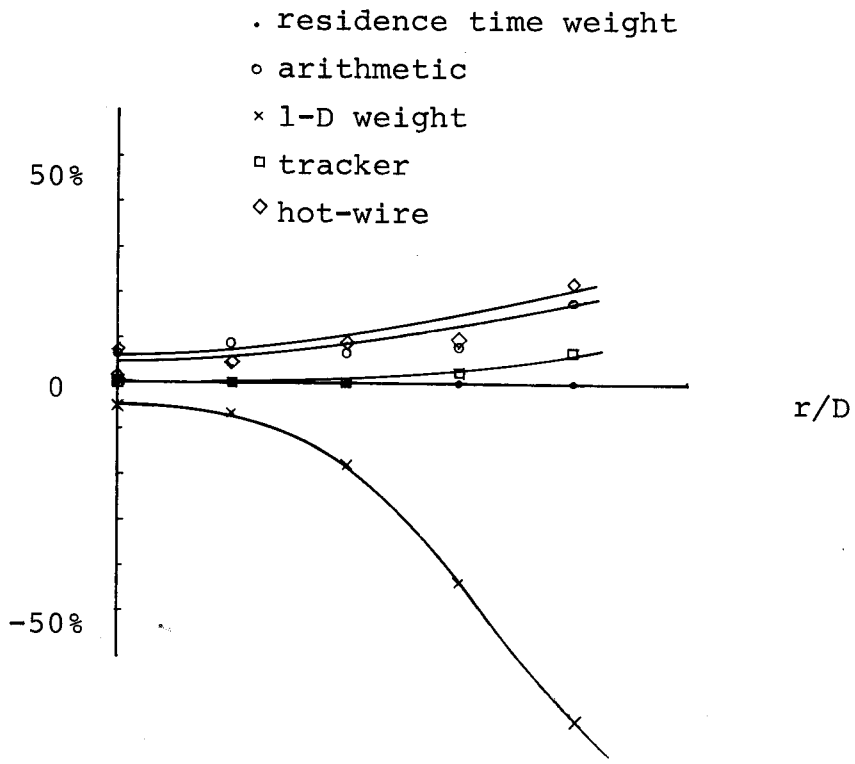

Fig. 5.5 Relative error in mean value, transverse scan. Re=10000, f_s=.3 MHz.

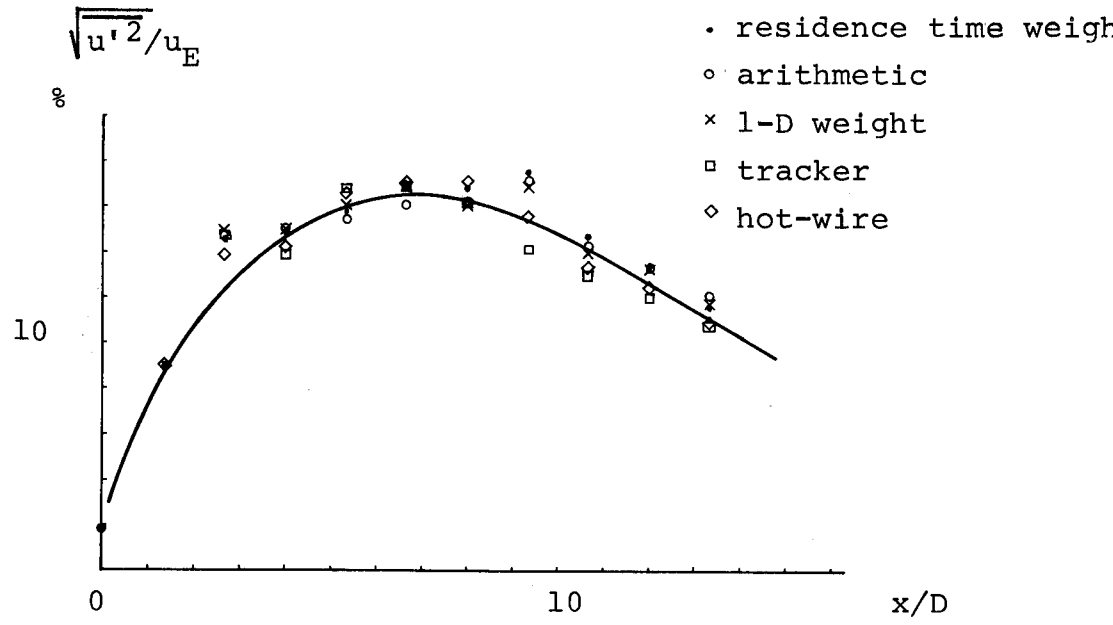

Fig. 5.6 rms value, axial scan. Re=10000, f_s=.3 MHz.

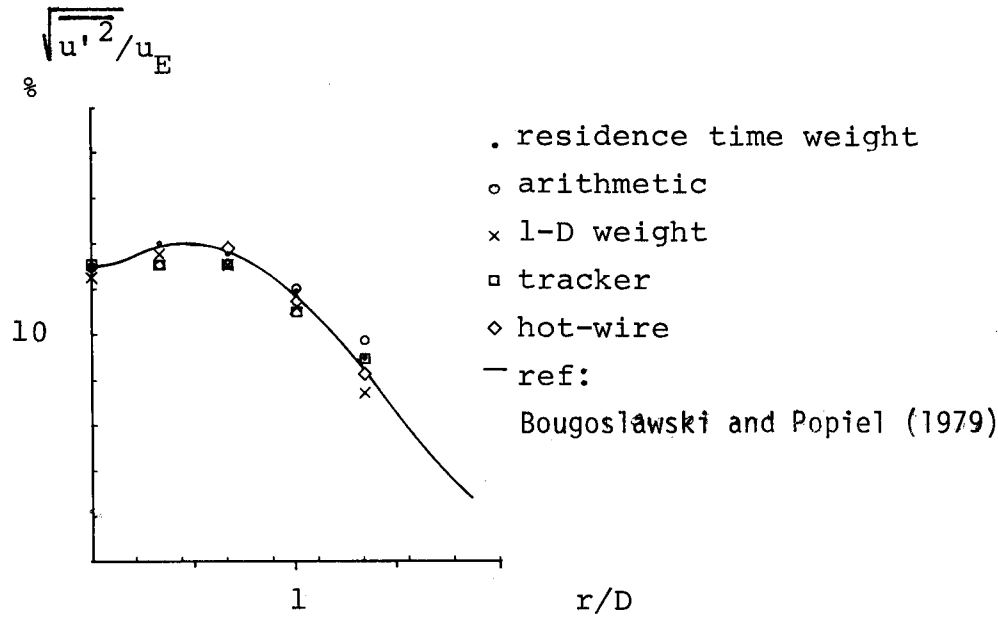

Fig. 5.7 rms value, transverse scan at x/D= 10.6.
Re=10000, f_s= .3 MHz.

show the relative difference between the mean values obtained with different methods. The differences are shown relative to the residence-time weighted data. The jet Re-number was Re=10,000. Figures 5.6 and 5.7 show the rms velocity at the positions of Figures 5.2 and 5.3. The differences between the various methods in rms measurements were insignificant. Figures 5.8 and 5.9 show mean velocity data at a higher Re-number (Re=20,000). In these measurements the frequency shift was higher relative to the Doppler frequency than in the previous data. The influence of the frequency shift is displayed in Figures 5.10a and b. The figure shows the difference between arithmetic, 1-D weighted and residence-time weighted counter data for the transverse scan for two different values of the ratio of frequency shift to Doppler frequency.

Considering the errors introduced by the arithmetic averaging and the 1-D correction method it must be noted that the differences only become appreciable for high turbulence intensities, e.g. in regions of the free jet, where measurements are known to be difficult and subject to large errors. In the measurement of turbulence of a more moderate turbulence intensity (below 10-20 pct.) the errors are smaller and some corrections may be successfully applied to bring the errors down to the order of 1 pct., even when residence-time weighting is not available.

Depending on the particular design of the electronic circuits various other bias effects caused by electronic noise in the signal can be expected to occur, especially in high velocity measurements, where the signal-to-noise ratio can be expected to be low. Also an increase in the variance of the measured statistical variables might occur in residence-time weighted data because of the additional randomness introduced by the measured value of the number of zero-crossings. These effects were not considered in the present investigation.

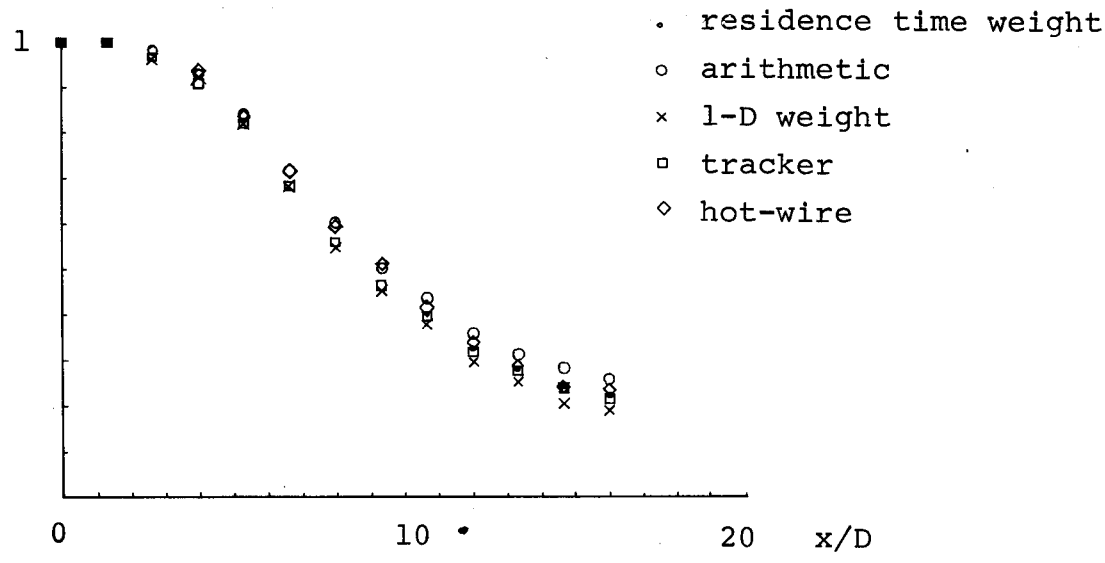

Fig. 5.8 Mean velocity measured along axis, Re=20000, f_s=1 MHz.

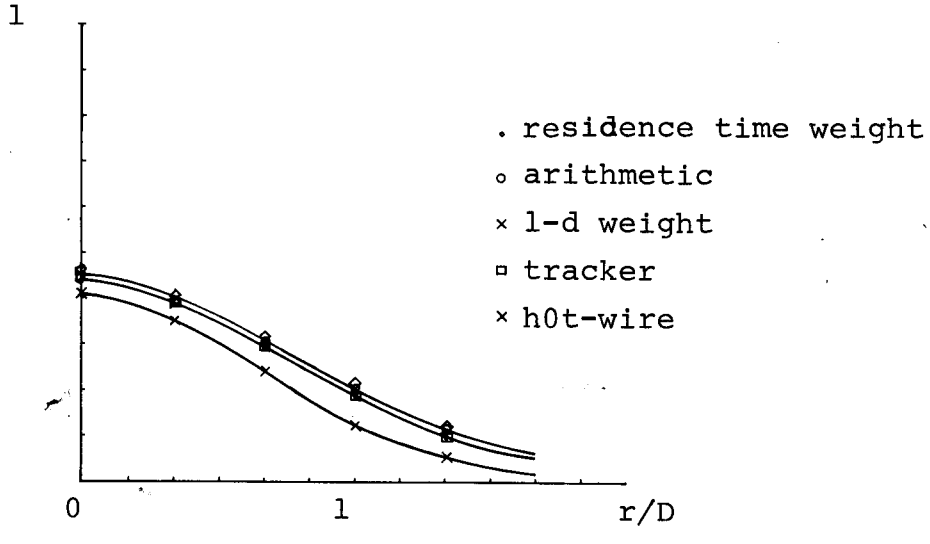

Fig. 5.9 Mean velocity, $\bar{u}$, transverse scan at x/D=10.6.

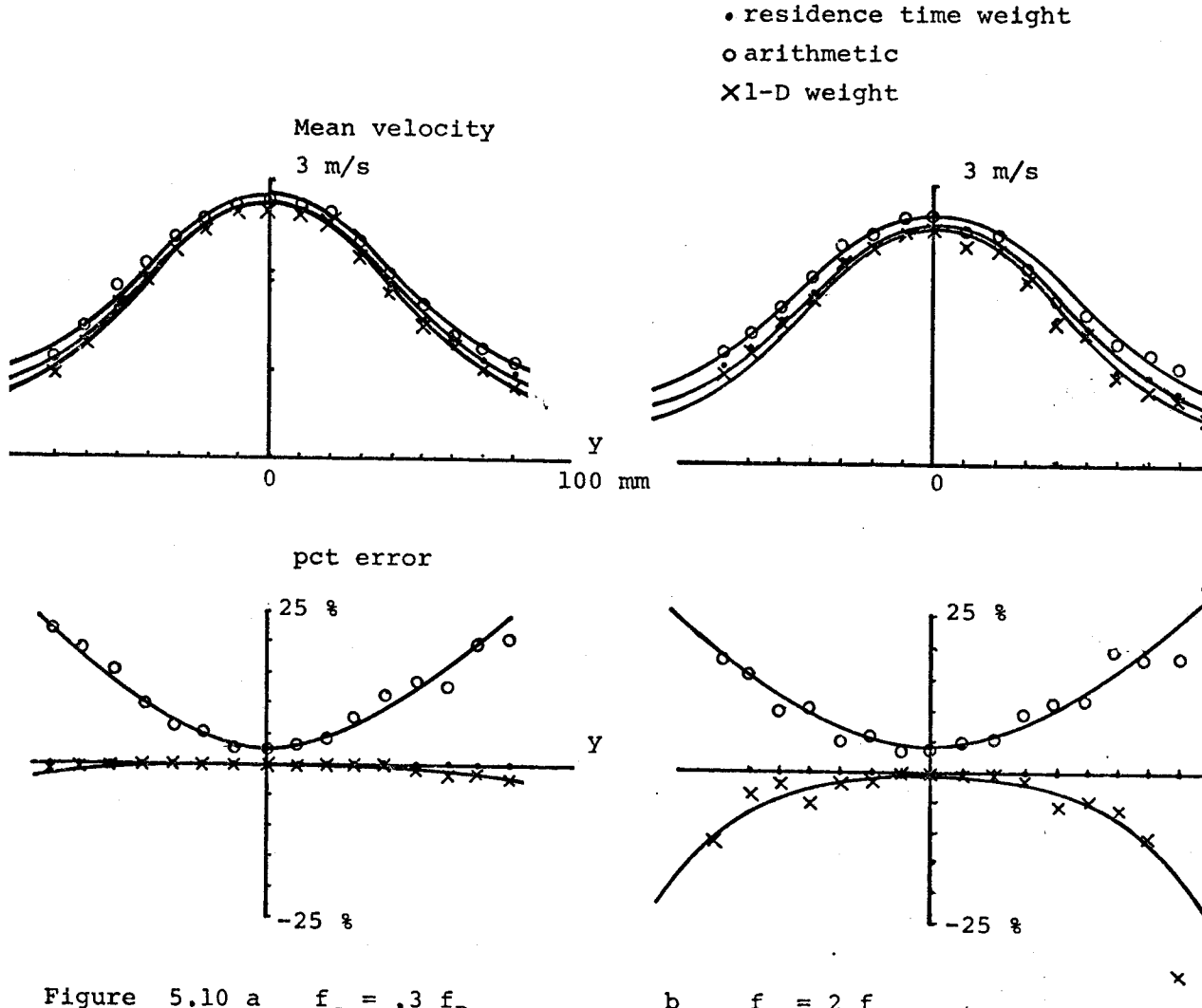

Figure 5.10 a $f_s = .3\ f_D$ b $f_s = 2\ f_D$

Mean velocity and pct. error in mean relative to residence time weighted data.

6. Measurement of Autocorrelation Function and Spectrum with the Counter LDA

6.1 Introduction

LDA measurements are generally considered more subject to noise than hot-wire measurements. That this is true at least for the analog, real-time output is obvious from a comparison of the output signals from a CTA and a continuous LDA processor on an oscilloscope. The noise in hot-wire measurements is primarily thermal noise in the input amplifier circuit. The noise in the output of a continuous LDA processor (e.g. a tracker) is dominated by the "ambiguity noise", the noise caused by the random phase fluctuations in the multi-particle LDA signal (see the tracker spectra displayed in Chapter 7). An effective way of removing or compensating for this noise has not yet been devised, and for this reason the tracker based LDA is generally more suited for the measurement of large fluctuations relative to the mean and in cases where flow reversals occur. In such cases the hot-wire instrument is handicapped by its limited flow acceptance angle. Observation of the counter analog output may lead one to believe that counter measurements are even more noisy than tracker measurements, and spectra formed from the counter analog output are indeed superimposed with a high frequency noise due to the sample-and-hold type output (see again Chapter 7). The interesting fact is, however, that the inherent noise level in burst type LDA data may be far lower than that of the continuous LDA signal. The reason is that the basic information in the signal, the time of flight across a certain number of interference fringes in the measuring volume, is undistorted in the single particle LDA. The fringe pattern in a well adjusted dual-beam LDA is well defined with equidistant fringe spacing throughout

the measuring volume. When the particle concentration is so low that the probability of more than one particle at a time in the measuring volume is negligible and/or facilities are available for the removal of data caused by two or more particles present simultaneously, no ambiguity noise can be generated.

The noise in the digital LDA counter data is primarily caused by shot noise in the signal and possibly a white shot noise level from background light or thermal noise in the detector and preamplifier. Other noise sources are truncation or round-off errors in the frequency (velocity), time interval and residence time data.

By using the autocorrelation estimator derived in Chapter 4 (eq. 4.5.21), which does not contain "self-products" or "zero-lag products" (i.e. the square of individual realizations), directly on the digital counter data, an autocorrelation function estimate is formed, which does not contain ambiguity noise and noise due to the sample-and-hold character of the analog output. Similar estimators were introduced by Mayo (1974) and Gaster and Roberts (1975) for purely Poisson distributed data (no velocity bias correction). As emphasized by these authors and shown already by Shapiro and Silverman (1960) Poisson sampling eliminates aliasing in the computed spectrum and allows the formation of spectral estimates for frequencies above the usual Nyquist frequency limit, which exists for equidistantly sampled data. More recently the properties of Poisson sampled spectra have been treated by Masry and Lui (1976) and Masry (1978a) and (1978b).

Concerning noise it was further shown by Gaster and Roberts (1975) on simulated data that the type of estimator, which does not contain "self-products", is insensitive to white noise added to the signal

(i.e. for our purpose noise with a correlation shorter than a particle transit time). In section 4.5 it was furthermore shown that even velocity gradients within the measuring volume do not cause additional noise (gradient noise) in the autocorrelation function and hence in the spectrum formed from the autocorrelation. Thus burst-type LDA data processing would appear to have many advantages compared to continuous (tracker data processing.

The primary source of noise in the following measurements is probably the quantization error caused by the 8-bit mantissa of the velocity data (in floating point format). This noise source has an rms value of about 0.25% of full scale and spectral roll off of ω^{-2}. Thus the high frequency end of the log-log spectrum will be obscured by this error. Unlike white noise added to the signal, the quantization noise does not cancel in the formation of the autocovariance and spectrum. In principle the quantization can be reduced by increasing the word length, but at high velocities the quantization will be determined by the finite clock frequency.

As shown in Chapters 3, 4, and 5 velocity bias can be eliminated by the residence time weighting and direction effects may be reduced by the addition of frequency shift. This gives the LDA an advantage over hot-wire measurements in high intensity turbulence, where the correction of hot-wire data for the effects of transverse cooling is questionable or impossible. Moreover, the small measuring volume readily obtained with the LDA seems to point to the possibility of obtaining better spatial and temporal resolution in the measurement of fine scale turbulence with the LDA than with the hot-wire.

The results of the present investigation show that it is indeed possible to obtain turbulence spectra with the LDA counter over a

considerable dynamic range. However, more work is needed to explore the noise sources and ultimate limitations to the resolution and dynamic range of burst-type LDA turbulence spectra and to exploit the unique potentials of the LDA in turbulence measurements.

6.2 Data Processing

As in Chapter 5, which dealt with mean and rms measurements, the data is sampled and processed in batches of a certain number NDATA data points, which together form one batch record of length TREC.

Each batch of data is sampled via the buffer interface (DISA 57 G 20) and transferred to memory directly in the format they are output from the counter by the program COLLEC. When the batch is complete the data is transferred to a data array in standard floating point format by the program TRANS and is then available for further data processing by high level (FORTRAN) data processing programs.

The data array contains the three words per data point, D(I,J), I = 1, 2, 3 and J = 1, 2 ···, NDATA, described in section 5.4.

Several versions of autocorrelation and spectrum programs have been tested. Common to them all is the batch structure described in section 5.4. Each data point contains information of the Doppler frequency (or the inverse, the measured time of flight), the time interval from the previous sample from which the absolute time within the batch can be computed, and the number of periods in a burst from which the residence time can be computed.

During a run the mean value of each batch is computed and the updated mean value of all previous batches within a given run is also computed. The latter is used to form the fluctuating component. Thus the computations require strict stationarity throughout the measurement to prevent low

frequency errors. (If the process is not strictly stationary it may be advantageous to use the individual batch mean values instead).

As always in turbulence measurements the best results are obtained if some information on the expected values is available and can be used to select the instrumental parameters. The integral scale of the flow should be known roughly either from guessing or from previous exploratory measurements. Continuing the discussion on the variance of the measured statistical quantities from section 5.5, we have for the autocovariance function and spectrum:

variance of autocovariance function:

$$\mathrm{var}[C_T(\tau)] \cong \overline{(u'^2)}^2 \left[\frac{2T_u}{T} + \frac{1}{\nu T}\right] \tag{6.2.1}$$

variance of spectrum:

$$\mathrm{var}[S_T(\omega)] \cong [S(\omega)]^2 \left[1 + \frac{\overline{u'^2}}{2\pi\nu S(\omega)}\right]^2 \tag{6.2.2}$$

Again we see that for a high average data rate, ν, the variance reduces to the form known for a continuous time series. The data rate at which a significant increase in spectral variance due to the random sampling is noticed depends on the value of the spectrum relative to the spectrum at zero frequency. The optimum sample rate for a fixed number of samples and a fixed batch length is

$$\nu_{opt} = \frac{\overline{u'^2}}{2\pi S(\omega)} \tag{6.2.3}$$

Both the measured autocovariance and the measured spectrum must be smoothed by suitable means. The time slot technique (eq. 4.5.20) reduces the variance of the autocovariance estimate by the factor $1/\nu\Delta\tau$, where $\Delta\tau$ is the slot width. The application of a window function and/or batch averaging result in a reduction of the variance of the spectrum. Batch averaging simply reduces the variance by one over the number of batches.

Convolution of the spectrum with a window function of efffective width $\Delta t = 2\pi/\Delta\omega$ where $\Delta\omega$ is the bandwidth of the final estimate reduces the variance by a factor $(2\pi/\Delta\omega T)$, where T is the length of the record used to compute the spectrum.

The expression for the variance of the direct transform applicable to the present measurements is then:

$$\mathrm{var}[\hat{S}_2(\omega)] = \frac{T_B}{T}\left[S(\omega) + \frac{\overline{u'^2}}{2\pi\nu}\right]^2 \qquad (6.2.4)$$

where T_B is the length of the batch and T is the total length of record. This is the expression derived by Gaster and Roberts (1975) except for a constant factor resulting from a different choice of window shape. Masry (1978) showed that this result is essentially unchanged in the case of fixed batch size (NDATA data points), which results in a random batch record length. The variance of the spectral estimtor based on the cosine transform of the autocovariance function is then

$$\mathrm{var}[\hat{S}_1(\omega)] = \frac{3}{4}\frac{\mathrm{NDATA}}{N}\left|S(\omega) + \frac{\overline{u'^2}}{2\pi\nu}\right|^2 \qquad (6.2.5)$$

where the factor $\frac{3}{4}$ arises because of the Hanning window applied in the correlation plane.

In accordance with the discussion in section 5.5 we still want the sampling period TREC to cover at least an integral scale. It then follows that the batch size should be approximately:

$$\mathrm{NDATA} \simeq \nu\cdot\mathrm{TREC} \simeq \nu\cdot 2T_u \qquad (6.2.6)$$

Thus measurements covering a large dynamic range require a large buffer memory and/or a large computer memory.

6.3 Measurement of Autocorrelation Function and Spectrum by the Slotted Time Lag Technique

The autocorrelation function is constructed by accumulating cross products of pairs of measurements in array elements according to the value of the time lag. Each array element corresponds to lag values within a given slot on the time lag axis. Similar methods were used or suggested by Smith and Meadows(1974), Mayo (1974), Scott (1974) and Gaster and Roberts (1975). The present method deviates from these earlier ones by processing the data in batches of a record length of about two integral scales of the flow and by assigning weights to each cross product according to the method described in section 4.5. The autocovariance estimate is then given by:

$$C(K) = \frac{\sum_{i\neq j}^{N} u'_i W_i \; u'_j W_j}{\sum_{i\neq j}^{N} W_i \; W_j} : \tau_{K-1} \leq t_j - t_i < \tau_K \qquad (6.3.1)$$

where τ_K is the upper limit for lag values in the K'th slot. As in 5.4.14-16 we have used the general expression W_i for the weighting factor to be able to compare the residence time weighting to the arithmetic and the 1-D averaging.

The most straightforward method to implement this estimator is to divide the time lag axis into N ≡ NSLOT equally spaced slots of width $\Delta\tau$ ≡ TAU = TLAG/NSLOT. The procedure in the autocorrelation program is then the following (See Figure 6.1 for a flow diagram of the FORTRAN procedure): First, the maximum time lag TLAG is chosen in accordance with the expected integral scale. Then, for each data point cross products are formed with all subsequent data points within the batch. The program keeps track of the time lag between data points by summing the time intervals between data points.

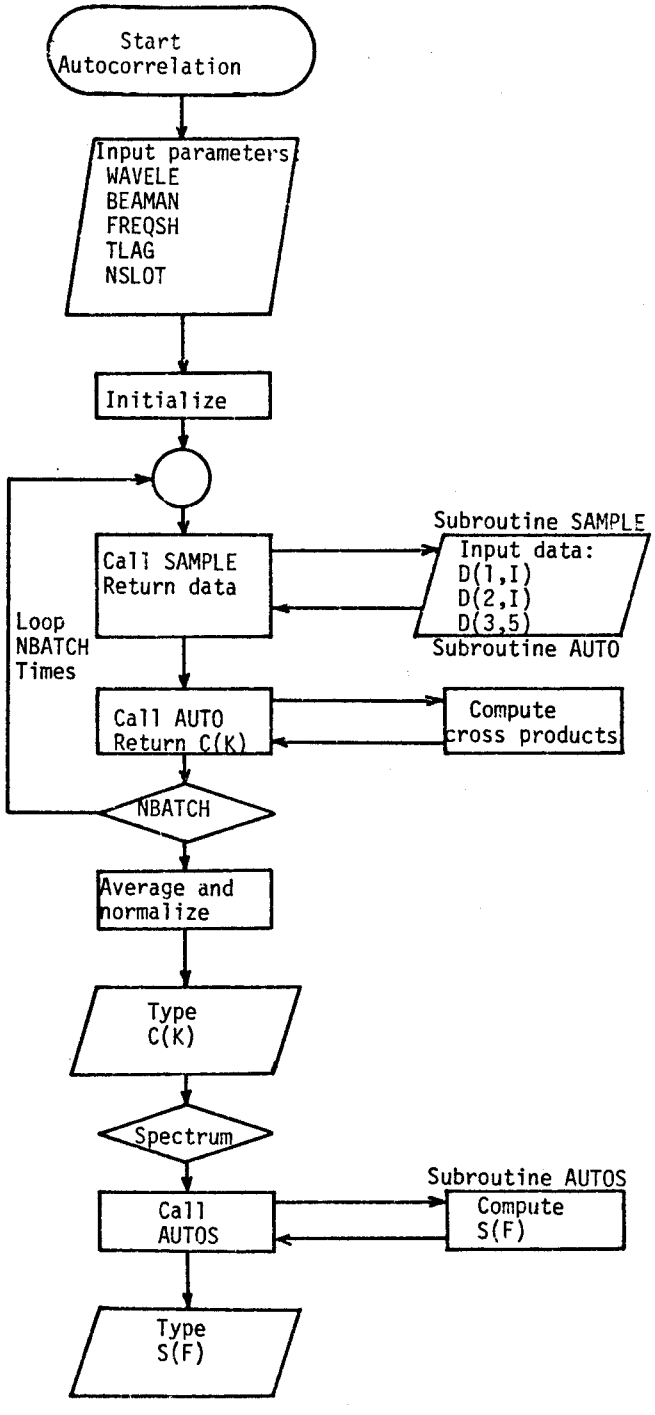


```
      SUBROUTINE AUTO
C
      DO 100 I = 1,NDATA-1
C
      LAG = 0.
C
      DO J = I+1,NDATA
      LAG = LAG + D(2,J)
      K = INT(NSLOT*LAG/TLAG)
      C1(K)=C1(K)+D(1,I)*D(1,J)
      W1(K)=W1(K)+D(3,I)*D(3,J)
200   CONTINUE
C
100   CONTINUE
C
      DO 300 K = 1,NSLOT
      C(K) = C1(K) / W1(K)
300   RETURN
```

Figure 6.1 Flow chart illustrating the computation of autocorrelation function with equispaced slots.

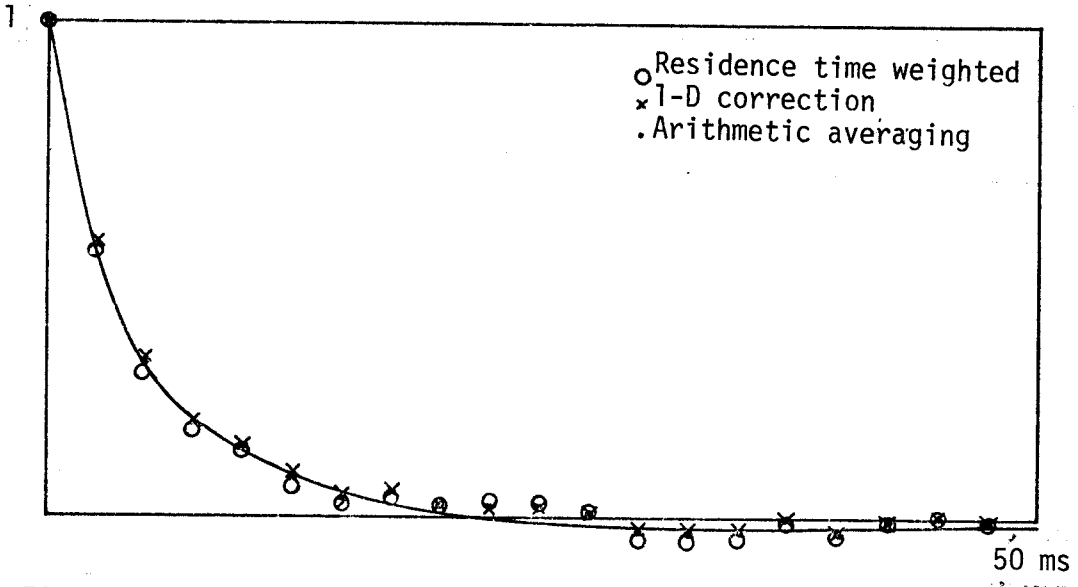

Figure 6.2 - Autocorrelation function measured at x = 10D, y = o · Re = 22000. Computed with three different averaging procedures, arithmetic, x1-D corrected and o residence time weighted.

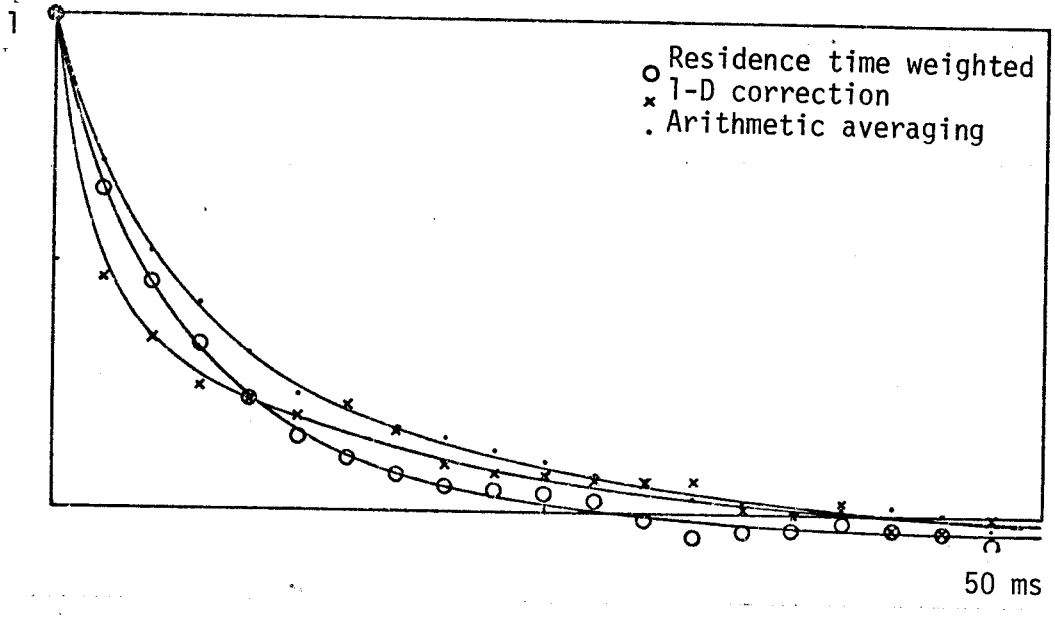

Figure 6.3 As Figure 6.2 but x = 10D, y = 0.2x.

Bartlett window:

$$D(L) = 1 - K/SLOT$$

$$K = 1,2,\cdots, NSLOT \qquad (6.3.8)$$

Hanning window:

$$D(K) = 0.5 + 0.5 \cos(\pi K/NSLOT) \qquad (6.3.9)$$

Results of measurements of autocorrelation and spectrum with the method of equidistantly slotted time lags are shown in Figure 6.2 to 6.5. Figure 6.2 shows the autocorrelation function of the axial velocity of the free jet described in Chapter 3 at an axial position of X/D = 10 and a Reynolds number of Re = 22000. The three curves show the results of arithmetic, 1-D and residence time weighting respectively. The three curves are based on the exact same data points. Figure 6.3 shows the results of a measurement made under the same conditions but at a position off-axis (x = 10 D, y = 0.25 X). The results show that the weighting is important for the measurement of the autocorrelation function, in particular for measurements in high intensity turbulence.

Figure 6.4 and 6.5 show the autocovariance function and spectrum obtained by the residence time weighted LDA counter data and by CTA at the axial position x = 10 D for Re = 22000. The LDA spectrum is based on an autocovariance function with 100 slots. The hot-wire spectrum is obtained from the Nicolet "Mini Ubiquitous", FET spectrum analyzer based on 256 records of 1024 points. The LDA and hot-wire spectra are in agreement at the low frequency end of the spectrum, but the LDA spectrum based on a 100 point transform does not have a dynamic range comparable to the hot-wire spectrum. To obtain better resolution and dynamic range by increasing the number of slots requires so many data points that the computing time becomes prohibitive. However, it may be possible to apply some form of averaging of adjacent estimators to obtain better dynamic range at the cost of decreased resolution.

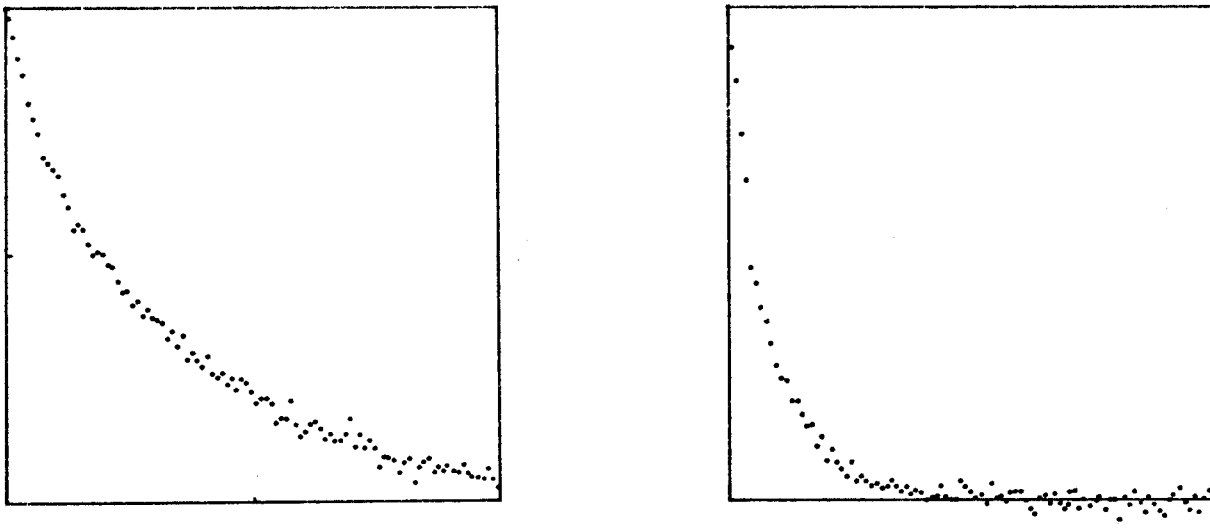

Figure 6.4 Autocorrelation function with equidistantly spaced slots measured at x = 10D, y = o, Re = 22000.

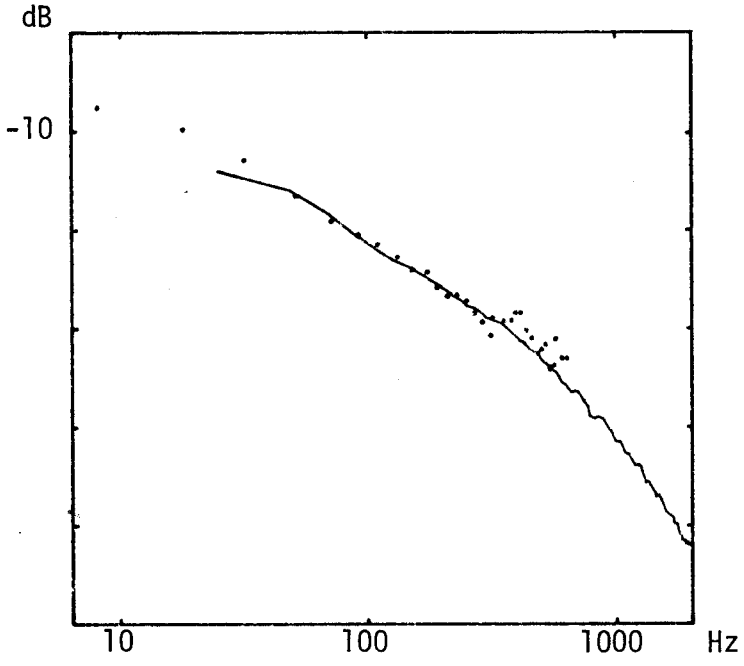

Figure 6.5 Spectrum from the autocorrelation function in Figure 6.4. · LDA measurements; - hot-wire measurements.

To speed up the computations the data array is restructured into the three words:

$$D(1,I) = (u_I - \bar{u}) \cdot W_I$$

$$D(2,I) = t_I - t_{I-1} \qquad (6.3.2)$$

$$D(3,I) = W_I$$

The cross products D(1,I)*D(1,J) are accumulated in an array C1(K) and the cross products D(3,I)*D(3,J) are accumulated in an array W1(K). The value of K is determined from the definition of the slots:

$$K = 1 + \mathrm{INT}\left(\sum_{N=I}^{J} D(2,N)/TAU\right) \qquad (6.3.3)$$

The autocovariance estimate C(K) is determined after the completion of NBATCH batches as

$$C(K) = C1(K)/WI(K) \qquad (6.3.4)$$

and assigned to the lag value

$$T(K) = (K-0.5)*TAU \qquad (6.3.5)$$

The autocorrelation function is found by normalization with C(1).

The spectrum is computed by a conventional cosine transform of the autocorrelation. Since no "zero-lag" value is present in the autocorrelation the spectrum is simply:

$$S(L) = \sum_{K=1}^{NSLOT} C(K)D(K)\cos(2\pi F(L)T(K)) \qquad (6.3.6)$$

where the frequencies F(L) are:

$$F(L) = L/(2*T(L)) \qquad (6.3.7)$$

and D(K) is a spectral smoothing window, e.g. a Bartlett or Hanning window:

A larger dynamic range can be obtained by the method of logarithmically distributed slots described by Gaster and Roberts (1975). By using logarithmically decreasing slot widths as the time lag is decreased and correspondingly spectral estimates of bandwidth increasing with frequency, a more efficient method is obtained for computing spectra covering a large dynamic range. The method used here is outlined with reference to the flow chart in Figure 6.6. The time lag range is defined by the selection of the number of slots per decade, NDE, and the number of decades, NDEC, resulting in the total number of points, NSLOT = NDE*NDEC. The slots are defined by the logarithmically decreasing slots:

$$T(I) = TLAG*10^{((I-1)/NDE-NDEC)} \tag{6.3.10}$$

and the autocovariance estimates

$$C(K) = C2(K)/W2(K) \tag{6.3.11}$$

are assigned to the time lag value

$$T(K) = TLAG*10^{((I-1.5)/NDE-NDEC)} \tag{6.3.12}$$

The spectral estimates are obtained as before as a cosine transform of the autocovariance function. Folllowing Gaster and Roberts (1975) we may introduce an adjustable 1/Q'th octave bandwidth and a spectral window accordingly. The spectral estimate is

$$S(L) = \sum_{K=1}^{NSLOT-R} C(K)D(K-R)\cos(2\pi QF(L)T(K)) \tag{6.3.13}$$

with

$$F(L) = L/2*T(L)) \tag{6.3.14}$$

and windows defined as before (eq. 6.3.8 and 6.3.9).

The logarithmic slot width procedure is able to provide smooth spectra with a good resolution at low frequencies and a large dynamic range. The

```
      SUBROUTINE AUTO
C
      TAU = TLAG*10.**(-NDEC)
      TF = 10.**(1./NDE)
C
      DO 100 I = 1,NDATA-1
C
      K = 1
      TK = TAU
      LAG = 0.
C
      DO 200 J = I+1,NDATA
      LAG = LAG + D(2,J)
110   IF (LAG .LT. TK) GO TO 120
      K = K + 1
      TK = TK * TF
      IF (K .GT. NSLOT) GO TO 130
      GO TO 110
120   C1(K)=C1(K)+D(1,I)*D(1,J)
      W1(K)=W1(K)+D(3,I)*D(3,J)
130   CONTINUE
200   CONTINUE
C
100   CONTINUE
C
      DO 300 K = 1,NSLOT
      C)K) = C1(K) / W1(K)
300   CONTINUE
      RETURN
```

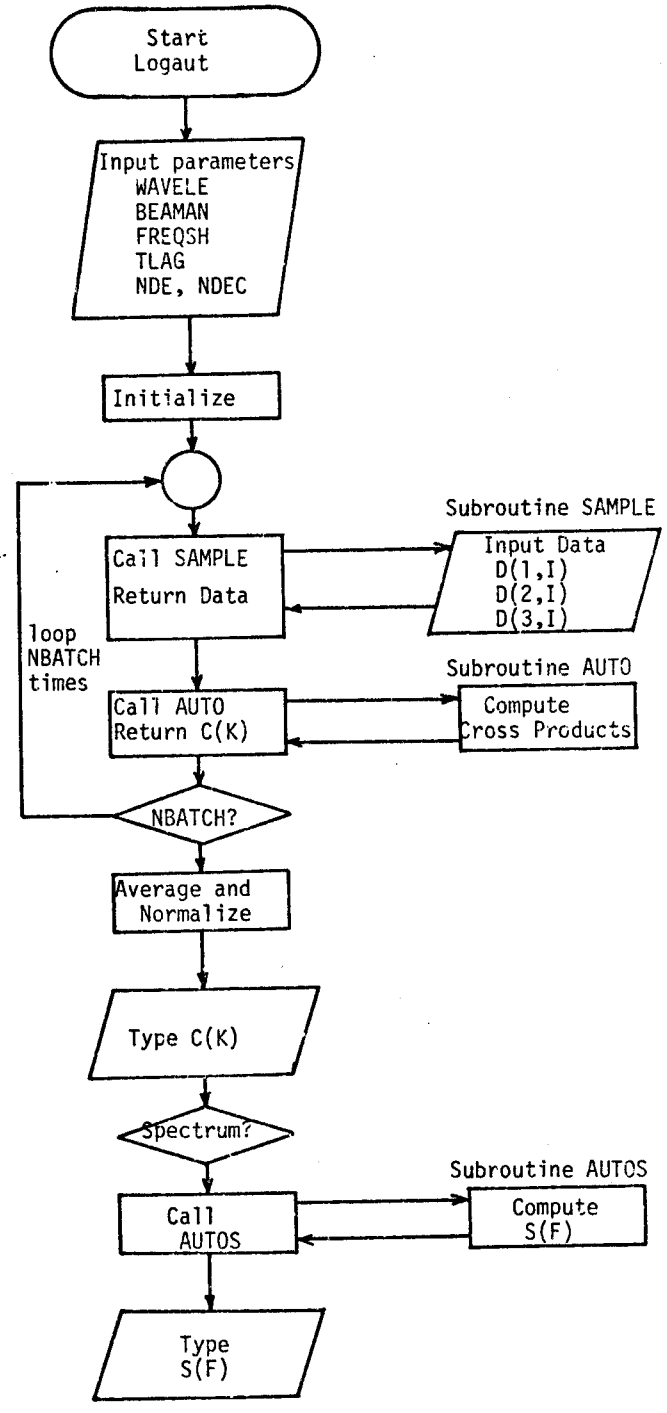

Figure 6.6 Flow chart illustrating the computation of the autocorrelation function with logarithmically spaced slots.

computation time is still excessive, however, compared to the regularly sampled, FFT- based method.

The main reason for the long computing time is the large number of cross products formed in each batch at the long lags. To reduce computing time a modification of the logarithmic slot procedure was used which increases the speed by an order of magnitude, but at the expense of having to adjust the data rate during the measurement.

The modification is essentially to sample only lag values within one decade and to adjust the data rate in such a way that only NDE data points are contained in a record of length $10 \cdot T(K)$, where $T(K)$ is the minimum lag in the decade processed. The program continually displays the optimum data rate. The first batches of the total of NBATCH batches are used to sample the short lags. The lags are increased in such a way that all lags are covered equally during the NBATCH batches. The computing time for forming the cross products is reduced because the data rate may be adjusted so that only a few points occur within each lag. It must be noted that the computer memory should still be large enough to hold a batch record of NDATA = $\nu \cdot T_u$ data points (eq. 6.2.5)

Figure 6.7 and 6.8 show LDA counter and hot-wire autocovariance functions and spectra obtained under the same conditions as in Figure 6.4 and 6.5. The dynamic range is increased without loss of resolution at the low frequency end and without increase in computing time. The LDA spectra are in good agreement with the hot-wire spectra measured at the same point and of comparable quality until the minus 20-30 dB point. At higher frequencies the LDA spectrum is still contaminated by noise. Figure 6.9 and 6.10 show corresponding autocorrelation function and spectrum at a higher velocity (Re = 44000).

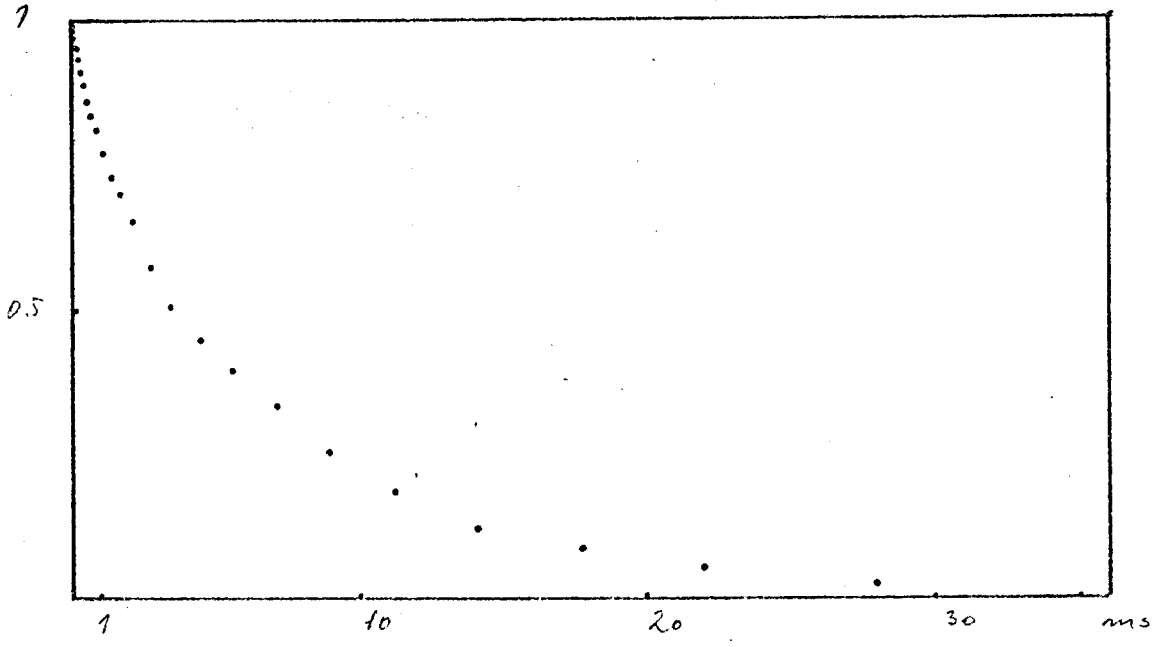

Figure 6.7 Autocorrelation function with logarithmically decreasing slots measured at x = 10D, y = o ; Re = 22000.

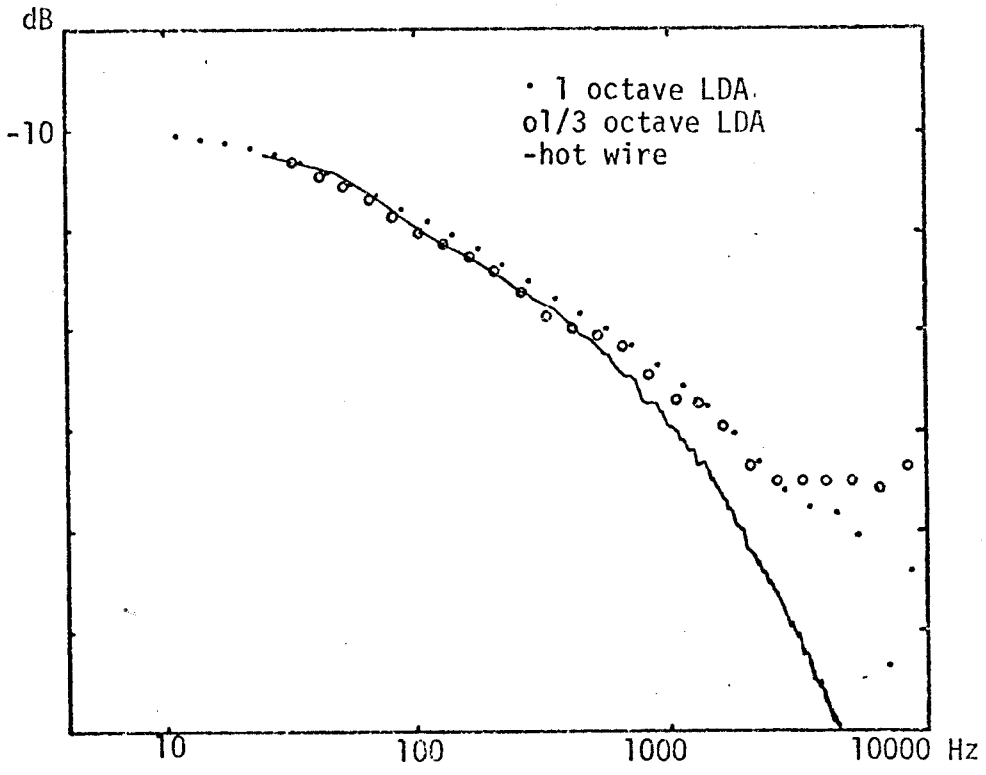

Figure 6.8 Spectrum from the autocorrelation function in Figure 6.7.

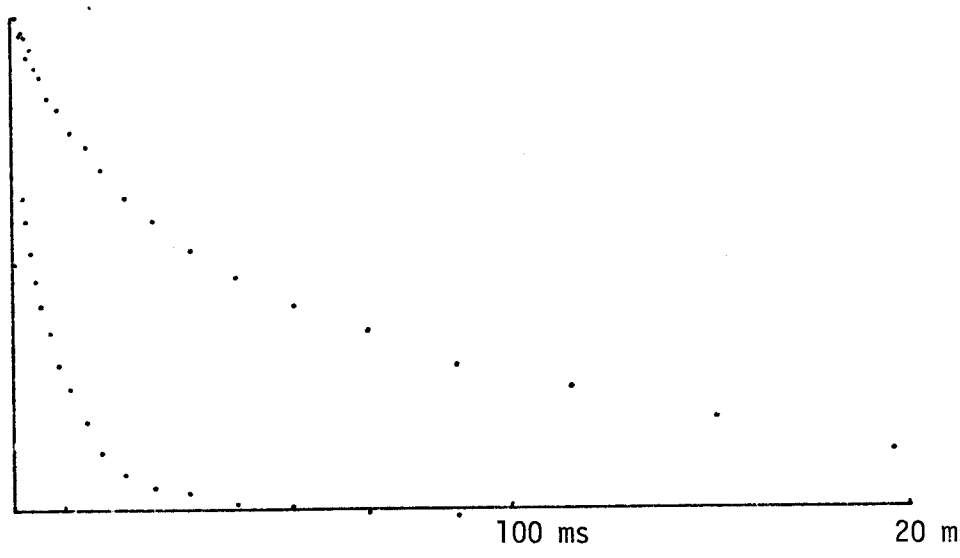

Figure 6.9 Autocorrelation function with logarithmically decreasing slots measured at x = 10D, y = o · Re = 44000.

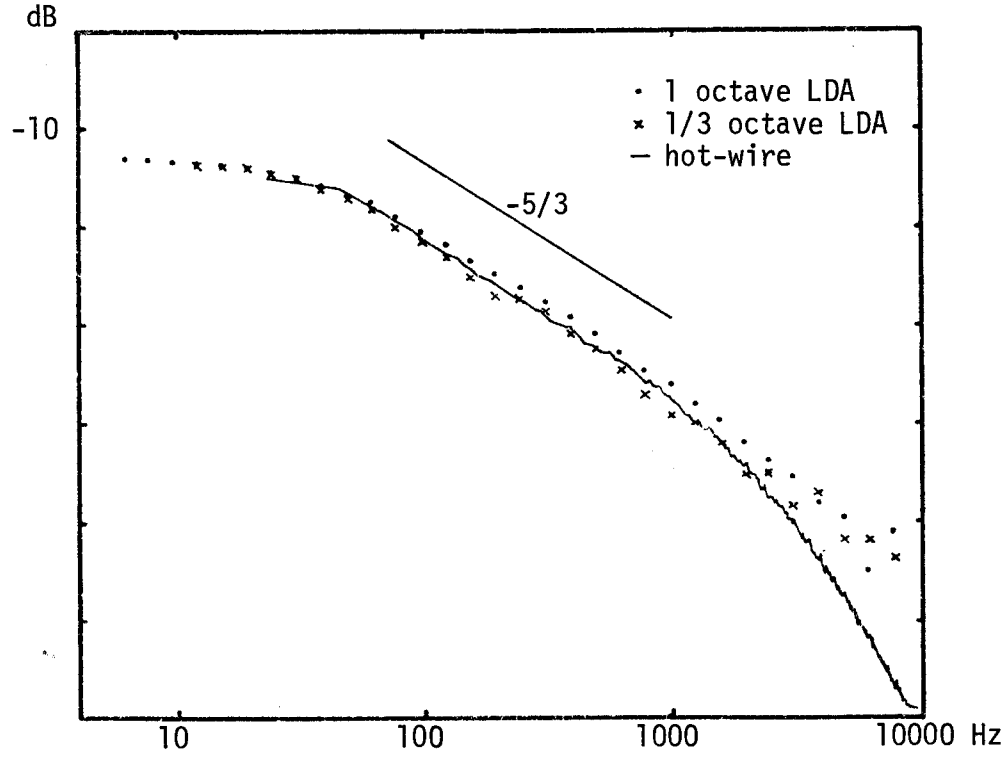

Figure 6.10a Spectrum from the autocorrelation function in Figure 6.9.

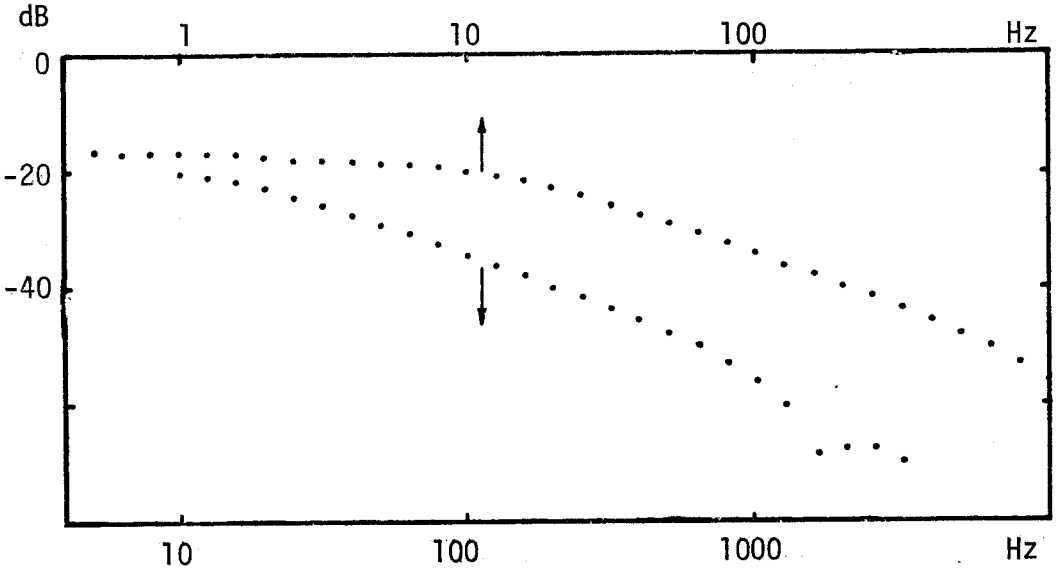

Figure 6.10b Spectrum from estimator $\hat{S}_1$ extending to very low frequencies. Flow conditions as in Figure 6.5.

It is conceivable that the sampling method described above (sampling only lag-values within one decade at a time) can be advantageously extended to sampling only one lag value at a time, if the experimental conditions allow a suitable adjustment of the data rate. This procedure in the time domain would be equivalent to the direct spectral estimate in the frequency domain described in the next section.

6.4 Measurement of Spectrum by Direct Fourier Transform.

The direct power spectral estimator S_2 (eq. (4.6.7), analogous to the classical periodogram, has been implemented in the batch processing technique used in the present system. The direct transform of the randomly sampled data has the advantage of allowing the formation of spectral estimates at any frequency independently. In this technique logarithmically spaced estimates (or any other system for frequency selection) are easily implemented. The disadvantage of the method is the requirement for repeated evaluation of cosine and sine functions. To reduce the time needed for computations the cosine and sine functions were discretized and stored in a "look-up" array.

There is a distinct difference between the sampling methods that are most straightforwardly used to form the spectral estimators ($S_1(\omega)$ and $S_2(\omega)$, a difference, which was already discussed in section 6.2. The autocovariance function which forms the basis for estimator $S_1(\omega)$ is formed from batches of a certain number of data points (NDATA). Thus the summation in eq. (6.2.1) is over a fixed number of samples. In the estimator $S_2(\omega)$ it is most practical to form the estimate by the method of block averaging (analogous to the method described in Welsh (1967)). Each block or batch estimate is formed from an expresion like eq. (4.6.2), but including a spectral window, which defines the bandwidth of the estimate and determines the end of the summation. Because of the random sampling $S_2(\omega)$ is formed

from a random number of samples. The expression for the complete estimator used here is:

$$\hat{S}_2(\omega) = \frac{1}{NBATCH} \sum_{B=1}^{NBATCH} \hat{S}_{2,B}(\omega) \tag{6.4.1}$$

where

$$\hat{S}_{2,B}(\omega) = \frac{T_B}{2\pi \left| \left(\sum_{i=1}^{N_B} t_i \right)^2 - \sum_{i=1}^{N_B} \Delta t_i^2 \right|}$$

$$\times \left| \left| \sum_{i=1}^{N_B} u_i \Delta t_i D(t_i) e^{i\omega t_i} \right|^2 - \sum_{i=1}^{N_B} (u_i \Delta t_i)^2 \right| \tag{6.4.2}$$

where $D(t_i)$ is the window function (see eq. (6.3.8) and (6.3.9)), and N_B is the (random) number of samples obtained within the window $D(t_i)$.

Sampling over a fixed time instead of a fixed number of data points has the further advantage that the residence time weighting is correct also for batch record lengths shorter than the integral scale. It is only necessary that all samples occurring during the sampling period are accepted (n memory overflow), and that periods between sampling are of equal lengths Sampling during a fixed period (resulting in a random number of samples in a batch) with the residence time weighting applied is completely equivalent to the conventional equispaced sampling with fixed batch length.

The method is illustrated in Figure 6.11 which shows a flow diagram of a FORTRAN program, which provides logarithmically spaced spectral estimates according to eqs. (6.4.1) and (6.4.2). Figure 6.12 shows a spectrum measured under the same experimental conditions as those of Figure 6.4 and 6.7. The same total number of data points was used and the spectra have the same bandwidth (1/3-octave bandwidth).

```
      SUBROUTINE SPEC
C
      SUM = 0.
      SUMC = 0.
      SUMS = 0.
      SUMD1 = 0.
      SUMD2 = 0.
      ARG = 0.
C
      DO 100 I = 1,NDATA
      ARG = ARG + D(2,I)
      IF (ARG .GT. 2.*PI) GO TO 110
      WIND = .5 * (1. - COS(ARG/Q))
      SUM = SUM + D(1,I)*D(1,I)*WIND*WIND
      SUMC = SUMC + D(1,I)*WIND*COS(ARG)
      SUMS = SUMS + D(1,I)*WIND*SIN(ARG)
      SUMD1 = SUMD1 + D(3,I)
      SUMD2 = SUMD2 + D(3,I)*D(3,I)
  100 CONTINUE
      SNUM = SUMC*SUMC + SUMS*SUMS - SUM
      SDEN = SUMD1*SUMD1 - SUMD2
C
      S(F) = S(F) + SNUM / SDEN
C
      RETURN
```

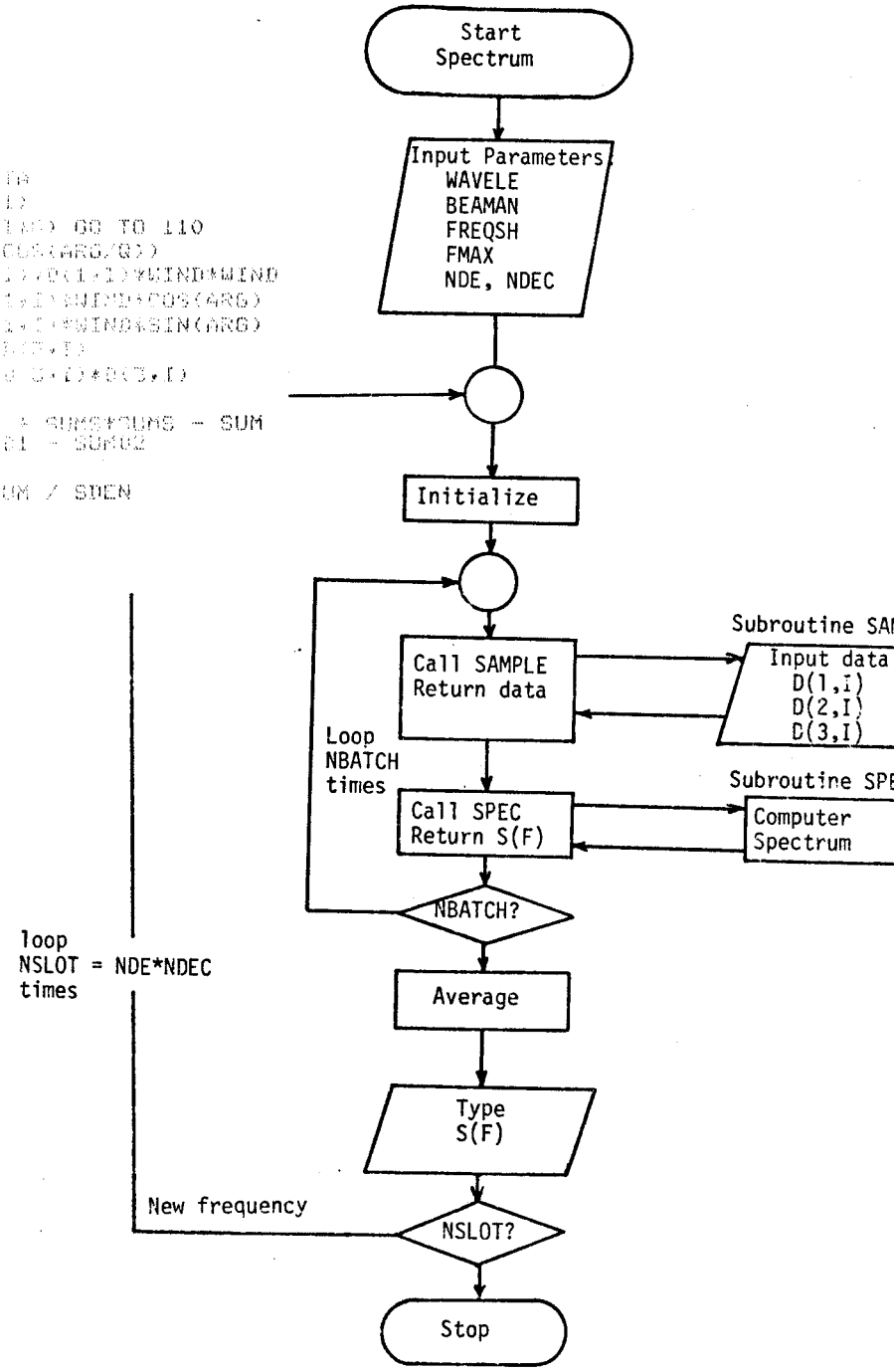

Figure 6.11 Flow chart illustrating the computation of the spectrum by the direct transform.

The variability of the direct transform was appreciably greater than that of the slotted autocovariance method even though the bandwidths were equal and the measuring time was appreciably longer. However, this may partly be due to a less efficient way of handling the data, and may be improved with further development of the data processing. At any rate, the direct method is more convenient to work with, since it can provide spectral estimates at a few, widely separated points relatively quickly, whereas the estimator $S_1(\omega)$ can only be formed after the measurement of the full covariance function.

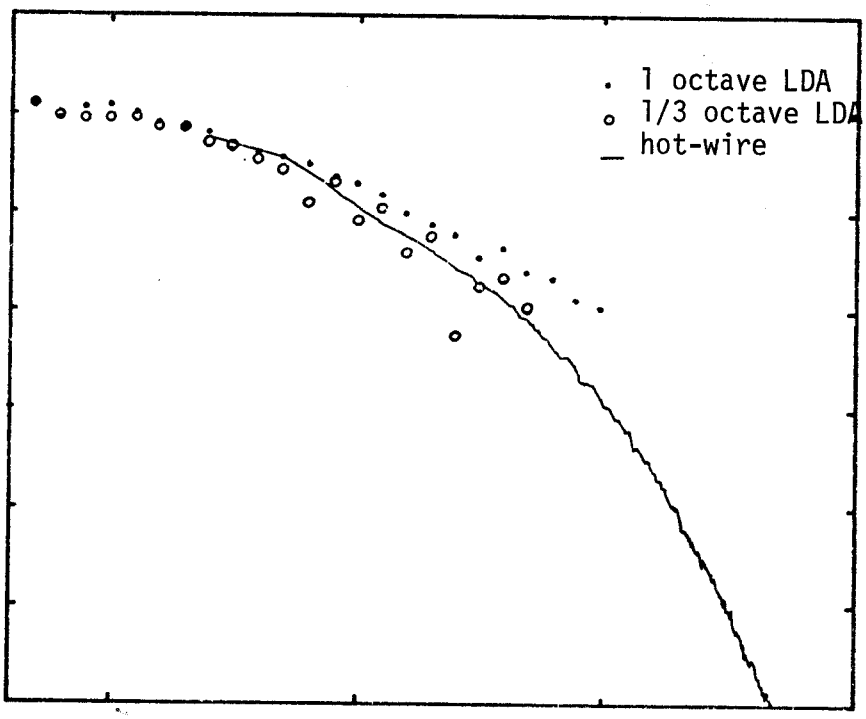

Figure 6.12 Spectrum from estimator $\hat{S}_2$ (direct transform). Flow conditions as in previous figures.

7. Characteristics of Tracker Output with Drop-Out Detection and Sample-and-hold Type Counter Analog Output

7.1 Drop-out Detection and Counter Analog Output

It is well known that the "continuous Doppler signal", even in cases where many particles are present simultaneously in the measuring volume, is characterized by random amplitude and phase fluctuations. No real tracker can track these phase fluctuations exactly, and no real tracker can stay locked to the signal during the amplitude minima occurring in the signal. Momentarily or permanently the lock between the tracker oscillator (VCO) and the signal can be broken and the tracker encounters a so-called drop-out. In modern trackers the tracking performance is monitored by a drop-out detector, which indicates the presence of a drop-out when the correlation between the signal and the tracker oscillator falls below a preset level. Under normal operating conditions drop-out is associated with signal amplitude fluctuations caused by phase cancellations between many particles in the measuring volume, and the duration of a drop-out is of the order of a few times the transit time for a particle through the measuring volume. In other cases drop-out may of course take place because of an absence of particles in the volume. Since tracking is normally reestablished after a drop-out lasting only a few particle transit times, drop-out periods are normally short compared to the time scales of the flow. A typical drop-out case is illustrated in Figure 7.1 which shows at the bottom the Doppler signal, next the control voltage to the tracker oscillator (the VCO control voltage) and at the top the tracker output including drop-out periods where the signal during drop-out has been replaced by the last measured value. It may be noted from the figure that the VCO control voltage during an amplitude minimum (where the maximum phase fluctuations occur) shows a characteristic spike resulting from

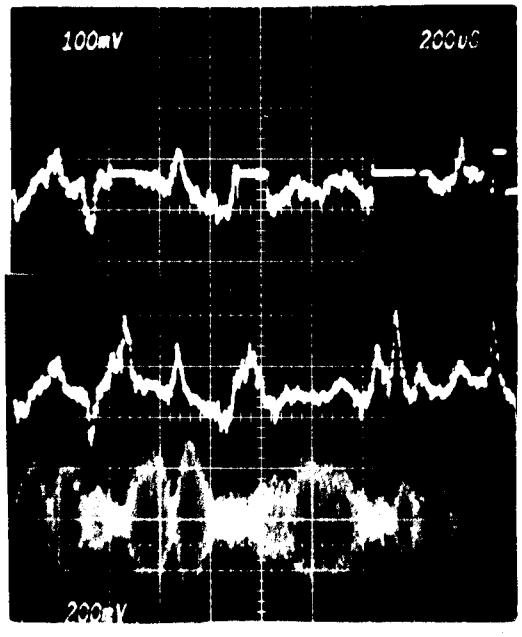

Fig. 7.1 Oscilloscope traces showing (from bottom): The Doppler signal, the tracker VCO signal and the tracker output with drop-out protection (the threshold set to eliminate the large phase fluctuations).

the attempt to stay locked during a phase jump.

With this particular tracker (DISA 55N20) a reduction in the rms ambiguity noise to 1/3 the value without drop-out detection can be obtained by adjusting the signal amplitude relative to the drop-out level in such a way that the tracker only is locked to the large amplitude bursts of the signal (drop-out percentage about 50).

The way the tracker output is processed during a drop-out has an important influence on the results of the measured statistical flow parameters such as mean and mean square velocity, higher moments, probability density, correlations and spectra. To examine this influence, we must make some assumptions about the occurrence of drop-out.

We assume that both the drop-out occurrence and the fraction of time "out" are independent of the instantaneous velocity. These assumptions are in concordance with the known properties of the many-particle Doppler signal presuming no correlation between velocity and spatial distribution of particles exists and presuming no effects (electronic or otherwise) cause the tracker to loose lock preferentially at any particular frequencies within its tracking range.

The case of the counter analog-out is more straightforward; most LDA-counter analog outputs are simply a digital-to-analog conversion of the measured Doppler frequency of a Doppler burst. The analog voltage is switched instantaneously to a new value at the occurrence of a data-ready pulse, and this value is held until the next data-ready pulse comes along. The output is thus a sample-and-hold type signal, but the sample times are random and obey the same statistics as described under LDA-burst processing (Section 4). In this analog mode, bias problems will occur if the mean sampling rate is lower than the Nyquist sampling rate for the velocity signal.

7.2 Effect of Tracker Drop-out

The statistics of the many-particle Doppler signal is described in detail in George and Lumley (1973) and George (1976). The probability that the Doppler signal amplitude R is below a given value, R_1 say, is given by

$$P[R<R_1] = 1 - \exp\left[-\frac{R_1^2}{2\overline{i^2}}\right] \qquad (7.2.1)$$

where $\overline{i^2}$ is the mean square Doppler current. If the dropout threshold is given, the drop-out percentage (the fraction of time the tracker is in drop-out condition) can be computed.

With the assumptions about the occurrence of drop-out given in Section 7.1 and further assuming (Lumley 1978) that the drop-out process can be assumed a Markov chain with a transition probability from "in" to "out" in any interval dt of μdt and a transition probability from "out" to "in" in the interval dt of νdt, we find that the probability of being "in" at any instant is $(1 + \mu/\nu)^{-1}$, while the probability of being "out" is $(1 + \nu/\mu)^{-1}$. The latter corresponds to the result computed from the amplitude probability distribution above. For all cases of interest $\nu/\mu << 1$, which is to say that the tracker is "in" most of the time.

To analyze the tracker output an indicator function I(t) is defined as suggested by Lumley (1978), i.e. a function which has the value +1 when the tracker is "in" and 0 when the tracker is "out". The expected value of I is clearly $\overline{I} = (1 + \mu/\nu)^{-2}$. The tracker output signal can thus be represented as:

$$\tilde{f}(t) = f(t) \cdot I(t)$$

where f(t) is the output without drop-out (the tracker response to the instantaneous velocity).

We now consider three ways of handling the signal during drop-out:

1. Setting the output equal to zero during drop-out.
2. Setting the output equal to the mean during drop-out.
3. Holding the signal at its last measured value during drop-out.

Case 1: Output equal to zero during drop-out:

The signal with drop-out is represented by:

$$\tilde{f} = f\, I \tag{7.2.2}$$

The mean value for the output is:

$$\bar{\tilde{f}} = \bar{f}\,\bar{I} = \frac{\nu}{\nu+\mu}\,\bar{f} \tag{7.2.3}$$

Thus the correct mean is not preserved.

The fluctuating component of f is given by:

$$\tilde{f}' = \tilde{f} - \bar{\tilde{f}} = fI - \overline{fI} = \bar{I}f'+I'f'+\bar{f}I' = f'I+\bar{f}I' \tag{7.2.4}$$

and thus

$$\overline{\tilde{f}'^{2}} = \overline{f'^{2}}\;\overline{I^2} + \bar{f}^2\,\overline{I'^{2}} \tag{7.2.5}$$

I(t) has a mean square value given by:

$$\overline{I^2} = \bar{I} = \frac{\nu}{\nu+\mu} \tag{7.2.6}$$

since $I = 1$, and thus a variance given by:

$$\overline{I'^{2}} = \overline{I^2} - \bar{I}^2 = \bar{I}(1-\bar{I}) \tag{7.2.7}$$

Thus

$$\overline{\tilde{f}'^{2}} = \bar{I}\,\overline{f'^{2}} + \bar{I}(1-\bar{I})\bar{f}^2$$

or

$$\overline{f'^{2}} = \left(\frac{\nu}{\nu+\mu}\right)\overline{f'^{2}} + \frac{\nu\mu}{(\nu+\mu)^2}\,\bar{f}^2 \tag{7.2.8}$$

The autocovariance of $\tilde{f}$, $R_{\tilde{f}} = \overline{\tilde{f}(t)\tilde{f}(t+\tau)} = \bar{\tilde{f}}^2 \cdot \rho_f$, where ρ is the autocorrelation function, is easily shown to be given by:

$$R_{\tilde{f}} = \overline{(\bar{I}f'(t)+I'(t)f'(t)+I'(t)\bar{f})\cdot(\bar{I}f'(t+\tau)+I'(t+\tau)f'(t+\tau)+I'(t+\tau)\bar{f})}$$

$$= \bar{I}^2 R_f + \bar{f}^2 R_I + R_f R_I \tag{7.2.9}$$

where R_f and R_I are the autocorrelations of f and I respectively.

Consider two limiting cases: (1a) The integral scale of the flow is much less than the average drop-out period, and (1b), the average drop-out period is much less than the flow integral scale.

Case (1a): Flow integral scale << average drop-out period.

Since the flow will become uncorrelated more rapidly than the drop-out signal we will have

$$\rho_f \rho_I \simeq \rho_f$$

or using equation (7.2.7) and equation (7.2.9)

$$R_f \cong \overline{I}\, R_f + \overline{I}(1-\overline{I})\, \overline{f}^2 \qquad (7.2.10)$$

Thus the autocovariance is reduced and goes to a non-zero value at large times.

By Fourier transforming equation (7.2.10) it follows immediately that

$$S_{\tilde{f}} \simeq \overline{I}\, S_f + \overline{I}\, (1-\overline{I})\, \overline{f}^2 \delta(\omega) \qquad (7.2.11)$$

Thus aside from the scale factor $\overline{I}$ and the spike at the origin, long drop-out periods have no effect on the spectrum. The fact that these drop-out occurrences must be independent of the flow field rules out the case of drop-out due to a scarcity of particles.

Case (1b): Average drop-out period << flow integral scale.

In this case the rate of decay of the drop-out correlation dominates the product and

$$\rho_f \rho_I \sim \rho_I$$

from which it follows that

$$R_{\tilde{f}} \cong \overline{I}^2 R_f + (\overline{f}^2 + f'^2) R_I \qquad (7.2.12)$$

Since the drop-out occurrence is assumed to be Markovian, the auto-correlation is given by

$$R_I = \overline{I'^2} e^{-(\mu+\nu)|\tau|} \simeq \frac{\mu}{\nu} e^{-\nu|\tau|} \tag{7.2.13}$$

since the signal is mostly "in". It follows immediately by Fourier transforming that

$$S_I(\omega) \simeq \frac{\mu}{\pi\nu^2} \frac{1}{1+(\omega/\nu)^2} \tag{7.2.14}$$

Thus the high frequency end of the noise spectrum rolls off as frequency squared.

It follows by Fourier transforming equation (7.2.12) and using equations (7.2.6) that

$$S_{\tilde{f}} \simeq \frac{\mu}{\mu+\nu} S_f + \frac{\mu}{\pi\nu^2} \cdot \frac{(\overline{f}^2+\overline{f'^2})}{1+(\omega/\nu)^2} \tag{7.2.15}$$

For the usual case where $\overline{f} > f'$, the flow spectrum, S_f, is seen to be completely obscured by the drop-out noise spectrum S_I.

Case 2: Output set equal to mean during drop-out.

We can now represent the output by:

$$\tilde{f}(t) = f(t)\, I(t) + \overline{f}(1-I(t)) \tag{7.2.16}$$

The mean value is now preserved:

$$\overline{\tilde{f}} = \overline{f}\,\overline{I} + \overline{f}(1-\overline{I}) = \overline{f} \tag{7.2.17}$$

but the variance (and higher moments) is not:

$$\tilde{f}' = f'I = f'(\overline{I}+I') \tag{7.2.18}$$

The mean square fluctuation and the autocovariance are given by equations (7.2.8) and (7.2.9) respectively with $\overline{f}$ set equal to zero. Thus the noise level introduced by the drop-out on these measurements is considerably reduced since the spectral height of the noise is now determined only by the drop-out and the mean square fluctuation. The results for the two cases considered above are listed below.

Case (2a): Flow integral scale << average drop-out period

From equations (7.2.10) and (7.2.11) it follows that

$$R_{\tilde{f}} \cong \bar{I}\, R_f \tag{7.2.19}$$

and

$$S_{\tilde{f}} \cong \bar{I}\, S_f \tag{7.2.20}$$

Thus both the autocovariance and spectrum shapes are accurately reproduced

Case (2b):

From equations (7.2.12) and(7.2.15) it follows immediately that

$$R_{\tilde{f}} \sim \bar{I}^2\, R_f + \overline{f'^2}\, R_I \tag{7.2.21}$$

and

$$S_{\tilde{f}} \simeq \frac{\mu}{\mu+\nu}\, S_f + \frac{\mu}{\pi\nu^2}\, \frac{\overline{f'^2}}{1+(\omega/\nu)^2} \tag{7.2.22}$$

The spectrum is slightly reduced and a noise spectrum of the order $\overline{F'^2}$ is added.

Case 3: Output holds last value.

This method is common practice in commerical LDA- trackers. The output signal can be represented by:

$$\tilde{f}(t) = f(t)\, I(t) + \hat{f}(t)[1-I(t)], \tag{7.2.23}$$

where

$$\hat{f}(t) = f(t_k) \text{ for } t_k \leq t < t_{k+1} \tag{7.2.24}$$

and t_k ($k = 1, 2, \ldots$) are the drop-out times.

The mean and all higher moments are now preserved:

$$\overline{\tilde{f}} = \overline{f}\,\overline{I} + \overline{\hat{f}}(1-\overline{I}) = \overline{f} \tag{7.2.25}$$

since $\overline{\hat{f}} = \overline{f}$. Thus also $\overline{f^n} = \overline{f^n}$.

The autocovariance of the output is:

$$R_f = \overline{I(t)I(t+\tau)}\ \overline{f'(t)f'(t+\tau)} + \overline{(1-I(t))(1-I(t+\tau))}\cdot\overline{\hat{f}'(t)\hat{f}'(t+\tau)} + \overline{I(t)(1-I(t+\tau))}\ \overline{f'(t)\hat{f}'(t+\tau)}$$

$$= \bar{I}^2 R_f + (1-\bar{I})^2 R_{\hat{f}} + R_I(R_f+R_{\hat{f}}-2R_{f\hat{f}})+2\bar{I}(1-\bar{I})R_{f\hat{f}}$$

where

$$R_{f\hat{f}} \equiv \overline{f'(t)\hat{f}'(t+\tau)}. \tag{7.2.26}$$

Consider again the two limiting cases,

Case (3a): Integral scale of flow << the drop-out period.

$$R_f R_I \simeq \bar{I}(1-\bar{I})R_f,\ R_{\hat{f}}R_I \simeq \overline{f'^2}R_I^2 \text{ and } R_{f\hat{f}}.$$

We also have $R_{\hat{f}}R_I \simeq \overline{f'^2}R_I^2$ since $R_{\hat{f}} \simeq \overline{f'^2}R_I$.

Finally we must have $R_{f\hat{f}} \simeq 0$ for large times since f(t) will most likely be uncorrelated with its value at the previous drop-out.

Thus the autocovariance reduces to:

$$R_{\tilde{f}} \simeq \bar{I}^2 R_f + (1-\bar{I})\overline{f'^2}R_I^2 \tag{7.2.27}$$

We thus get the correct spectrum slightly reduced plus some low frequency noise due to the drop-out periods.

Case (3b): Average drop-out period << than flow integral scale.

Here we have:

$$R_f \simeq R_{\hat{f}} \simeq R_{f\hat{f}} \text{ and } R_f R_I \simeq \overline{f'^2}R_I.$$

Thus

$$R_{\tilde{f}} \simeq R_f + (R_f+R_{\hat{f}} - 2R_{f\hat{f}})R_I \tag{7.2.28}$$

or

$$S_{\tilde{f}}(\omega) \simeq S_f(\omega) + \frac{\mu}{\pi\nu^2}\cdot\overline{(\Delta f)^2}\left(\frac{1}{1+(\omega/\nu)^2}\right) \tag{7.2.29}$$

The spectrum is increased with a noise term, which is the Fourier transform of a spike at the origin of duration $T_I \simeq 1/\mu$, and a magnitude determined by the difference $\overline{\Delta f^2} = R_f + R_{\hat{f}} - 2R_{f\hat{f}}$, which for $1/\mu \ll T_f$ is small compared to $\overline{f'^2}$. Thus the noise term in the spectrum is reduced relative to case 2b.

In summary, drop-out can affect all statistical properties of the tracker output. The magnitude of the disturbing effect depends on the manner in which the tracker compensates for the drop-out. In the usual mode of operation of the tracker, where drop-outs are short compared to the integral scale of the flow, drop-out is best handled by holding the last measured output until the tracker has again acquired lock. This method preserves all moments of the velocity distribution and adds the least amount of noise to the spectrum. Higher order approximations during drop-out can be envisioned, e.g. linear extrapolation from the last measured value. Such methods might further reduce noise in tracker output, but these methods have not been tested as far as the author is aware. If drop-out periods long compared to the integral scale occur, it might be best to set the output equal to a running average of previously measured values.

It should be noted that the analyses of this section are valid only as long as the occurrence of drop-out and the velocity field are statistically independent. While this can be shown to be approximately the case when the drop-out is due to the random phase fluctuations, this will seldom be the case when drop-out results from an absence of scattering particles. Thus care should be exercised in applying the cases (1a), (2a), and (3a) above to cases of extended drop-out which very often result from an absence of particles.

7.3 Measured Spectra of Tracker and Counter Analog Out

The power spectrum of the tracker and counter analog outputs were measured with a Nicolet "Mini-Ubiquitous" digital spectrum analyzer. The LDA-instruments measured the velocity at the center-line of the free jet at x/D = 10 under different conditions of drop-out percentage and data rate. The spectrum analyzer computed the average of 256 fast Fourier transforms of digitally sampled records of the signal. Figure 7.2a and b show the output of the DISA 55 L 22 tracker in the time domain and in the frequency domain respectively (tracker bandwidth 4% of i.f. frequency, drop-out percentage zero). The spectral level beyond 1 kHz is ambiguity noise. Figure 7.3 shows a corresponding hot-wire spectrum (1mm x 5μ tungsten wire). The spectra below 1 kHz are identical, but the dynamic range of the hot-wire is much better than that of the tracker.

Figures 7.4a and b, 7.5a and b and 7.6a and b show the effect of increasing amount of drop-out on the time trace and spectrum respectively. Figure 7.4a shows the characteristic spikes associated with the ambiguity noise.

Increasing amount of drop-out results eventually in a ω^{-2} roll-off at high frequencies as predicted in the previous section (Figure 7.7), but at intermediate drop-out percentages two effects are present: The ambiguity noise decreases as mentioned in the introduction, but is replaced by the drop-out noise.

Figure 7.8 shows a spectrum of the counter analog output at a high data rate (20 kHz). The measurement is performed under the same circumstances as the previous ones. The counter acts here nearly as a continuous FM demodulator, and the spectrum shows the characteristic ambiguity noise level associated with continuous LDA signal processors. Figures 7.9a and b

and 7.10a and b show time trace and spectrum at lower data rate. The spectrum below 500 Hz is still accurate, but the high frequency part is swamped by the drop-out or sample-and-hold noise. Figure 7.11 measured with a counter data rate of 100 Hz is practically identical to Figure 7.7 measured with the tracker at a drop-out percentage of 80%.

Obviously the analog outputs from neither tracker nor counter can compete with the hot-wire signal as far as noise level and dynamic range are concerned. The advantage of the continuous LDA lies in its ability (with frequency shift included) to measure large fluctuations, even reversing flows without bias. The burst-type LDA does not suffer from ambiguity and can also be corrected for bias. As explained in Chapters 4, 6 and 7 the burst-type LDA may eventually be able to compete with the hot-wire also as concerns spectral resolution and dynamic range.

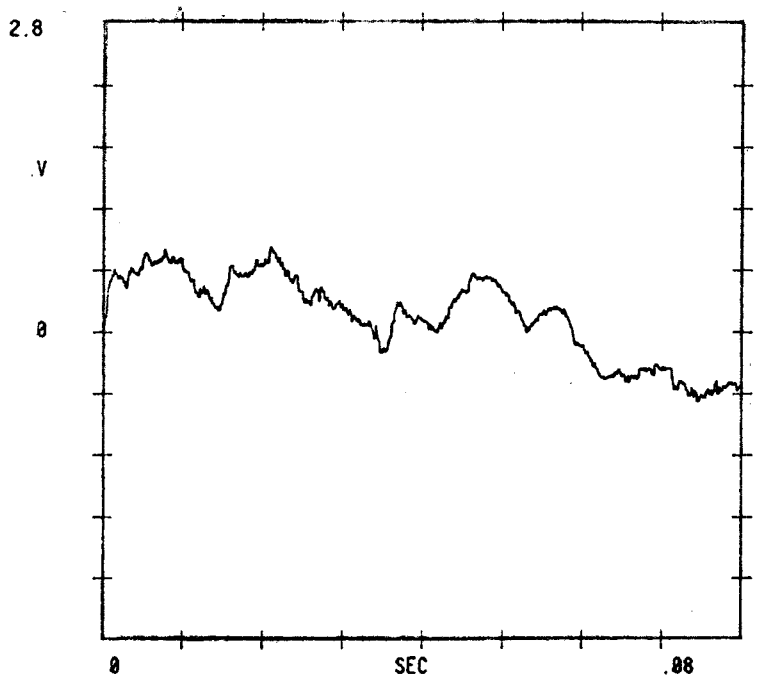

Fig. 7.2a Tracker output in time domain.
(Range 1.5 MHz, Bandwidth 4%).

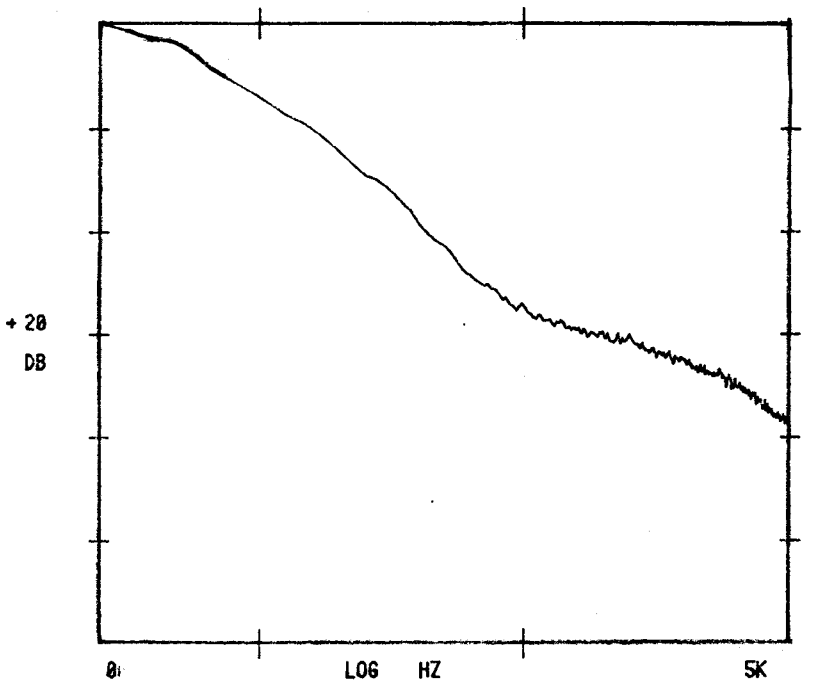

Fig. 7.2b Tracker output in frequency domain.

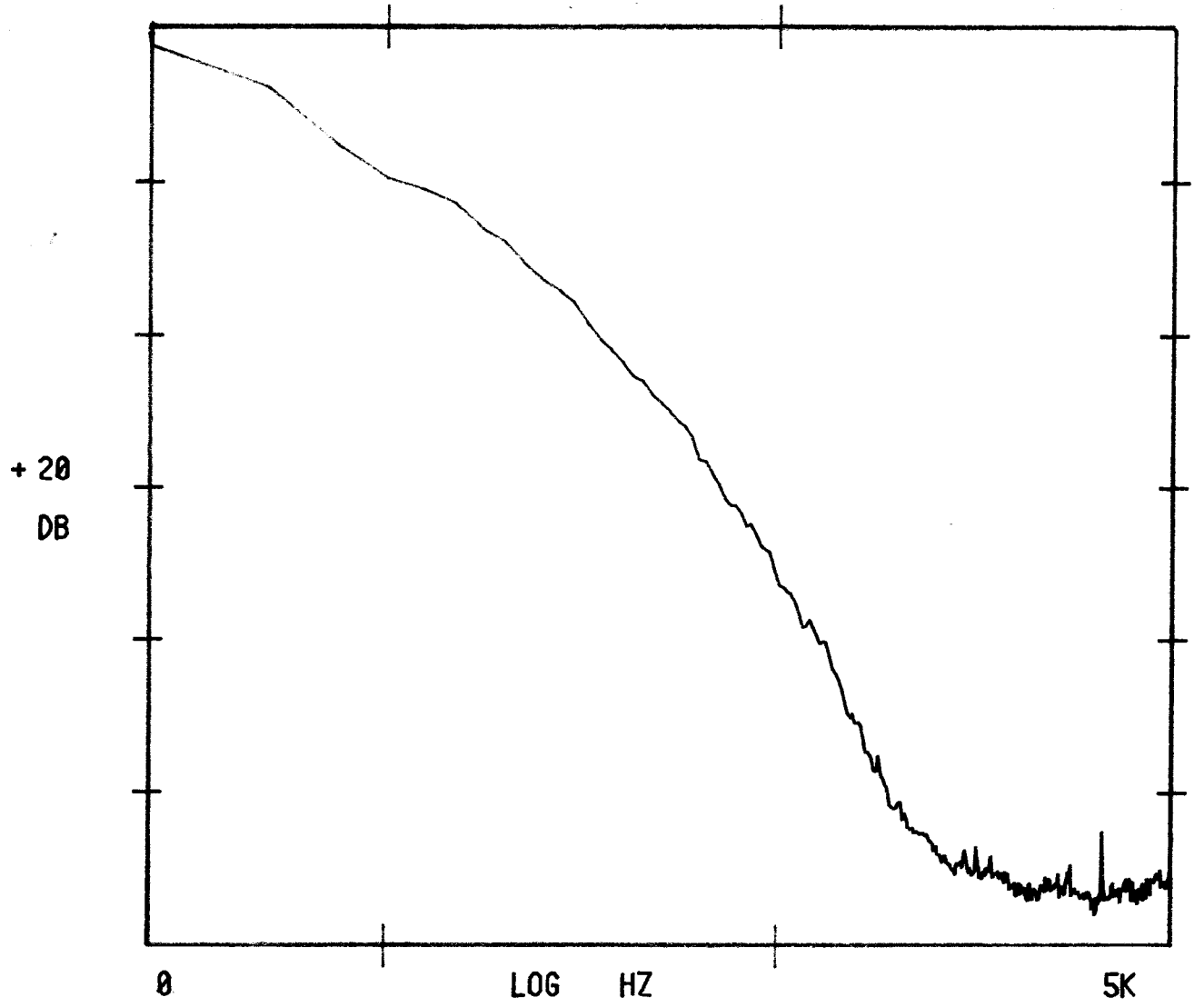

Fig. 7.3 Hot-wire spectrum corresponding to the tracker spectrum of Fig. 7.2b.

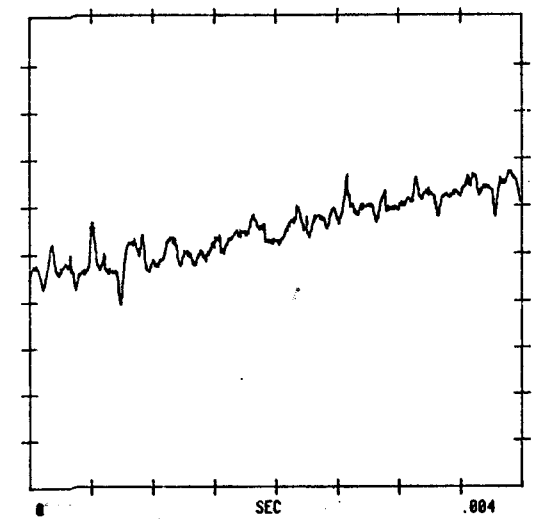

7.4a Tracker output in the time domain. Drop-out pct 0
(Range 1.5 MHz, B.W. 4%, f_D-.2 MHz, f_s-.3 MHz)

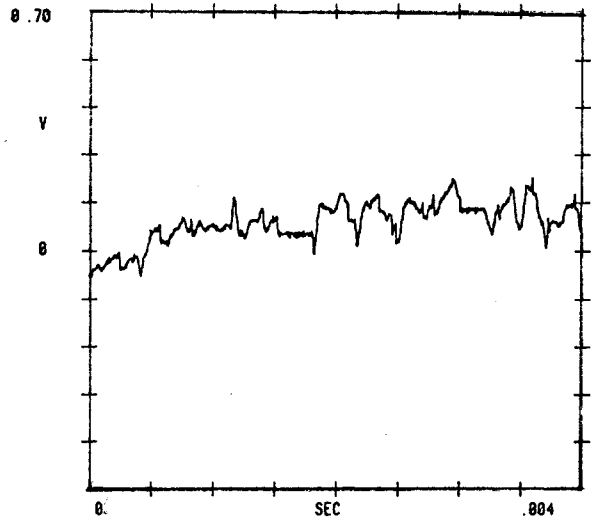

Fig. 7.5a Tracker output in time domain. Drop-out pct. 10.
(Parameters as in Fig. 7.4a)

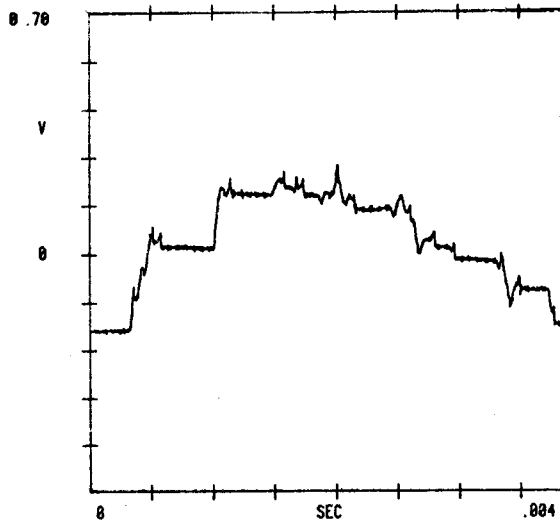

Fig. 7.6a Tracker output in time domain. Drop-out pct.
(Parameters as in Fig. 7.4a).

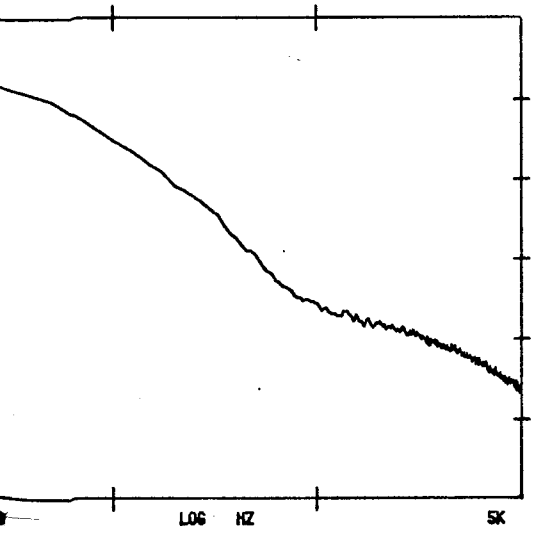

.4b Spectrum corresponding to Fig. 7.4a

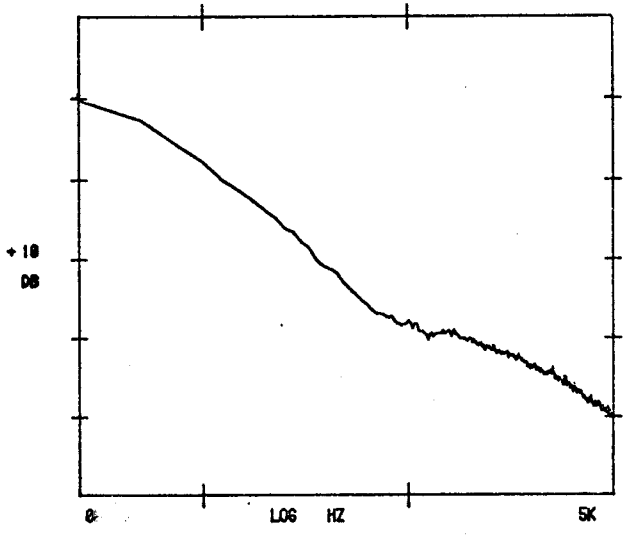

Fig. 7.5b Spectrum corresponding to Fig. 7.5a.

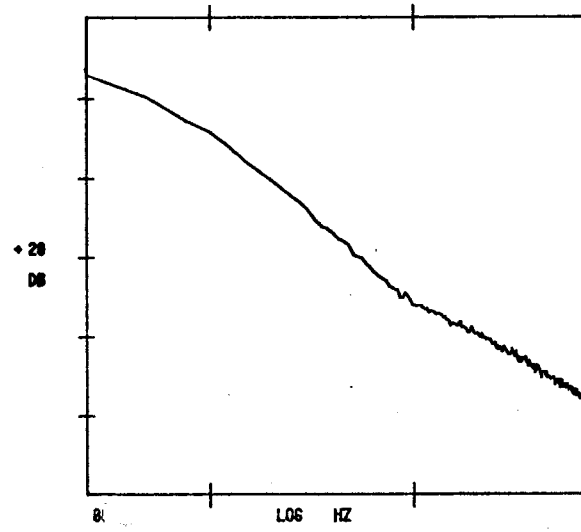

Fig. 7.6b Spectrum corresponding to Fig. 7.6a.

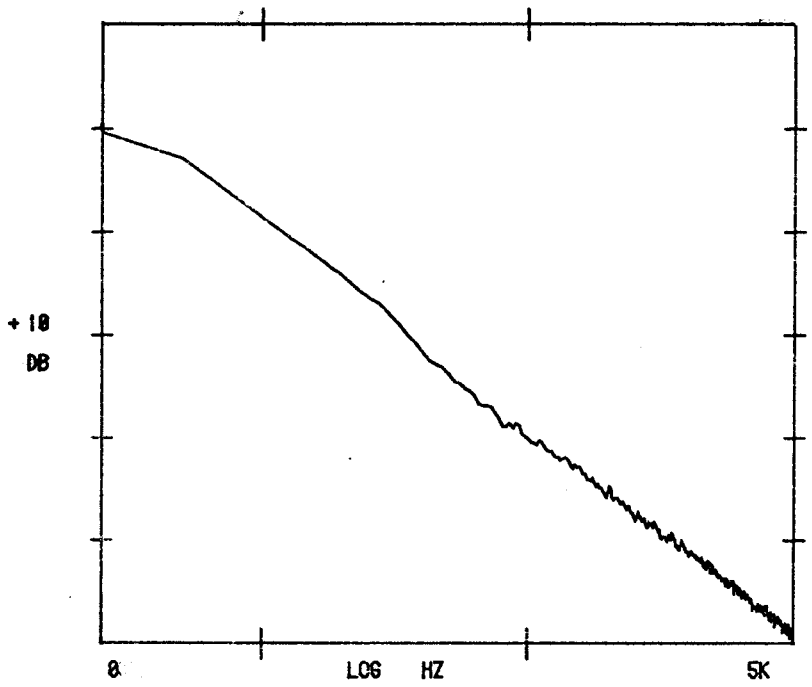

Fig. 7.7 Spectrum of tracker output at drop-out pct. 80. (Parameters as in Fig. 7.4a).

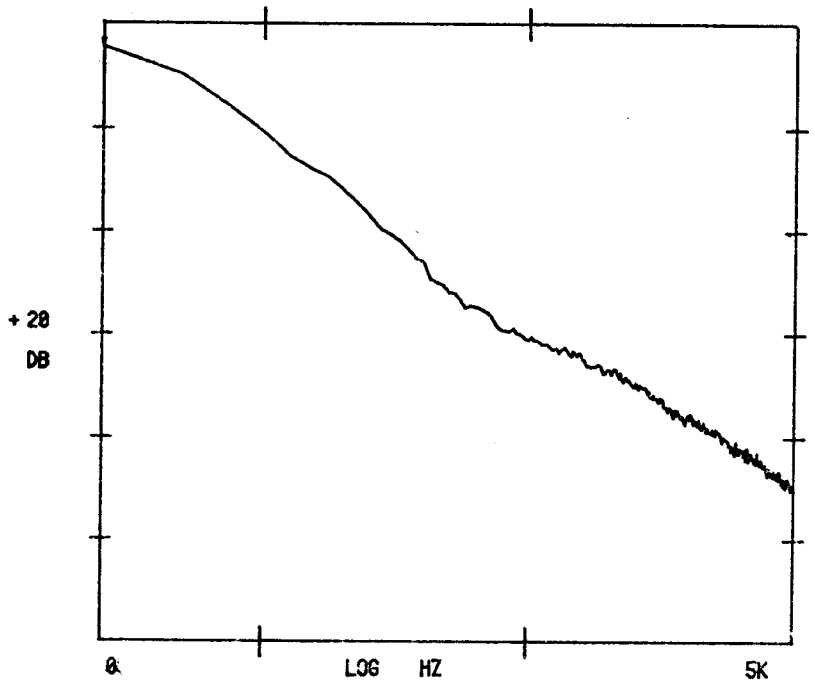

Fig. 7.8 Spectrum of LDA-counter analog out at a high data rate (d.r. 20 kHz)

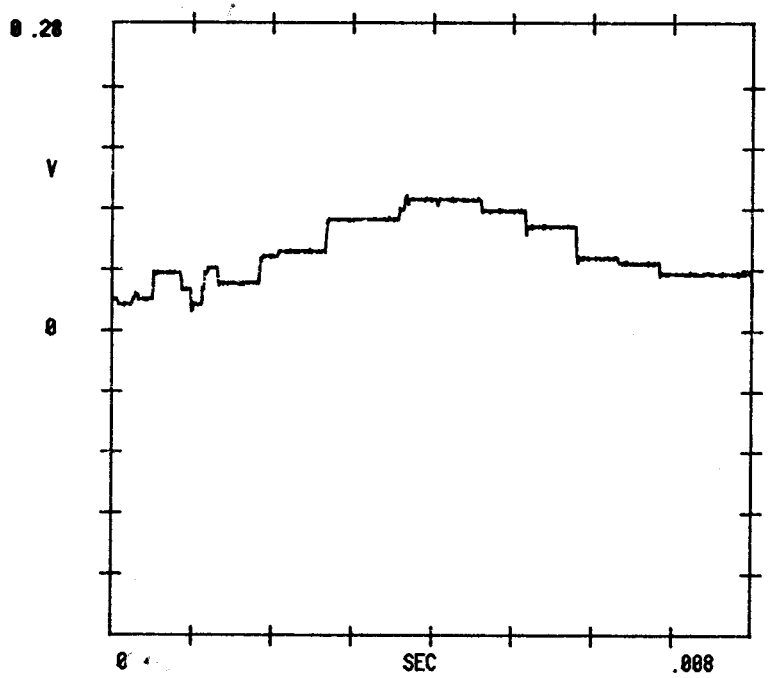

Fig. 7.9a Analog out of counter in time domain. D.r. 6kHz. (high pass 16 kHz, low pass 4 MHz, f_D .2 MHz, f_s=.3 MHz).

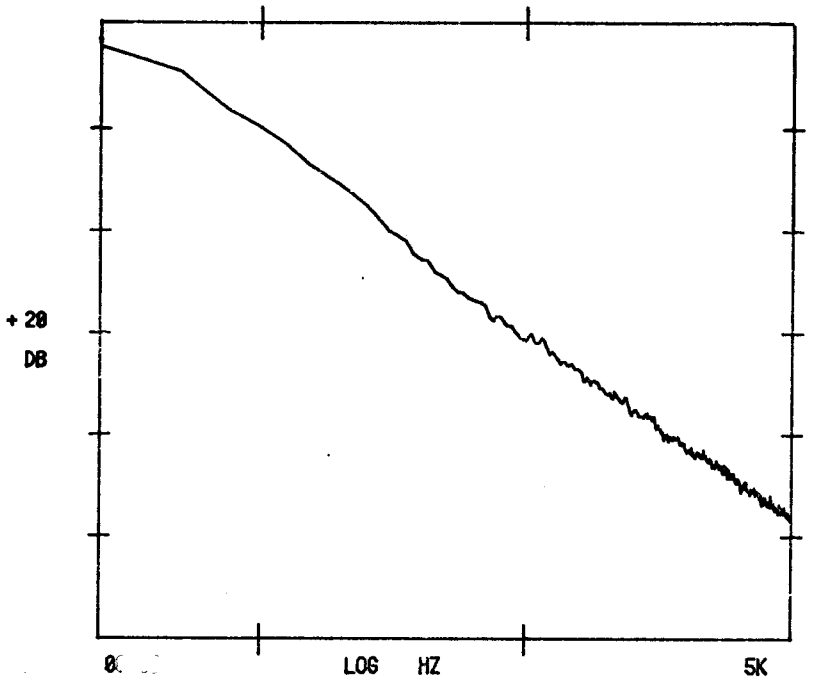

Fig. 7.9b Spectrum corresponding to Fig. 7.9a.

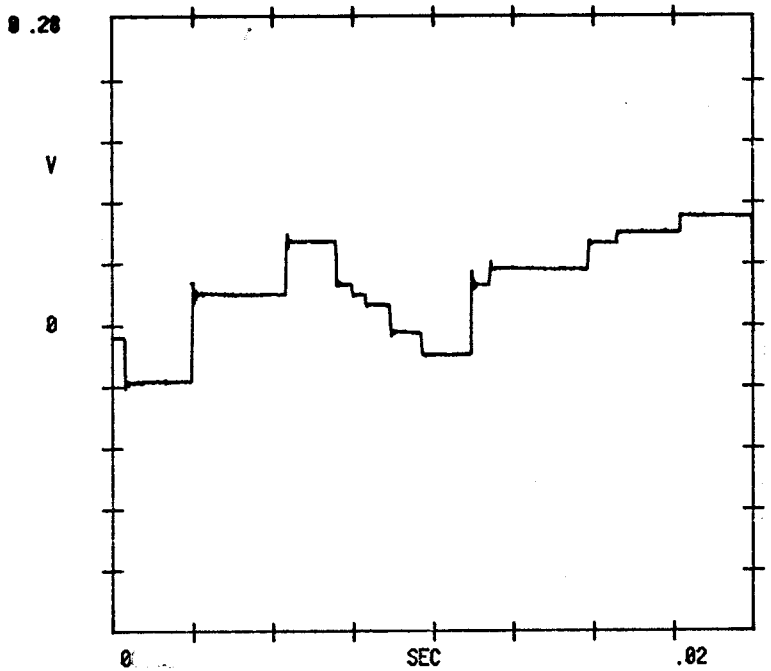

Fig. 7.10a Counter analog out in time domain. D.r. 1.8 kHz. (Parameters as in Fig. 7.9a).

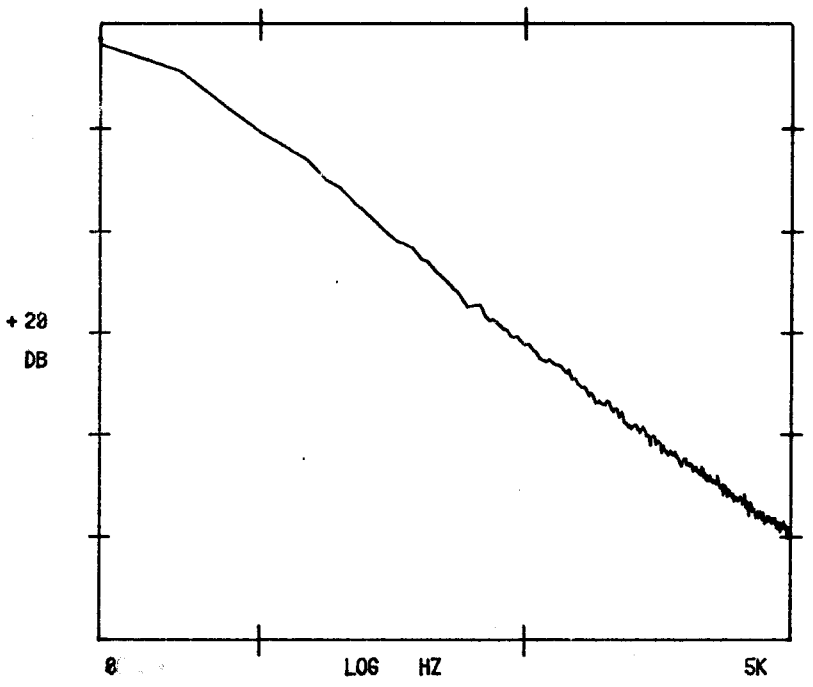

Fig. 7.10b Spectrum corresponding to Fig. 7.10a.

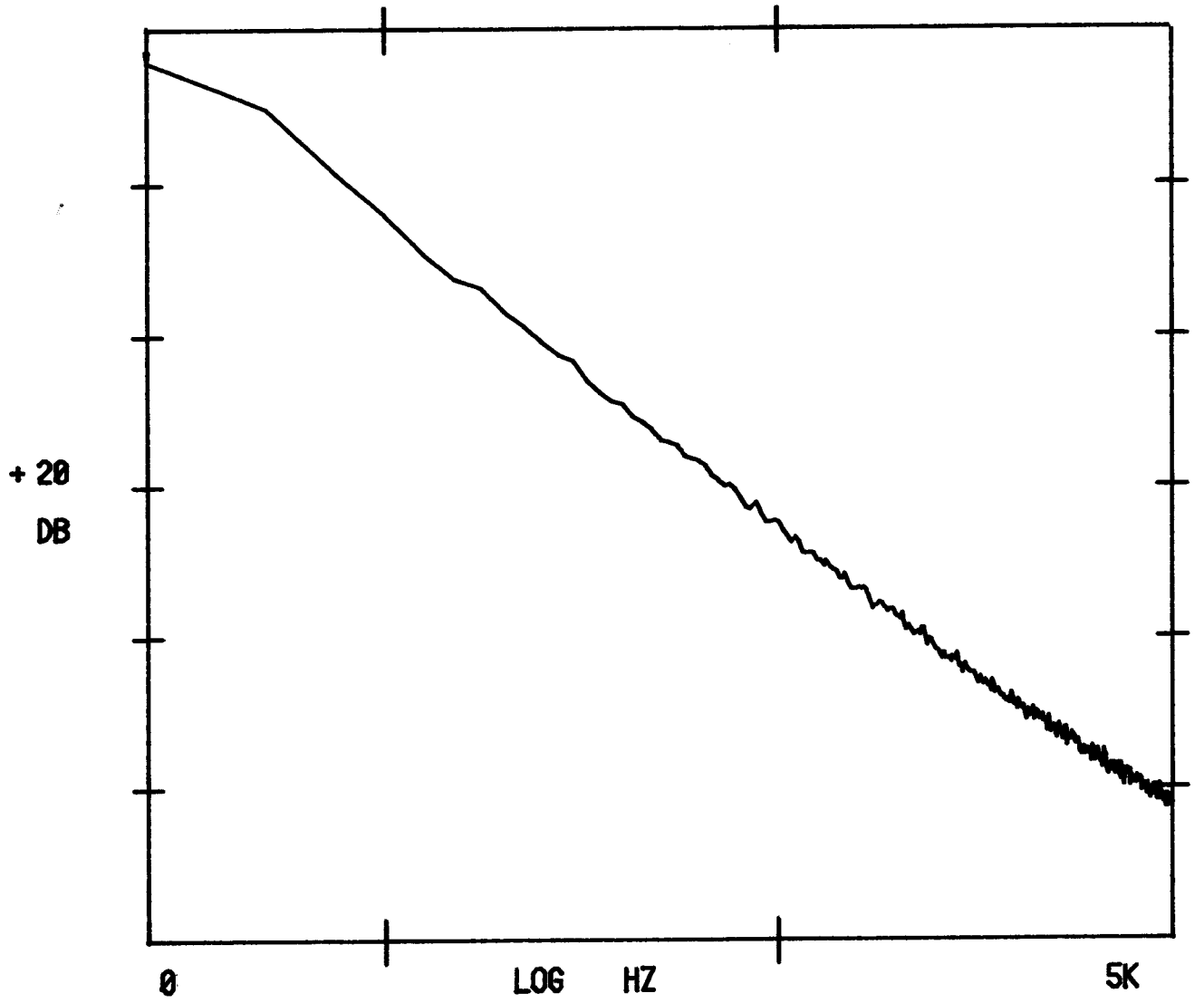

Fig. 7.11 Spectrum of counter analog output at a data rate of 100 Hz. (Parameters as in Fig 7.9a).

8. Summary and Conclusions

The dual-beam, fringe mode LDA has been investigated with particular emphasis on turbulence measurements. The theory of residence-time weighted burst-type LDA signal and data processing has been presented and formulas for mean and mean-square velocity, correlation function and spectrum have been derived. It has been shown that a weighting factor equal to the measured residence-time applied to each measured velocity data point completely removes the so-called velocity bias not only in mean and mean-square measurements, but also in measurements of autocorrelation function and spectrum. Furthermore it has been shown that the particular methods used to form the spectrum result in the cancellation or the elimination of various noise sources such as ambiguity noise, gradient noise and added white noise, which can otherwise be a problem in LDA turbulence measurements.

The residence-time weighting and two other methods of forming statistical averages, the one-dimensional correction and the straight arithmetic averaging, were compared to LDA-tracker and to hot-wire measurements. The measurements were carried out on a free, axisymmetric jet in air, and the LDA-counter measurements were made with a burst counter directly interfaced to a mini-computer. Measurements were made of mean and mean-square velocity for axial and transverse scans of the jet, and the relative differences were displayed in the figures. The results showed that residence-time weighting is necessary for turbulence measurements beyond 10-20 pct. intensity. The effect of frequency shift and angular effects are such that the one dimensional correction is best when no frequency shift is used. In this case the one-dimensional correction gives only minor (< 2 pct.) errors up to 15 pct. turbulence.

Two methods of implementing the spectral measurements from the randomly

sampled LDA data were carried out. The first is analogous to the Blackman-Tukey method, in which the spectrum is formed as a cosine transform of the autocovariance function. The other is based on a direct transform analogous to the classical periodogram. Measurements of the velocity spectrum of the jet were performed by both methods. The effect on the autocorrelation function of the various weighting methods was illustrated, and the LDA spectra were compared to hot-wire spectra measured simultaneously or taken from previous publications.

The spectrum measurements showed that the burst-type counter LDA is able to measure spectra with a relatively low noise level and dynamic range approaching that of hot-wire spectra. However, the LDA spectrum is still disturbed by noise sources at the high frequency end. This noise may be reduced by a finer resolution of the velocity data, and by more efficient computing and data processing methods. The residence time weighted LDA spectra have the advantage of measuring a single velocity component and allowing measurements in highly turbulent flow.

In a separate chapter, the effect of LDA-tracker drop-out and the sample-and-hold character of the counter analog output was investigated. An analysis of the drop-out effect was presented and compared to results of both LDA and hot-wire spectral measurements in the jet.

The results of the present work confirm the importance of the burst-type LDA in turbulence measurements. It would appear that the burst-type LDA has the potential of providing interesting results from measurements in highly turbulent flows to complement previous hot-wire measurements as well as provide results in cases where measurements have so far been impractical or impossible. Although more turbulence data from counter-LDA measurements are beginning to appear, some of the unique properties of the

burst-type LDA still remain largely unexploited: the ability to apply the residence time correction in highly turbulent flow, the interpretation of the uncorrected (arithmetic) averaging as a mass flow weighted average, and the unique capability of measuring only the seeded component of a mixing or reacting flow. These topics present challenging opportunities for further research with the burst-type LDA.

Appendix A

Measuring Volume Cross Section

Consider the ellipsoidal volume figure A1 with half axes a,b and c:

$$\frac{x^2}{a^2} + \frac{y^2}{b^2} + \frac{z^2}{c^2} = 1 \tag{A.1}$$

The distance between fringes is δ and the number of fringes within 2a is $N_f = 2a/\delta$. We allow a frequency difference f_s between the laser beams, which corresponds to a motion of the fringe planes along with $\hat{x}$-axis with velocity $u_f = -f_s \cdot \delta$.

We define:

$$Q \equiv N_e/N_f \tag{A.2}$$

and

$$R \equiv u_f/|\underline{u}| \tag{A.3}$$

where N_e is the number of zero-crossings needed by the electronics and R is the ratio of the fringe velocity to the magnitude of the instantaneous velocity vector.

Assuming a constant flow velocity $\underline{u} = (u,v,w)$ across the measuring volume, the particle trajectory may be described by:

$$\underline{e} = (x_p, Y_p, z_p) = (x_o+ut, y_o+vt, z_o+wt) \tag{A.4}$$

The arithmetic is simplified by a change of coordinates:

$$\alpha = \frac{u}{a'}, \quad \beta = \frac{v}{b'}, \quad \gamma = \frac{w}{c} \tag{A.5}$$

and

$$\xi_o = \frac{x_o}{a'} \qquad \eta_o = \frac{y_o}{b'} \qquad \zeta_o = \frac{z_o}{c} \tag{A.6}$$

whereby the ellipse is transformed to a sphere.

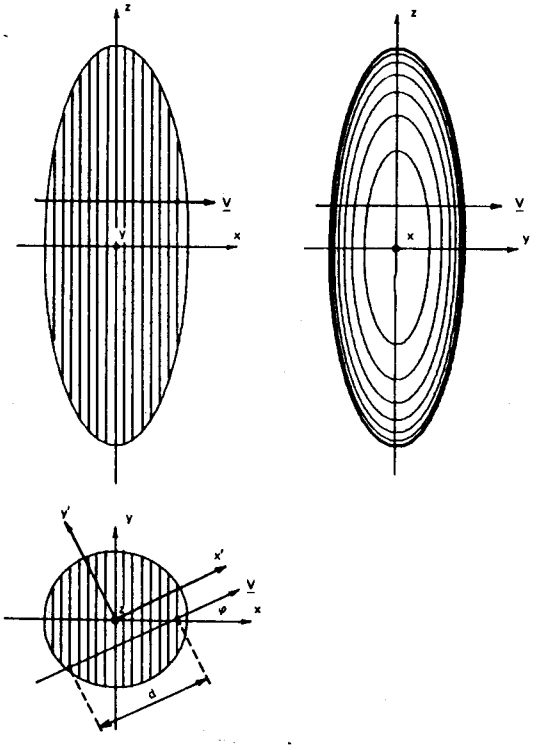

Figure A1 The measuring volume projected onto the three coordinate planes $\theta = 20°$.

The intersection points between the particle trajectory and the sphere is given by:

$$(\alpha t+\xi_o)^2 + (\beta t+\eta_o)^2 + (\gamma t+\zeta_o)^2 = 1 \tag{A.7}$$

or

$$At + Bt + C = 0 \tag{A.8}$$

with

$$A = \alpha^2 + \beta^2 + \gamma^2 \tag{A.9}$$

$$B = 2(\alpha\xi_o+\beta\eta_o+\gamma\zeta_o) \tag{A.10}$$

$$C = \xi_o^2+\eta_o^2+\zeta_o^2-1 \tag{A.11}$$

The instants in time at which the particle enters and leaves the volume is given by:

$$t = \frac{-B}{2A} \pm \sqrt{\frac{B^2-4AC}{4A^2}} \tag{A.12}$$

and the time spent in the volume (the residence time) by:

$$\Delta t = \sqrt{\frac{B^2-4AC}{A^2}} \tag{A.13}$$

The number of times a particle crosses a fringe in the volume, the number of zero-crossings of the Doppler burst, is then:

$$N_z = \frac{(u-u_f)\Delta t}{\delta} \tag{A.14}$$

The condition for a measurement is:

$$N_z = \frac{u-u_f}{\delta}\Delta t \geq Ne \tag{A.15}$$

or

$$\frac{u-u_f}{2a}\Delta t \geq Q \tag{A.16}$$

or

$$\frac{B^2}{4} - AC - A^2 \frac{a^2Q^2}{(u-u_f)^2} \geq 0 \qquad (A.17)$$

Inserting A, B and C we get an inequality expressing the initial positions ξ_o, η_o and ζ_o which would lead to a measurement. The intersection of the trajectories forming the boundary (expressed by the equality in A.17) with the (η,ζ)-plane is an ellipse:

$$C_1 \eta_o^2 + C_2 \xi_o^2 + C_3 \eta_o \xi_o + C_4 = 0 \qquad (A.18)$$

with

$$\left.\begin{aligned} C_1 &= \alpha^2 \quad \gamma^2 \\ C_2 &= \alpha^2 + \beta^2 \\ C_3 &= -2\beta\gamma \end{aligned}\right\} \qquad (A.19)$$

and

$$\left.\begin{aligned} C_4 &= (\alpha^2 + \beta^2 + \gamma^2)^2 \frac{a^2Q^2}{(u-u_f)^2} - (\alpha^2 + \beta^2 + \gamma^2) \end{aligned}\right\}$$

A rotation removes the product term:

$$\begin{aligned} \eta_o &= \eta_o' \cos \phi_o - \zeta_o' \sin \phi_o \\ \zeta_o &= \eta_o' \sin \phi_o + \zeta_o' \cos \phi_o \end{aligned} \qquad (A.20)$$

Inserting into (A.18), dividing by $\cos^2 \phi_o$ and rearranging terms leads to the following condition for the removal of the product term:

$$\tan \phi_o = \begin{cases} \gamma/\beta \\ -\beta/\gamma \end{cases} \qquad (A.21)$$

and the following expression for the ellipse in the new coordinates:

$$\eta_o'^2/b_o^2 + \zeta_o'^2/c_o^2 = 1 \qquad (A.22)$$

with

$$b_o^2 = C_4/\alpha^2 \quad \text{and} \quad c_o^2 = C_4/(\alpha^2 + \beta^2 + \gamma^2)$$

The area A' of this ellipse is:

$$A' = \pi \frac{C_4}{\alpha\sqrt{\alpha^2+\beta^2+\gamma^2}} \tag{A.23}$$

or in the original coordinates:

$$A = \pi\, abc\, \frac{1}{u} \sqrt{\frac{\underline{u}^2}{a^2} + \frac{\underline{v}^2}{b^2} + \frac{\underline{w}^2}{c^2}} \left[1 - \frac{a^2Q^2}{(u-u_j)^2} \left(\frac{\underline{u}^2}{a^2} + \frac{\underline{v}^2}{b^2} + \frac{\underline{w}^2}{c^2}\right)\right] \tag{A.24}$$

The cross section S is just the projection of this area normal to $\underline{u}$:

$$S = \frac{\underline{u}}{|\underline{u}|} \cdot \hat{x}\, A = \frac{\underline{u}}{|\underline{u}|} A \tag{A.25}$$

or

$$S = \pi\, a\, b\, c\, R\left(1 - a^2Q^2R^2\left(\frac{|\underline{u}|}{u-u_s}\right)^2\right) \tag{A.26}$$

with

$$R = \frac{1}{|\underline{u}|} \sqrt{\frac{\underline{u}^2}{a^2} + \frac{\underline{v}^2}{b^2} + \frac{\underline{w}^2}{c^2}} \tag{A.27}$$

The cross section relative to the geometrical cross section in the (y,z)-plane is:

$$\sigma = a\, R\left(1 - a^2 Q^2 R^2 \left(\frac{|\underline{u}|}{u-u_f}\right)^2\right) \tag{A.28}$$

Appendix B

Moments of the Particle Distribution Function ($g_1(x,t)$)

George and Lumley (1973) compute the moments of the particle distribution function $g_1(\underline{x})$, which expresses the static particle distribution at time t. The present problem differs from that of George and Lumley only by: 1) The probability of two or more particles in the measuring volume at any one time is negligible, and 2) g_1 is a function of time as well as of spatial coordinate $\underline{x}$. In the general case, i.e. for any particle concentration and volume size, we may use the derivation of George and Lumley, if we note that the time dependence of g_1 enters only through $\underline{x}$, since the variations of g_1 with time reflects the motion of the particle. Thus

$$g_1(\underline{x},t) = g_1(\underline{x}(t)), \tag{B.1}$$

where

$$\underline{x}(t) = \underline{a} + \int_0^t \underline{U}(t)dt \tag{B.2}$$

$\underline{a}$ is the initial position of the particle, and capital letters denote Lagrangian quantities, i.e. the coordinates of individual particles.

Expressing g_1 in this form, we may directly take over the results of George and Lumley (1973):

$$\overline{g_1(\underline{x}(t))} = \mu \tag{B.3}$$

and

$$g_1(\underline{x}(t))\, g_1(\underline{x}'(t')) = \mu^2 + \mu\, \delta(\underline{x}(t) - \underline{x}'(t')) \tag{B.4}$$

Introducing

$$\underline{x}'(t') = \underline{x}'(t) + \int_t^{t'} \underline{U}(t)dt \tag{B.5}$$

we get:

$$\overline{g_1(\underline{x},t)\, g_1(\underline{x}',t')} = \mu^2 + \mu\delta\left[\underline{x}(t)-\underline{x}'(t)-\int_t^{t'} \underline{U}(t)dt\right] \qquad (B.6)$$

If we can make Taylor's hypothesis ("frozen turbulence"), the second moment can be simplified. We can replace $\underline{U}(t)$ by the Eulerian velocity at location $\underline{x}$, $\underline{u}(\underline{x},t)$, and since Taylor's hypothesis entails $\underline{u} << \overline{\underline{u}}$, we may write for short times:

$$\int_t^{t'} \underline{U}(t)dt \cong \int_t^{t'} \underline{u}(\underline{x}',t)dt \cong \overline{\underline{u}}(\underline{x})\cdot(t'-t) \qquad (B.7)$$

Thus

$$\overline{g_1(\underline{x},t)\, g_1(x',t')} = \mu^2 + \mu\delta\left[\underline{x}(t) - \underline{x}'(t) - \overline{\underline{u}}(\underline{x})\cdot(t'-t)\right] \qquad (B.8)$$

References

Adrian, R.J., Orloff, K.L. (1977). *Laser Anemometer Signals: Visibility Characteristics and Application to Particle Sizing*. Appl. Opt. 16: 677-84.

Asalor, T.D., Whitelaw, J.H. (1976). *The Influence of Combustion-Induced Particle Concentration Variations on Laser-Doppler Anemometry*. In Proc. LDA Symp., Copenhagen 1975, 115-37. Copenhagen: PO Box 70, 2740 Skovlunde, Denmark, 736 pp.

Asher, J.A., Scott, P.F., Wang, J.C. (1974). *Parameters Affecting Laser Velocimeter Turbulence Spectra Measurements*. Final Rep. (AEDC-TR-74-54) Contract No. F40600-72-C-0013, Oct. 1974.

Berman, N.S., Dunning, T.W. (1973). *Pipe Flow Measurements of Turbulence and Ambiguity Using Laser-Doppler Velocimetry*. J. Fluid Mech. 61: 289-99.

Boguslawski, L., Popiel, Cz.O. (1979). *Flow Structure of the Free Round Turbulent Jet in the Initial Region*. J. Fluid Mech., 90 pt 3, 531-39.

Bouis, X., Gourtot, S., Pfeiffer, H.T. (1977). *Laser Anemometry: Measurement of the Spectral Power Density of Velocity Variations in Turbulent Flow*. ISL-R-126/76 Contract No. DRME-75/055 (B77-32497/86A)

Bovin, A., Wolf, E. (1965). *Electromagnetic Field in the Neighborhood of the Focus of a Coherent Beam*. Phys. Rev., 138, 1561-1565.

Born, M., Wolf, E. (1959). *Principles of Optics*. Pergamon Press, Oxford.

Buchhave, P. (1976). *Biasing Errors in Individual Particle Measurements with the LDA-Counter Signal Processor*. In Proc. LDA Symp., Copenhagen, 1975, 258-78.

Buchhave, P., George, W.K., Jr., Lumley, J.L. (1979). *The Measurement of Turbulence with the Laser-Doppler Anemometer*. Annual Review of Fluid Mech., V. 11, 443-503, Annual Reviews, Inc., Palo Alto, Calif.

Drain, L.E. (1972). *Coherent and Noncoherent Methods in Doppler Optical Beat Velocity Measurement.* J. Phys. D5: 481-95.

Durrani, T.S., Greated, C.A., (1977). *Laser Systems in Flow Measurement.* New York & London: Plenum. 289 pp.

Durst, F. (1974). *Informal Presentation.* In: Proc. Second Int. Workshop on Laser Velocimetry, March 27-29, 1974. (Bull No. 144), Purdue University, West Lafayette, Ind.

Durst, F., Melling, A., Whitelaw, J.H.,(1976). *Principles and Practice of Laser-Doppler Anemometry.* New York: Academic, 405 pp.

Edwards, R.V., Angus, T.C., French, M.J., Dunning, T.W.,Jr., (1971). *Spectral Analysis of the Signal from the Laser-Doppler Flowmeter: Time Dependent Systems.* J. Appl. Phys. 42: 837-50.

Erdman, J.C., Gellert, R.I., (1976). *Particle Arrival Statistics in Laser Anemometry of Turbulent Flow.* Appl. Phys. Lett. 29: 408-11.

Gaster, M., Roberts, J.B. (1975). *Spectral Analysis of Randomly Sampled Signals.* J. Inst. Maths. Applics. 15: 195-216.

Gaster, M., Roberts, J.B. (1977). *The Spectral Analysis of Randomly Sampled Records by a Direct Transform.* Proc. R. Soc. London Ser. A 354: 27-58.

George, W.K.,Jr. (1973). *The Laser Doppler Velocimeter and Its Application to the Measurement of Turbulence.* J. Fluid Mech. 60: 321-62.

George, W.K., Jr., (1976). *Limitations to Measuring Accuracy Inherent in the Laser-Doppler Signal.* In Proc. LDA Symp., Copenhagen, 1975.

George, W.K., Jr., (1979). *Processing of Random Signals*. In: Proc. of the Dynamic Flow Conf. 1978, P.O. Box 121, DK-2740, Skovlunde, Denmark. 757-800.

Hanson, S. (1973). *Broadening of the Measured Frequency Spectrum in a Differential Laser Anemometer Due to Interference Plane Gradients*. J. Phys. D, 6, 164-171.

Hanson, S. (1974). *Coherent Detection in Laser-Doppler Velocimeters*. Opto-Electronics 6: 263-69.

Hinze, J.O. (1975). *Turbulence*. McGraw-Hill, Inc.

Hosel, W., Rodi, W. (1977). *New Biasing Elimination Method for Laser-Doppler Velocimeter Counter Processing*. Rev. Sci. Instrum. 48: 910-19.

Jenkins, G.M., Watts, D.G. (1968). *Spectral Analysis and Its Applications*. Holden-Day, San Francisco.

Karpuk, M.E., Tiederman, W.G., Jr. (1976). *Effect of Finite-Size Probe Volume Upon Laser-Doppler Anemometer Measurments*. AIAA J. 14: 1105-9.

Lading, L., (1973). *Analysis of Signal-To-Noise Ratio of the Laser-Doppler Velocimeter*. Opto-Electronics 5: 175-87.

Lading, L., Edwards, R.V., (1976). *The Effect of Measurement Volume on Laser-Doppler Anemometer Measurements as Measured on Simulated Signals*. In: Proc. LDA Symp., Copenhagen 1975, 64-80.

Lumley, J.L. (1978) private communication.

Masry, E., Lui, Ming-Chuan, C. (1976). *Discrete-time Spectral Estimation of Continuous-Parameter Processes - a New Consistent Estimate.* IEEE Trans. on Inf. Theory, IT-22, 298-304.

Masry, E. (1978)a. *Poisson Sampling and Spectral Estimation of Continuous-Time Processes.* IEEE Trans. on Inf. Theory, IT-24, 173-83.

Masry, E.(1978)b. *Alias-Free Sampling: An Alternative Conceptualization and its Applications.* IEEE Trans. on Inf. Theory, IT-24, 317-24.

Mayo, W.T. Jr. (1974) A *Discussion of the Limitations and Extensions of Power Spectrum Estimation with Burst Counter LDV Systems.* In: Proc. of the Second Int. Workshop on Laser Velocimetry, March 27-29, 1974 (Bull. No. 144), Purdue Univ., West Lafayette, Ind.

Mayo, W.T., Shay, M.T., Riter, S. (1974). *The Development of New Digital Data Processing Techniques for Turbulence Measurements with a Laser Velocimeter.* Final Rep. (AEDC-TR-74-53), USAF Contract No. F40600-73-C-003, Aug. 1974.

Mayo, W.T. Jr. (1979). *Spectrum Measurements with Laser Velocimeters.* In: Proc. of the Dynamic Flow Conf. 1978, P.O. Box 121, DK-2740, Skovlunde, Denmark. 851-868.

McLaughlin, D.K., Tiederman, W.G. (1973). *Biasing Correcting for Individual Realization of Laser Anemometer Measurements in Turbulent Flows.* Phys. Fluids,16: 2082-88.

Mehta, C.L. (1970). *Theory of Photoelectron Counting.* In: Progress in Optics, V. VIII, ed. E. Wolf, No. Holland Publishing Co., Amsterdam, London.

Middleton, D. (1960). *Statistical Communication Theory.* Mc-Graw-Hill Book Co., New York.

Morel, T. (1975). *Comprehensive Design of Axisymmetric Wind Tunnel Contractions*. J. Fluids Eng. ASME Trans. Sect. I, V. 97 #2, 225-233.

Quigley, M.S., Tiederman, W.G. Jr. (1977). *Experimental Evaluation of Sampling Bias in Individual Realization Laser Anemometry*. AIAA J. 15: 266-68.

Rudd, J.M. (1969). *A New Theoretical Model for the Laser-Doppler Meter*. J. of Phys. E, 2, 55-58.

Scott, P.F. (1974). *Theory and Implementation of Laser Velocimeter Turbulence Spectrum Measurements*. In: Proc. of the Second Inter. Workshop on Laser Velocimetry, March 27-29, 1974 (Bull. No. 144), Purdue Univ., West Lafayette, Ind.

Shapiro, H.S., Silverman, R.A. (1960). *Alias-Free Sampling of Random Noise*. J. Soc. Ind. Appl. Math. 8: 225-48.

Smith, D.M., Meadows, D.M. (1974). *Power Spectra from Random-Time Samples for Turbulence Measurements with a Laser Velocimeter*. In: Proc. of the Second Int. Workshop on Laser Velocimetry, March 27-29, 1974. (Bull. No. 144), Purdue Univ., West Lafayette, Ind.

Tennekes, H., Lumley, J. L. (1972). *A First Course in Turbulence*, Cambridge: MIT Press.

Tiederman, W.G.,Jr. (1977). *Interpretation of Laser Velocimeter Measurements in Turbulent Boundary Layers and Regions of Separation*. Paper presented at 5th Biennial Symp. on Turbulence, Oct. 1977, Univ. Missouri, Rolla.

Wang, J.C.F. (1976). *Measurement Accuracy of Flow Velocity via a Digital Frequency Counter Laser Velocimeter Processor.* In: Proc. of the LDA Symp., Copenhagen 1975, 150-75. Copenhagen: P.O. Box 70, 2740 Skovlunde, Denmark. 736 pp.

Wyganski, I., Fiedler, H. (1969). *Some Measurements in the Self-Preserving Jet.* J. Fluid Mech., 38 pt 3, 577-612.